HAL open science

Inversion in a four-terminal superconducting device on the quartet line: I. Two-dimensional metal and the quartet beam splitter

Régis Mélin

▶ To cite this version:

Régis Mélin. Inversion in a four-terminal superconducting device on the quartet line: I. Two-dimensional metal and the quartet beam splitter. Physical Review B, 2020, 102 (24), pp.245435. 10.1103/PhysRevB.102.245435 . hal-03084480

HAL Id: hal-03084480

https://hal.science/hal-03084480v1

Submitted on 31 May 2023

HAL is a multi-disciplinary open access archive for the deposit and dissemination of scientific research documents, whether they are published or not. The documents may come from teaching and research institutions in France or abroad, or from public or private research centers.

L'archive ouverte pluridisciplinaire **HAL**, est destinée au dépôt et à la diffusion de documents scientifiques de niveau recherche, publiés ou non, émanant des établissements d'enseignement et de recherche français ou étrangers, des laboratoires publics ou privés.

Inversion in a four-terminal superconducting device on the quartet line. I. Two-dimensional metal and the quartet beam splitter

Régis Mélin
Université Grenoble-Alpes, CNRS, Grenoble INP, Institut NEEL, 38000 Grenoble, France

(Received 5 August 2020; revised 3 November 2020; accepted 30 November 2020; published 31 December 2020)

In connection with the recent Harvard group experiment on graphene-based four-terminal Josephson junctions containing a grounded loop, we consider voltage biasing at opposite voltages on the quartet line and establish lowest-order perturbation theory in the tunnel amplitudes between a two-dimensional (2D) metal and four superconducting leads in the dirty limit. We present in addition general nonperturbative and nonadiabatic results. The critical current on the quartet line $I_c(\Phi/\Phi_0)$ depends on the reduced flux Φ/Φ_0 via interference between the three-terminal quartets (3TQs) and the nonstandard four-terminal split quartets (4TSQs). The 4TSQs result from synchronizing two Josephson junctions by exchange of two quasiparticles "surfing" on the 2D quantum wake, and this mechanism is already operational at equilibrium. Perturbation theory in the tunnel amplitudes shows that the 3TQs are π-shifted but the 4TSQs are 0-shifted if the contacts have linear dimension which is large compared to the elastic mean free path. We establish the gate voltage dependence of the quartet critical current oscillations $I_c(\Phi/\Phi_0)$. It is argued that "observation of $I_c(0) \neq I_c(1/2)$" implies "evidence for the four-terminal 4TSQ" for finite bias voltage on the quartet line and arbitrary interface transparencies. This statement relies on physically motivated approximations leading to the Ambegaokar-Baratoff-type formula for the quartet critical current-flux relation. It is concluded that the recent experiment mentioned above finds evidence for the four-terminal 4TSQ.

DOI: 10.1103/PhysRevB.102.245435

I. INTRODUCTION

A superconductor such as aluminum is characterized by a macroscopic phase variable φ and a gap Δ separating the collective BCS ground state from the first quasiparticles. A BCS superconductor supports dissipationless supercurrent flow in response to phase gradients.

BCS theory assigns given numerical values to the phase φ of a single superconductor, even if φ is a non-gauge-invariant quantity that cannot be observed under any experimental condition. BCS theory also yields an absence of the Meissner effect, i.e., BCS superconductors do not repel magnetic field. These paradoxes were resolved [1,2] by the so-called Higgs mechanism, i.e., a theory of superconductivity that takes Coulomb interactions into account and describes the dynamics of the collective modes in the so-called "Mexican-hat" potential.

Following the seminal works [1,2] on gauge invariance mentioned above, Josephson calculated [3] the supercurrent through a tunnel junction connecting two superconductors S_1 and S_2 with phases φ_1 and φ_2. The phase φ of a single superconductor is not gauge-invariant, thus it is not observable. The difference $\varphi_1 - \varphi_2$ between the phases of S_1 and S_2 is gauge-invariant. The latter is observable as the following dissipationless current through a superconductor-insulator-superconductor S_1IS_2 Josephson junction:

$$I = I_c^{(2T)} \sin(\varphi_1 - \varphi_2), \tag{1}$$

which has its maximal value set by the two-terminal critical current $I_c^{(2T)}$.

Equation (1) describes the tunneling of single Cooper pairs between the superconductors S_1 and S_2. Composite objects made of two or more Cooper pairs tunnel in the same quantum event at larger interface transparency. The possibility of two-Cooper-pair tunneling yields the $\sin[2(\varphi_1 - \varphi_2)]$ term in the following equation:

$$I = \left[I_c^{(1),1} + I_c^{(2),1} + \cdots\right] \sin(\varphi_1 - \varphi_2) \tag{2}$$

$$+ \left[I_c^{(2),2} + \cdots\right] \sin[2(\varphi_1 - \varphi_2)] \tag{3}$$

$$+ \cdots . \tag{4}$$

Due to their internal structure, both Cooper pairs are coupled to each other by the Fermi exclusion principle since they are located within the same coherence volume $\sim\xi^3$ in the same time window $\tau_\Delta = \hbar/\Delta$, where the zero-energy coherence length is $\xi = \xi_{\rm ball}(0)$ in the ballistic limit:

$$\xi_{\rm ball}(0) = \frac{\hbar v_F}{\Delta}, \tag{5}$$

with v_F the Fermi velocity.

The expansion given by Eqs. (2)–(4) shows fast convergence under usual experimental conditions: Eqs. (2)–(4) are usually dominated by $I_c^{(1),1}$, such that $|I_c^{(1),1}| \gg |I_c^{(2),1}|$ and $|I_c^{(1),1}| \gg |I_c^{(2),2}|$.

The present paper is the first of a series of three papers I, II, III, and it will be followed by paper II [23] and paper III [24]. These papers demonstrate that *multiterminal Josephson junctions* offer a playground for investigating the physics of two-Cooper-pair tunneling in connection with an interpretation of a recent experiment realized in the Harvard group [4].

 ©2020 American Physical Society

Namely, the terms similar to $I_c^{(1),1} + I_c^{(2),1} + \cdots$ in Eq. (2) become ac in the multiterminal Josephson effect (typically in the range of a GHz or 10 GHz), thus not contributing to the dc-current response. This offers an experimental signal controlled solely by higher-order dc-contributions similar to $I_c^{(2),2} + \cdots$ in Eq. (3), without the terms similar to $I_c^{(1),1} + I_c^{(2),1} + \cdots$ in the dc-current; see Eq. (2).

Concerning multiterminal Josephson junctions, it was shown in Refs. [5,6] that nonstandard effects appear in "supercurrent splitting" if three superconducting leads are connected at a distance shorter than $\sim\xi$. The three-terminal quartets (3TQs) and higher-order resonances such as the three-terminal sextets and octets were predicted to be revealed upon voltage biasing (S_a, S_b, S_c) at (V_a, V_b, V_c); see Refs. [5,6]. This four-fermion quartet resonance can be viewed as being "glued" by the interfaces in the absence of preexisting quartets in the bulk of BCS superconductors. Namely, energy conservation puts a constraint on the bias voltages V_a and V_b, which have to be "on the quartet line" $V_a + V_b = 0$ in the (V_a, V_b) voltage plane (S_c being grounded at $V_c = 0$). The predicted [5–12] Josephson anomaly on the quartet line $V_a + V_b = 0$ originates from quantum mechanically synchronizing the three superconductors (S_a, S_b, S_c), via the following gauge-invariant static combination of their respective macroscopic phase variables:

$$\varphi_{q,\,3T} = \varphi_a + \varphi_b - 2\varphi_c. \tag{6}$$

The Josephson relations imply that the phase combination $\varphi_a(t) + \varphi_b(t) - 2\varphi_c(t)$ is time t-independent, with $\varphi_a(t) = 2eVt/\hbar + \varphi_a$, $\varphi_b(t) = -2eVt/\hbar + \varphi_b$, and $\varphi_c(t) = \varphi_c$. The previous difference $\varphi_1 - \varphi_2$ between the phases φ_1 and φ_2 of S_1 and S_2 enters the two-terminal dc-Josephson current-phase relation given by Eq. (1). Conversely, in a three-terminal Josephson junction, the nonstandard combination given by Eq. (6) implies that the 3TQ current I_q is given by

$$I_q = I_{c,\,q} \sin \varphi_{q,\,3T} \tag{7}$$

in the limit of tunnel contacts. Equation (7) depends on the phases of the three superconductors through the 3TQ phase $\varphi_{q,\,3T}$ in Eq. (6), not only on the two-body $\varphi_1 - \varphi_2$ entering Eq. (1) for the two-terminal dc-Josephson effect.

The prediction of the 3TQ was confirmed experimentally by the Grenoble group [13] (with a metallic structure) and by the Weizmann Institute group [14] (with a semiconducting nanowire double quantum dot). The recent Harvard group experiment [4] provides evidence for unanticipated features of the quartets in the graphene-based four-terminal device schematically shown in Fig. 1, in connection with the additional parameter provided by the flux Φ in the loop.

The four-terminal Josephson junction in Fig. 1 is an opportunity to investigate interference in the quartet current, in the spirit of a superconducting quantum interference device (SQUID) [15]. Several experiments on multiterminal devices containing loops have been proposed recently [8,16,17] in the absence of voltage biasing, i.e., at equilibrium, where all parts of the circuit are grounded.

The device in Fig. 1 was proposed recently [18,19] to probe Weyl points and nontrivial topology. The voltage biasing conditions are different in Refs. [18,19] for topology and Refs. [5,6] for the quartets: the voltages are incommensurate

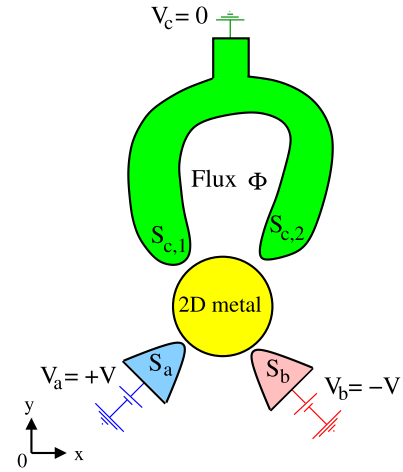

FIG. 1. The four-terminal superconducting device: The superconducting leads S_a, S_b, and S_c are voltage-biased at (V_a, V_b, V_c), with $V_a = -V_b \equiv V$ on the quartet line and S_c is grounded at $V_c = 0$. The loop in S_c terminates at the contact points S_{c_1} and S_{c_2} on the 2D metal used to describe the sheet of graphene gated away from the Dirac points in the Harvard group experiment [4]. The loop is threaded by the magnetic flux Φ.

in Refs. [18,19], so as to sweep the (φ_a, φ_b) Brillouin zone of the superconducting phases. Experiments related to the theoretical proposal on topology [18,19] were attempted recently [20–22].

Coming back to the Harvard group experiment [4], the emergence of a quartet anomaly in four-terminal configurations naturally raises the question of making the theory of the quartets with four terminals, instead of three terminals as in the previous theoretical [5–12] and experimental [13,14] investigations. In this sequence of papers I (current paper), II [23], and III [24], the $(S_a, S_b, S_{c_1}, S_{c_2})$ four-terminal device is biased at (V_a, V_b, V_c, V_c), where $V_c = 0$ is the reference voltage of the grounded S_c containing a loop threaded by the magnetic flux Φ and terminated by S_{c_1} and S_{c_2} (see Fig. 1). Our strategy in this series of papers is to develop a theory that is intended to interpret the following unexpected features reported by the Harvard group [4]:

(i) A quartet Josephson anomaly appears on the $V_a + V_b = 0$ quartet line, once one of the elements of the conductance matrix is plotted in color as a function of the (V_a, V_b) voltages [4]. This is compatible with the theoretical prediction of the quartets for three superconducting terminals [5,6], and with the previous Grenoble [13] and Weizmann Institute [14] group experiments.

(ii) In addition, the four-terminal Harvard group experiment [4] demonstrates oscillations of the quartet current as a function of the reduced flux Φ/Φ_0 in the loop.

(iii) An "inversion" appears [4] in a low bias voltage window if the experimental data for the amplitude of the quartet anomaly are plotted as a function of Φ/Φ_0. Namely, the quartet anomaly is stronger at $\Phi/\Phi_0 = 1/2$ than at $\Phi/\Phi_0 = 0$ even if superconductivity should naively be stronger at $\Phi/\Phi_0 = 0$ than at $\Phi/\Phi_0 = 1/2$. The present paper (paper I) addresses a theoretical description of "inversion in $I_c(\Phi/\Phi_0)$ between $\Phi/\Phi_0 = 0$ and $\Phi/\Phi_0 = 1/2$" on the basis of

perturbation theory in the tunnel amplitudes within the simplest $V = 0^+$ adiabatic limit. In addition, the model is generalized beyond the perturbative and adiabatic regimes.

(iv) Gating away from the Dirac point in the Harvard group experiment [4] favors π-periodicity of $I_c(\Phi/\Phi_0)$ with respect to 2π-periodicity. The present paper turns out to be compatible with this observation.

(v) A small voltage scale V_* emerges [4] in the bias voltage V-dependence of the quartet signal. Paper II [23] addresses how inversion is produced by increasing the bias voltage V on the quartet line, in the simple situation of a 0D quantum dot. Paper III [24] addresses whether a "Floquet mechanism" similar to that of paper II [23] can extrapolate to the 2D metal of paper I, in connection with answering the question of why the voltage V_* for the inversion is much smaller than the gap in the Harvard group experiment [4].

In short, the progression between the three papers is about different levels of the modeling: The present paper (paper I) starts from the four-terminal split quartets (4TSQs) treated in perturbation in the tunnel amplitudes and in the $V = 0^+$ adiabatic limit with a 2D metal. Paper I also addresses how the nonstandard four-terminal quartets can be generalized to arbitrary device parameters. Paper II [23] addresses the full Floquet theory at finite bias voltage for a zero-dimensional (0D) quantum dot, i.e., how the Floquet spectra and populations can produce inversion in $I_c(\Phi/\Phi_0)$ between $\Phi/\Phi_0 = 0$ and $\Phi/\Phi_0 = 1/2$. Paper III [24] combines the present paper I and paper II [23], by addressing finite bias voltage for a 2D metal of paper I within physically motivated approximations.

The results of the present paper, which are not presented as theoretical support in the experimental Harvard group paper [4], are the following:

(i) Rigorous microscopic calculation for the sign and the amplitude of the critical currents through a 2D metal within perturbation theory in the tunnel amplitudes and in the adiabatic limit, taking disorder in the superconducting leads in the dirty limit into account.

(ii) Physically motivated approximations for addressing the nonstandard 4TSQ at arbitrary interface transparencies and finite bias voltage.

In this paper, we propose a simple model for the Harvard group experiment [4] (see Secs. III, IV, V, VI, and VII), and next the model is analyzed in connection with this experiment (see Secs. VIII, IX, and X).

The detailed structure of the present paper is as follows. Section II summarizes the three papers of the series. The model and the methods are presented in Secs. III and IV, respectively. The three-terminal 3TQ and the four-terminal 4TSQ current-phase relations are next calculated from perturbation theory in the tunnel amplitudes combined to the adiabatic limit; see Sec. V. Section VI deals with the interference between the three-terminal 3TQ and the four-terminal 4TSQ. The importance of two space dimensions is pointed out in Sec. VII, in connection with the 2D quantum wake. Section VIII shows that "relative shift of π between the three-terminal 3TQ and the four-terminal 4TSQ" implies "inversion in the critical current $I_c(\Phi/\Phi_0)$ between the reduced flux values $\Phi/\Phi_0 = 0$ and $\Phi/\Phi_0 = 1/2$." The consequence of the model for the gate voltage dependence of the magnetic field oscillations is discussed in Sec. IX in connection with the Harvard group's experimental paper [4]. Section X discusses arbitrary interface transparencies and finite bias voltage within the proposed approximations. A summary and final remarks are provided in Sec. XI.

II. THE THREE PAPERS OF THE SERIES

In this section, we present an overview of the three papers of the series. Specifically, the following items (A), (B), and (C) detail which features of the Harvard group experiment [4] will be addressed and explained in which paper, i.e., the present paper I or papers II [23] or III [24].

(A) The present paper (paper I) starts with the simplest predictive approach, i.e., perturbation theory in the interface transparencies in the adiabatic limit where $(S_a, S_b, S_{c_1}, S_{c_2})$ are biased at $(V, -V, 0, 0)$ on the quartet line, with $V = 0^+$. In the context of Cooper pair splitting in a three-terminal normal metal–superconductor–normal metal (NSN) device, a similar perturbative approach [25,26] turned out to usefully uncover the important elementary processes of "elastic cotunneling" [25,26] and "crossed Andreev reflection" [25–27]. Concerning the four-terminal Josephson junction in Fig. 1, the following perturbative calculations reveal the 3TQ [5,6] interfering with the nonstandard 4TSQ.

More precisely, perturbation theory and the adiabatic limit lead to the three processes that are shown in Fig. 2:

(a) The three-terminal $3TQ_1$, $3TQ_2$ in which two pairs (from S_a and from S_b biased at $\pm V$, respectively) exchange partners and recombine as two outgoing pairs transmitted at the same contact with S_{c_1} for the $3TQ_1$ (or at the contact with S_{c_2} for the $3TQ_2$); see Figs. 2(a), 2(d) and 2(e).

(b) The four-terminal statistical fluctuations of the split quartets (4TFSQs) take one pair from S_a and another one from S_b biased at $\pm V$, respectively. Both of them split and recombine as one pair transmitted into S_{c_1} and another one into S_{c_2}; see Figs. 2(b) and 2(f). The 4TFSQs contribute solely to small sample-to-sample statistical fluctuations of the supercurrent.

(c) The four-terminal split quartets (4TSQs) exchange a quasiparticle between two pairs taken from S_a and S_b biased at $\pm V$, respectively. The 4TSQs realize a "four-terminal quartet beam splitter," namely, they take two pairs from S_a and S_b, make their wave-function overlap, and transmit a pair into S_{c_1} and another one into S_{c_2} in the outgoing state; see Figs. 2(c) and 2(f). Contrary to the 4TFSQs of the previous item (b), the four-terminal 4TSQs turn out to be robust against averaging their critical current in the presence of multichannel contacts.

It is demonstrated that the three-terminal $3TQ_1$, $3TQ_2$ [see the above item (a)] and the four-terminal 4TSQ [the above item (c)] are π- and 0-shifted, respectively, due to the minus sign in the wave function of a Cooper pair for the former, and to the additional exchange of two quasiparticles via the quantum wake for the latter. The critical current is larger at $\Phi/\Phi_0 = 1/2$ than at $\Phi/\Phi_0 = 0$, i.e., the model of this paper produces the inversion between $\Phi/\Phi_0 = 0$ and $\Phi/\Phi_0 = 1/2$, which is also obtained in the Harvard group experiment [4].

In addition, an approximation on disorder is implemented to address general values of the parameters, i.e., finite bias voltage on the quartet line and arbitrary interface transparencies.

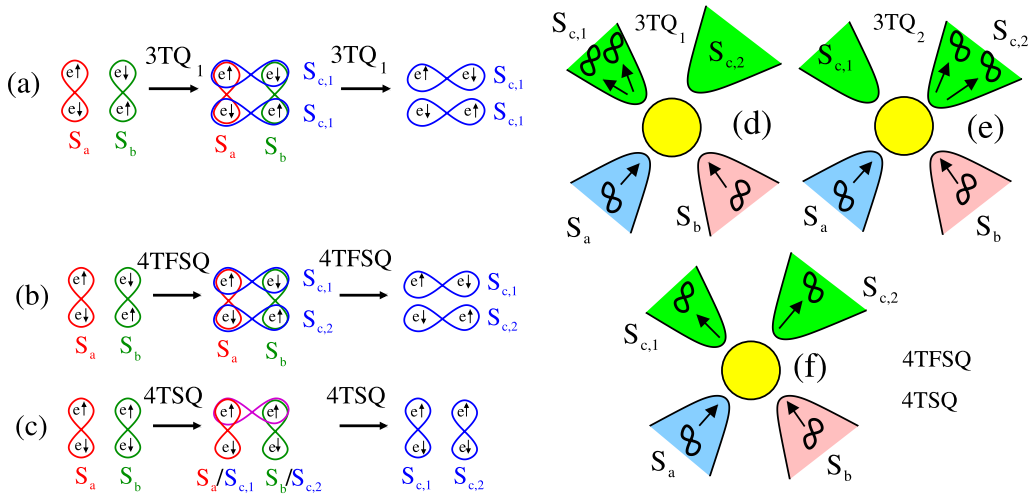

FIG. 2. Artist view of the microscopic processes: The three-terminal quartets [$3TQ_1$, panels (a) and (d)], the $3TQ_2$ [panel (e)], the four-terminal statistical fluctuations of the split quartet current [4TFSQ, panels (b) and (f)], and the four-terminal split quartets [4TSQ, panels (c) and (f)]. The two pairs taken from S_a and S_b biased at $\pm V$ exchange partners according to the "intermediate state" represented schematically in panels (a), (b), and (c) for the three-terminal $3TQ_1$ and the four-terminal 4TFSQ and 4TSQ, respectively. Two Cooper pairs are transmitted together into S_{c_1} [$3TQ_1$ in panels (a) and (d)] or into $S_{c,2}$ [$3TQ_2$ in panel (e)]. Alternatively, a single Cooper pair is transmitted into S_{c_1} and another one into S_{c_2} by the four-terminal 4TFSQ in panels (b) and (f), and by the 4TSQ in panels (c) and (f). A four-particle resonance is produced for the 3TQ and the 4TFSQ in panels (a) and (b), i.e., the two Cooper pairs from S_a and S_b recombine after exchanging partners. The 4TSQs in panel (c) involve interchanging a quasiparticle "surfing" on the quantum wake between the $S_{c,1}$ and $S_{c,2}$ contacts, from two Cooper pairs originating from S_a and S_b. The microscopic mechanism is different for the 3TQ and the 4TFSQ [panels (a) and (b)], or for the 4TSQ [panel (c)].

Now, we provide items (B) and (C) summarizing the goals of papers II [23] and III [24] of this series, in connection with explaining the Harvard group experiment [4]:

(B) We propose in the next paper (paper II [23]) a "Floquet level and population mechanism" by which an inversion between $\Phi/\Phi_0 = 0$ and $\Phi/\Phi_0 = 1/2$ is produced by tuning the bias voltage V on the quartet line. Most of the description in paper II [23] is based on a simplified 0D quantum dot configuration supporting a single level at zero energy. Paper II [23] relies on a combination of analytical theory and extensive numerical calculations. An interesting link is established in paper II [23], which relates the inversion in the critical current between $\Phi/\Phi_0 = 0$ and $\Phi/\Phi_0 = 1/2$ to repulsion between the Floquet levels as a function of the bias voltage V on the quartet line. Robustness of the inversion is established with respect to crossing over from weak to strong Landau-Zener tunneling by changing the couplings between the dot and the superconducting leads, and with respect to introducing several energy levels in a multilevel quantum dot. It turns out that the complementary "Floquet mechanism" of paper II [23] for the inversion tuned by the voltage V is different in nature from what is proposed here in paper I.

(C) The last paper of the series (paper III [24]) "merges" the present paper I and paper II [23] into an approximation scheme for the effect of bias voltage within the model proposed here in paper I. A link is established to the proximity effect, taking the specificities of the three- and four-terminal 3TQ and 4TSQ through a 2D metal into account. To illustrate this point, let us consider a two-terminal normal metal–superconductor (NS) Andreev interferometer containing a loop in its N part. Electrons with charge $-e$ from N are Andreev-reflected as holes with charge e, and a Cooper with charge $-2e$ is transmitted into S. Doubling the charge for the quartet mechanism, a pair of electronlike quasiparticles with charge $-2e$ can be reflected as a pair of holelike quasiparticles with charge $2e$ while two Coopers with charge $-4e$ are transmitted into S_c. We investigate in paper III [24] whether this can produce inversion in the critical current on the quartet line between $\Phi/\Phi_0 = 0$ and $\Phi/\Phi_0 = 1/2$ [for instance in connection with Fig. 3(c) in Ref. [28]]. In addition, we obtain the emergence of a small energy scale that is compatible with the observation [4] of a small voltage scale V_* in the variations of the critical current with bias voltage V.

The above items (A), (B), and (C) summarize the main motivations for investigating the three complementary mechanisms of the present paper I, and papers II [23] and III [24].

III. THE MODEL

This section presents the model used in this first paper of the series. The Hamiltonians are provided in Sec. III A. The voltage biasing conditions are given in Sec. III B. The critical current on the quartet line is defined in Sec. III C, in connection with making the link between our calculations and the Harvard group experiment [4].

A. The Hamiltonians

The assumptions of the model are presented in this subsection. The essential features of the Harvard group experiment [4] are listed in Sec. III A 1. The Hamiltonians are presented next: first the BCS Hamiltonian of the superconducting leads (see Sec. III A 2), next the Hamiltonian of the 2D metal used to model the sheet of graphene (see Sec. III A 3), and

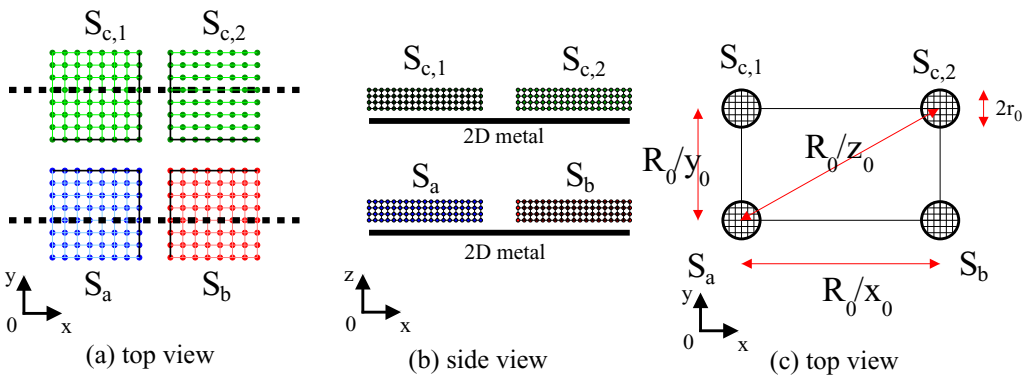

FIG. 3. The four-terminal superconducting device: Panel (a) shows a schematic top view of the Harvard group device [4], with four superconducting terminals S_a, S_b, $S_{c,1}$, and $S_{c,2}$ evaporated on top of the sheet of graphene that is in the (x, y) plane of the figure. The grounded loop connecting $S_{c,1}$ to $S_{c,2}$ is not shown in panel (a). Panel (b) shows cuts in the (x, z) plane along the dashed lines in panel (a). Panel (c) shows in the (x, y) plane a schematic top view of the geometry considered in this paper, with superconducting contacts having radius r_0, which can be smaller or larger than the zero-energy dirty-limit BCS coherence length. The separation between the superconducting contacts is R_0/x_0 along the x-axis, R_0/y_0 along the y axis, and R_0/z_0 along the diagonals. The superconducting leads S_a and S_b are biased at $\pm V$, while $S_{c,1}$ and $S_{c,2}$ belong to the same superconducting loop defined in S_c which is grounded at $V_c = 0$ and contains a loop pierced by flux Φ; see Fig. 1.

finally the term of the Hamiltonian describing the contacts between the 2D metal and the superconducting leads (see Sec. III A 4).

1. The essential ingredients

We start by presenting the ingredients of the Harvard group experiment [4] that are important to our theoretical description. The model relies on the following facts:

(i) The superconductors are connected on a 2D metal that consists of graphene gated away from the Dirac point; see Figs. 1 and 3.

(ii) The experiment involves four terminals instead of three as in the previous theoretical [5–12] and experimental [13,14] papers; see Figs. 1 and 3.

The discussion starts with two limiting cases for the device parameters:

(a) The limit of low-transparency interfaces between the 2D metal and the superconducting leads.

(b) The $V = 0^+$ adiabatic limit with voltage-biasing on the quartet line.

The theory is next generalized to arbitrary interface transparencies and finite bias voltage within a physically motivated approximation regarding disorder.

The assumptions about the geometry are illustrated in Fig. 3. Panels (a) and (b) show the geometry of the Harvard group experiment [4], with four superconducting contacts S_a, S_b, $S_{c,1}$, and $S_{c,2}$ evaporated on top of the sheet of graphene. Panel (a) shows the top view of the experimental configuration in the plane of the (x, y)-coordinates. Panel (b) shows the side views in the (x, z)-plane, i.e., cuts along the dashed lines in panel (a). Figure 3(c) represents the (x, y)-plane top view of the model considered in this paper, in which four superconducting leads S_a, S_b, $S_{c,1}$, and $S_{c,2}$ form contacts of radius r_0 on the 2D metal, where r_0 can be smaller or larger than the zero-energy dirty-limit BCS coherence length. The separation between the contacts in Fig. 3(c) corresponds to the parameters R_0/x_0 and R_0/y_0 along the x- and y-axis directions, respectively, and to R_0/z_0 along the diagonals.

2. BCS Hamiltonian of the superconducting leads

Now, we present the standard BCS Hamiltonian of each superconducting lead taken individually. In zero flux $\Phi/\Phi_0 = 0$, all superconducting leads are described by

$$\mathscr{H}_{\rm BCS} = -W \sum_{\langle i,j\rangle} \sum_{\sigma=\uparrow,\downarrow} (c^+_{i,\sigma} c_{j,\sigma} + c^+_{j,\sigma} c_{i,\sigma}) \tag{8}$$

$$-\Delta \sum_i (e^{i\varphi} c^+_{i,\uparrow} c^+_{i,\downarrow} + e^{-i\varphi} c_{i,\downarrow} c_{i,\uparrow}), \tag{9}$$

where the summation $\sum_{\langle i,j\rangle}$ runs over the pairs of nearest neighbors on a 3D tight-binding cubic lattice while $\sum_i$ runs over the tight-binding sites. The notation $\sigma = \uparrow, \downarrow$ stands for the spin. The first term in Eq. (8) is the kinetic energy. The second term given by Eq. (9) is the BCS mean field pairing with superconducting gap Δ. The macroscopic superconducting phase variable is generically denoted by φ in Eq. (9), and it takes the values φ_a, φ_b, $\varphi_{c,1}$, or $\varphi_{c,2}$ according to which of the superconducting leads S_a, S_b, $S_{c,1}$, or $S_{c,2}$ is considered.

A magnetic field in the loop is taken into account in the following gauge:

$$\varphi_{c,1} = \varphi_c - \frac{\Phi}{2}, \tag{10}$$

$$\varphi_{c,2} = \varphi_c + \frac{\Phi}{2}, \tag{11}$$

with a phase gradient along the loop S_c terminated by S_{c_1} and S_{c_2}, which is supposed to have a large perimeter compared to the superconducting coherence length.

3. Hamiltonian of the 2D metal

Now the 2D metal Hamiltonian is presented (see the yellow region in Fig. 1):

$$\mathscr{H}_{\rm 2D\,metal} = -W \sum_{\langle i,j\rangle} \sum_{\sigma=\uparrow,\downarrow} (c^+_{i,\sigma} c_{j,\sigma} + c^+_{j,\sigma} c_{i,\sigma}), \tag{12}$$

where the summation $\sum_{\langle i,j\rangle}$ runs over pairs of neighbors on a 2D tight-binding lattice.

In the following calculations, the 2D metal is considered to be infinite in the x- and y-axis directions, which is compatible with the large sheet of graphene used in the Harvard group experiment [4], having a typical dimension $\sim 10\,\mu$m.

We simply take the continuum limit for a 2D Fermi gas with a circular Fermi surface, parametrized by the single Fermi wave vector k_F and the bandwidth W. The assumption of a circular Fermi surface can be realized approximately from the generic tight-binding Hamiltonians given by Eq. (12) at low or high filling, and it provides a useful phenomenological basis for describing a sheet of graphene gated away from the Dirac point, with a minimal number of parameters and only two essential ingredients: spin-1/2 fermions and 2D.

In spite of its simplicity, it turns out that this circular Fermi surface 2D Fermi gas Hamiltonian will be well suited for addressing how the gate voltage on the sheet of graphene in the Harvard group experiment [4] couples to the signal on the quartet line. Approaching the Dirac points with gate voltage could be interesting for future experiments, which would require taking into account the additional ingredient of the full dispersion relation of graphene, including the Dirac cones.

4. Tunneling between the superconductors and the 2D metal

Now, we present the tunnel Hamiltonian between the 2D metal and each of the superconducting leads S_N among $\{S_a, S_b, S_{c_1}, S_{c_2}\}$. This coupling Hamiltonian consists of hopping between both sides of the junction:

$$\mathscr{H}_{T,N} = -J_N \sum_{\langle i_N, j_N\rangle} \sum_{\sigma=\uparrow,\downarrow} (c^+_{j_N,\sigma} c_{i_N,\sigma} + c^+_{i_N,\sigma} c_{j_N,\sigma}), \qquad (13)$$

where the summation $\sum_{\langle i_N, j_N\rangle}$ runs over the pairs of sites on both sides of the interfaces.

The notations used throughout the paper for labeling the interfaces between the 2D metal and the four S_a, S_b, $S_{c,1}$, and $S_{c,2}$ superconducting leads are the following: We denote by a_p, b_p, $c_{1,p}$, and $c_{2,p}$ the tight-binding sites on the superconducting side of the contacts, and by α_p, β_p, $\gamma_{c_1,p}$, and $\gamma_{c_2,p}$ their counterpart on the 2D metal.

B. Voltage biasing conditions

The voltage biasing conditions are made explicit in this subsection. The four-terminal $(S_a, S_b, S_{c_1}, S_{c_2})$ device in Fig. 1 is voltage-biased on the quartet line at (V_a, V_b, V_c, V_c), with $V_a = -V_b \equiv V$ and $V_c = 0$. We implement the $V = 0^+$ adiabatic limit combined to perturbation theory in $\{J_N\}$ in Secs. V, VI, VII C, VIII, and IX; see Eq. (13) for J_N. In addition, Sec. X addresses the more general conditions of finite bias voltage V on the quartet line and arbitrary interface transparencies, within the physically motivated approximation for disorder introduced in Sec. IV D.

C. A relevant physical quantity

In this subsection, we present the definition of the critical current on the quartet line. This quantity is measured in the Harvard group experiment [4], and it is evaluated theoretically in all three papers in the series. The "critical current on the quartet line" $I_c(V, \Phi/\Phi_0)$ is called "the critical current" for short:

$$I_c(V, \Phi/\Phi_0) = \max_{\varphi_{q,3T}} I_S(\varphi_{q,3T}, V, \Phi/\Phi_0), \qquad (14)$$

where $I_c(V, \Phi/\Phi_0)$ is gauge-invariant, and the quartet phase $\varphi_{q,3T}$-sensitive $I_S(\varphi_{q,3T}, V, \Phi/\Phi_0)$ can be calculated in any gauge. This is why it is legitimate to use the specific gauge given by Eqs. (10) and (11).

IV. THE METHODS

This section introduces the methods used in this paper. The calculation of the currents is presented in Sec. IV A. Section IV B deals with their perturbative expansion in the tunnel amplitudes. Superconducting diffusion modes are next introduced in Sec. IV C. Section IV D presents the approximations on disorder that will be used in Sec. X to address arbitrary interface transparencies and finite bias voltage on the quartet line.

A. Calculation of the current

This subsection explains the method to evaluate the currents from the Keldysh Green's functions. Section IV A 1 presents the bare Green's functions in the absence of the tunnel coupling between the different leads. The Dyson equations are next presented in Sec. IV A 2. Section IV A 3 deals with how the current is expressed with the Keldysh Green's function. The transport formula is next specialized to the equilibrium and adiabatic limits in Sec. IV A 4.

1. Bare Green's functions

In this subsection, we present the Green's functions in the absence of the tunnel coupling between the different parts of the circuit, i.e., the bare Green's functions with $J_N = 0$ in Eq. (13).

The two-component Bogoliubov–de Gennes wave functions for spin-up electrons and spin-down holes yield the 2×2 matrix advanced (or retarded) Green's function describing propagation between the tight-binding sites $\mathbf{x}_1$ and $\mathbf{x}_2$ at times t_1 and t_2:

$$\hat{g}^A_{\mathbf{x}_1,\mathbf{x}_2}(t_1, t_2) = -i\theta(t_1 - t_2) \begin{pmatrix} \langle\{c_{\mathbf{x}_1,\uparrow}(t_1), c^+_{\mathbf{x}_2,\uparrow}(t_2)\}\rangle & \langle\{c_{\mathbf{x}_1,\uparrow}(t_1), c_{\mathbf{x}_2,\downarrow}(t_2)\}\rangle \\ \langle\{c^+_{\mathbf{x}_1,\downarrow}(t_1), c^+_{\mathbf{x}_2,\uparrow}(t_2)\}\rangle & \langle\{c^+_{\mathbf{x}_1,\downarrow}(t_1), c_{\mathbf{x}_2,\downarrow}(t_2)\}\rangle \end{pmatrix}, \qquad (15)$$

where $\{A, B\} = AB + BA$ is an anticommutator between the fermionic creation or annihilation operators A and B. Equation (15) is useful in connection with the Dyson equations, and it can be used to address the time-periodic dynamics underlying the emergence of a dc-current of quartets [5,6], as well as arbitrary device parameters (i.e., arbitrary interface transparencies and finite bias voltage on the quartet line).

Considering the 2D metal [see the Hamiltonian given by Eq. (12), taken at low or high filling] and Fourier transforming from the time variables t_1 and t_2 to frequency ω, Eqs. (A8) and (A9) in Appendix A imply the following limiting long-distance behavior of the Green's function for $k_F R \gg 1$:

$$g^{A,(1,1)}_{\text{2D metal}}(R,\omega) = g^{A,(2,2)}_{\text{2D metal}}(R,\omega) \tag{16}$$

$$\simeq \frac{i}{W\sqrt{k_F R}}\cos\left(k_F R - \frac{\pi}{4}\right), \tag{17}$$

$$g^{R,(1,1)}_{\text{2D metal}}(R,\omega) = g^{R,(2,2)}_{\text{2D metal}}(R,\omega) \tag{18}$$

$$\simeq -\frac{i}{W\sqrt{k_F R}}\cos\left(k_F R - \frac{\pi}{4}\right), \tag{19}$$

where the (1,1) and (2,2) labels in the superscript denote the Nambu "spin-up electron" and "spin-down hole" components, respectively. The notation $R = |\mathbf{x}_1 - \mathbf{x}_2|$ stands for the separation between $\mathbf{x}_1$ and $\mathbf{x}_2$ in real space. Equations (16)–(19) assume that the separations R_0/x_0, R_0/y_0, and R_0/z_0 between the contacts are small compared to the zero-energy ballistic-limit coherence length given by Eq. (5); see Fig. 3 for the notations R_0/x_0, R_0/y_0, and R_0/z_0. Taking the short-junction limit $\Delta R/v_F \ll 1$ amounts to substituting the electron and hole wave vectors $k = k_e$ and $k = k_h$ in Eqs. (16) and (17) and Eqs. (18) and (19), respectively, with the Fermi wave vector k_F, without accounting for their different energy-ω dependence $k_{e,h} = k_F \pm \omega/v_F$.

A sanity check of Eqs. (16)–(19) is provided in Sec. I of the Supplemental Material [29] for a double junction between a 2D normal metal and 3D normal leads. In particular, it is mentioned at the end of Sec. I in the Supplemental Material [29] that Eqs. (16)–(19) imply the magnetic proximity effect at a 2D metal–3D ferromagnet interface, namely that magnetization is induced in the 2D metal.

Considering now the superconducting leads [see the Hamiltonian given by Eqs. (8) and (9)], the ballistic nonlocal Green's function of the 3D superconductor S_N with gap Δ and phase φ_N is the following:

$$\begin{aligned}\hat{g}^A_{\mathbf{x}_1,\mathbf{x}_2}(\omega) &= \frac{1}{W}\frac{1}{k_F R}\exp\left\{\left(-\frac{|\mathbf{x}_1-\mathbf{x}_2|}{\xi_{\text{ball}}(\omega - i\eta)}\right)\right\}\\ &\times\left[\frac{\sin(k_F R)}{\sqrt{\Delta^2-(\omega-i\eta)^2}}\begin{pmatrix}-(\omega-i\eta) & \Delta e^{i\varphi_N}\\ \Delta e^{-i\varphi_N} & -(\omega-i\eta)\end{pmatrix}\right.\\ &\left.+\cos(k_F R)\begin{pmatrix}-1 & 0\\ 0 & 1\end{pmatrix}\right]\Bigg\}.\end{aligned} \tag{20}$$

The Dynes parameter $\eta \ll \Delta$ is viewed as a requirement for making the difference between the "advanced" and "retarded" Green's functions, or as a phenomenological parameter to capture the experimental linewidth broadening and relaxation in superconductors [10,30–33]. In addition, the ballistic-limit BCS coherence length appearing in Eq. (20) is given by

$$\xi_{\text{ball}}(\omega - i\eta) = \frac{\hbar v_F}{\sqrt{\Delta^2-(\omega-i\eta)^2}}, \tag{21}$$

which goes to Eq. (5) if $\omega - i\eta \to 0$.

At equilibrium, i.e., if $V = 0$, the hopping amplitude $\hat{J}_N$ between the 2D metal and the superconducting lead S_N is given by the diagonal 2×2 Nambu matrix

$$\hat{J}_N = \begin{pmatrix} J_N & 0\\ 0 & -J_N\end{pmatrix}. \tag{22}$$

2. Dyson equations at equilibrium

Now, we consider $J_N \neq 0$ in Eq. (22) and start with equilibrium conditions, i.e., all leads are grounded at $V = 0$ and the superconductors are phase-biased. All parts of the circuit then have identical chemical potential taken as the energy reference.

The fully dressed advanced and retarded Green's functions $\hat{G}^A$ and $\hat{G}^R$ describe the 2D metal connected by finite hopping amplitudes $\{\hat{J}_N\}$ to the superconducting leads. Their values are obtained from the Dyson equations, which take the following form in a compact notation:

$$\hat{G}^{A,R} = \hat{g}^{A,R} + \hat{g}^{A,R}\otimes\hat{J}\otimes\hat{G}^{A,R}, \tag{23}$$

where the symbol $\otimes$ is a convolution over time variables [such as the time variables t_1 and t_2 in Eq. (15)] which becomes a simple product after Fourier transforming to the frequency/energy ω. A summation over all possible tight-binding sites between the 2D metal and the superconducting leads is carried out according to

$$\hat{G}^{A,R}_{\alpha_r,\beta_s}(\omega) = \hat{g}^{A,R}_{\alpha_r,\beta_s}(\omega) + \sum_{\gamma_p}\hat{g}^{A,R}_{\alpha_r,\gamma_p}(\omega)\hat{J}_{\gamma_p,c_p}\hat{G}^{A,R}_{c_p,\beta_s}(\omega) \tag{24}$$

$$= \hat{g}^{A,R}_{\alpha_r,\beta_s}(\omega) + \sum_{\gamma_p,\gamma_q}\hat{g}^{A,R}_{\alpha_r,\gamma_p}(\omega)\hat{J}_{\gamma_p,c_p}\hat{g}^{A,R}_{c_p,c_q}(\omega)\hat{J}_{c_q,\gamma_q}\hat{G}^{A,R}_{\gamma_q,\beta_s}(\omega), \tag{25}$$

where a closed set of linear equations is obtained at second order for $\{\hat{G}^{A,R}_{\alpha_r,\beta_s}\}$ in Eq. (25).

3. Finite bias voltage on the quartet line

Finite bias voltage $V \neq 0$ on the quartet line implies a single Josephson frequency $2eV/\hbar$ for the considered four-terminal Josephson junction biased at opposite voltages; see Sec. IV A 3. The periodic time dynamics is encoded in the Nambu tunnel amplitudes between the 2D metal and the superconducting leads $\{S_N\}$: Eq. (22) is replaced by

$$\hat{J}_N(t) = \begin{pmatrix} J_N\exp(ieV_N t/\hbar) & 0\\ 0 & -J_N\exp(-ieV_N t/\hbar)\end{pmatrix}, \tag{26}$$

where V_N is the voltage $V_N = 0, \pm V$ at which superconducting lead S_N is biased. At finite voltage V, and after Fourier transforming from time t to frequency ω, the "advanced" and "retarded" Green's functions in Eqs. (23)–(25) become infinite matrices having labels in the extended space of the harmonics of the Josephson frequency, in addition to being matrices in Nambu.

The fully dressed Keldysh Green's function takes the form [34,35]

$$\hat{G}^{+,-} = (\hat{I} + \hat{G}^R\otimes\hat{J})\otimes\hat{g}^{+,-}\otimes(\hat{I} + \hat{J}\otimes\hat{G}^A). \tag{27}$$

The "bare" Keldysh Green's function is given by

$$\hat{g}^{+,-}(\omega) = n_F(\omega)[\hat{g}^A(\omega) - \hat{g}^R(\omega)], \tag{28}$$

where $n_F(\omega)$ is the Fermi-Dirac distribution function, which reduces to the step function $n_F(\omega) = \theta(-\omega)$ in the limit of zero temperature.

The current $I_{\alpha\to a}$ flowing from the 2D metal to the superconducting lead S_a at the $\alpha - a$ contact is given by [34,35]

$$-I_{\alpha\to a} = \frac{e}{\hbar}\sum_p \int d\omega \{ [\hat{J}_{a_p,\alpha_p}\hat{G}^{+,-}_{\alpha_p,a_p}]_{(1,1)/(0,0)}(\omega) \quad (29)$$

$$-[\hat{J}_{a_p,\alpha_p}\hat{G}^{+,-}_{\alpha_p,a_p}]_{(2,2)/(0,0)}(\omega) \quad (30)$$

$$-[\hat{J}_{\alpha_p,a_p}\hat{G}^{+,-}_{a_p,\alpha_p}]_{(1,1)/(0,0)}(\omega) \quad (31)$$

$$+[\hat{J}_{\alpha_p,a_p}\hat{G}^{+,-}_{a_p,\alpha_p}]_{(2,2)/(0,0)}(\omega)\}, \quad (32)$$

where "(1,1)" or "(2,2)" in the first pair of labels correspond to the Nambu components, as in the above equations. The notation $(n, m) = (0, 0)$ in the second pair of labels denotes the static dc-component in the extended space of the harmonics of the Josephson frequency $(neV/\hbar, meV/\hbar)$. The variable p in Eqs. (29)–(32) runs over the tight-binding sites at the interface between the 2D metal and the superconductors; see Fig. 3 for the geometry of the contacts. Equations (27)–(32) are the starting point of the demonstration of the generalized Ambegaokar-Baratoff formula at finite bias voltage V on the quartet line; see the forthcoming Sec. X B 1.

4. Specializing to equilibrium and the adiabatic limit

Now, we come back to the equilibrium limit $V = 0$. The Keldysh Green's function given by Eq. (27) simplifies as

$$G^{+,-}_{\rm eq}(\omega) = n_F(\omega)[\hat{G}^A(\omega) - \hat{G}^R(\omega)]. \quad (33)$$

Inserting Eq. (33) into Eqs. (29)–(32) for the current as a function of $\hat{G}^{+,-}$ leads to the equilibrium current though the multichannel "α, a" contact:

$$-I_{\alpha\to a,\rm eq} = \frac{e}{\hbar}\sum_p \int d\omega n_F(\omega)$$

$$\times \{ [\hat{J}_{a_p,\alpha_p}(\hat{G}^A_{\alpha_p,a_p} - \hat{G}^R_{\alpha_p,a_p})]_{(1,1)}(\omega) \quad (34)$$

$$-[\hat{J}_{a_p,\alpha_p}(\hat{G}^A_{\alpha_p,a_p} - \hat{G}^R_{\alpha_p,a_p})]_{(2,2)}(\omega) \quad (35)$$

$$-[\hat{J}_{\alpha_p,a_p}(\hat{G}^A_{a_p,\alpha_p} - \hat{G}^R_{a_p,\alpha_p})]_{(1,1)}(\omega) \quad (36)$$

$$+[\hat{J}_{\alpha_p,a_p}(\hat{G}^A_{a_p,\alpha_p} - \hat{G}^R_{a_p,\alpha_p})]_{(2,2)}(\omega)\}, \quad (37)$$

where α_p and a_p label the tight-binding sites on the 2D metal and superconducting sides, respectively. Equations (34)–(37) are the starting point of the perturbative expansion of the current in powers of J_0/W; see the forthcoming Sec. V.

The matrices $\hat{J}$ [defined by Eq. (22)] and $\hat{G}$ [defined by Eq. (23)] appearing in Eqs. (34)–(37) are 2×2 in Nambu, and the "(1,1)" or "(2,2)" Nambu component of their product is evaluated according to the labels in the subscript.

The equilibrium current $I_{\alpha\to a,\rm eq}$ given by Eqs. (34)–(37) depends on all superconducting phase variables φ_a, φ_b, φ_{c_1}, and φ_{c_2}. Gauge invariance implies that

$$I_{\alpha\to a,\rm eq} = I_{\alpha\to a}(\varphi_a + \alpha, \varphi_b + \alpha, \varphi_{c_1} + \alpha, \varphi_{c_2} + \alpha) \quad (38)$$

is independent of α because a global superconducting phase is not measurable.

At finite bias voltage V on the quartet line, the phase variables are given by $\varphi_a = \varphi_a^{(0)} + \psi$, $\varphi_b = \varphi_a^{(0)} - \psi$, $\varphi_{c_1} = \varphi_{c_1}^{(0)}$, and $\varphi_{c_2} = \varphi_{c_2}^{(0)}$, where $\psi = 2eVt$ is linear in the time variable t. Assuming in addition adiabatic voltage biasing at $V = 0^+$ leads to slow time dependence of the variable ψ. Then, the adiabatic-limit current is obtained by averaging Eq. (38) over ψ:

$$I_{\alpha\to a,\rm adiab} = \int \frac{d\psi}{2\pi}$$

$$I_{\alpha\to a}(\varphi_a^{(0)} + \psi + \alpha, \varphi_b^{(0)} - \psi + \alpha, \varphi_{c_1}^{(0)} + \alpha, \varphi_{c_2}^{(0)} + \alpha). \quad (39)$$

Energy conservation puts the constraint that, on the quartet line, $I_{\alpha\to a,\rm adiab}$ in Eq. (39) depends only on the gauge-invariant quartet phase variable $\varphi_{q,3T} = \varphi_a^{(0)} + \varphi_b^{(0)} - 2\varphi_c^{(0)} \equiv \varphi_a + \varphi_b - 2\varphi_c$. Gauge invariance implies that the current $I_{\alpha\to a,\rm adiab}$ is independent of α, similarly to the previous Eq. (38) corresponding to equilibrium with $V = 0$.

B. Perturbative expansion of the adiabatic current

This subsection presents how the Dyson Eq. (23) is used in the forthcoming Sec. V to produce a systematic expansion of the current in powers of the tunnel amplitudes $\{J_N\}$ between the 2D metal and the superconductors $\{S_N\}$. Iterating Eq. (23) produces the series

$$G = g \quad (40)$$

$$+ g\otimes J\otimes g \quad (41)$$

$$+ g\otimes J\otimes g\otimes J\otimes g \quad (42)$$

$$+ g\otimes J\otimes g\otimes J\otimes g\otimes J\otimes g \quad (43)$$

$$+ g\otimes J\otimes g\otimes J\otimes g\otimes J\otimes g\otimes J\otimes g \quad (44)$$

$$+ g\otimes J\otimes g\otimes J\otimes g\otimes J\otimes g\otimes J\otimes g\otimes J\otimes g \quad (45)$$

$$+ g\otimes J\otimes g\otimes J\otimes g\otimes J\otimes g\otimes J\otimes g\otimes J\otimes g\otimes J\otimes g \quad (46)$$

$$+ \cdots, \quad (47)$$

which is inserted into Eqs. (34)–(37) for the equilibrium current.

At each order $J_a^{2m_a}J_b^{2m_b}J_{c_1}^{2m_{c_1}}J_{c_2}^{2m_{c_2}}$ in the tunnel amplitudes $\{J_N\}$, the expansion given by Eqs. (40)–(47) produces a finite number of "closed loop diagrams" contributing to the dc-current, where m_a, m_b, m_{c_1}, and m_{c_2} are four positive integers.

As seen from Eqs. (34)–(37) and from Eqs. (40)–(47), this diagrammatic expansion has a simple structure, due to the fact that all terms in the Hamiltonian are quadratic; see Eqs. (8), (9), (12), and (13). The diagrams consist of alternations between the following:

(i) The tunnel amplitudes in and out of the 2D metal; see Eq. (22).

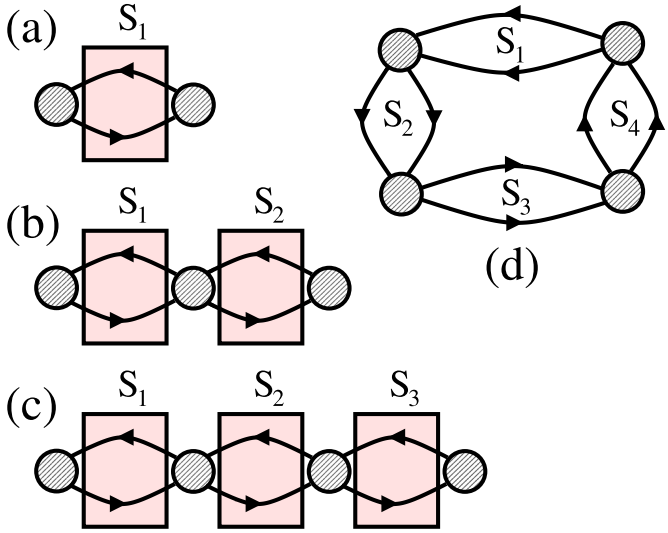

FIG. 4. Structure of the diagrammatic series: The "superconducting diffusion modes" are made of pairs of nonlocal Green's functions in the superconducting leads denoted by S_1,...,S_4 in the figure, which are among $\{S_a,\ S_b,\ S_{c,1},\ S_{c,2}\}$. The nonlocal superconducting modes connect the "nodes" corresponding to the dashed circled area. The nodes contain dressing by higher-order tunneling processes taking place locally between the 2D metal and the superconductors, and nonlocal transmission through the 2D metal. Panels (a), (b), and (c) show the "diffuson-like diagrams" with superconducting diffusion modes formed of Green's functions oriented in opposite directions. Panel (c) shows a "weak-localization-like diagram" with the same orientation for the pairs of the nonlocal superconducting Green's function.

(ii) Propagation through the 2D metal [see Eqs. (16)–(19)] or through one of the superconducting leads [see Eq. (20)].

Some of the relevant diagrams are shown schematically in the forthcoming Figs. 4, 5, 6, 7, and 8.

The equilibrium current is obtained as a series of diagrams that are labeled by the four positive integers $(m_a, m_b, m_{c_1}, m_{c_2})$ mentioned above. Assuming identical tunnel amplitudes $J_0 \equiv J_a = J_b = J_{c_1} = J_{c_2}$ for all contacts produces the prefactor $(J_0)^m$, with $m = m_a + m_b + m_{c_1} + m_{c_2}$. For instance, the three-terminal $3TQ_1$, $3TQ_2$ appear at the order $m = 8$; see the forthcoming Sec. V A. The four-terminal 4FTSQ and 4TSQ appear at the orders $m = 8$ and $m = 12$, respectively; see the forthcoming Secs. V B and V C.

Each Green's function propagating through any superconducting lead S_N is within the electron-electron, hole-hole, electron-hole, or hole-electron Nambu channel. Each electron-hole or hole-electron conversion produces $\exp(\pm i\varphi_N)$, where φ_N is the macroscopic phase variable of the superconductor S_N (which is among $\{S_a, S_b, S_{c_1}, S_{c_2}\}$). To each diagram is thus associated the overall factor

$$\exp\left[i\left(n_a\varphi_a + n_b\varphi_b + n_{c_1}\varphi_{c_1} + n_{c_2}\varphi_{c_2}\right)\right], \tag{48}$$

where $(n_a, n_b, n_{c_1}, n_{c_2})$ are four (positive or negative) integers counting the number and the sign of the electron-hole or hole-electron conversions in the leads $\{S_a, S_b, S_{c_1}, S_{c_2}\}$, respectively, within a given quantum process.

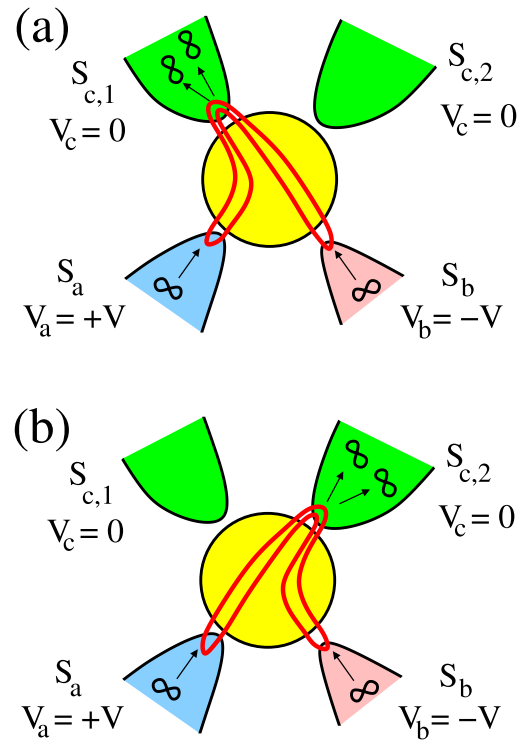

FIG. 5. The lowest-order three-terminal $3TQ_1$, $3TQ_2$ diagrams in a real-space representation [in panels (a) and (b), respectively]: Two pairs are taken from (S_a, S_b) biased at $(V, -V)$. After making a quartet from taking the square of the wave function of a pair, the two outgoing Cooper pairs are transmitted into the grounded S_{c_1} for the $3TQ_1$ [panel (a)] or into S_{c_2} for the $3TQ_2$ [panel (b)]. The $3TQ_1$ and $3TQ_2$ current-phase relations are given by Eqs. (66) and (67), respectively.

Voltage biasing at $V_a = -V_b \equiv V$ on the quartet line (see Sec. III B) implies a constraint on $(n_a, n_b, n_{c,1}, n_{c,2})$ coming from conservation of energy between the following:

(i) The energy $n_a eV_a$ of the n_a pairs taken from S_a, and the energy $n_b eV_b$ of the n_b pairs taken from S_b.

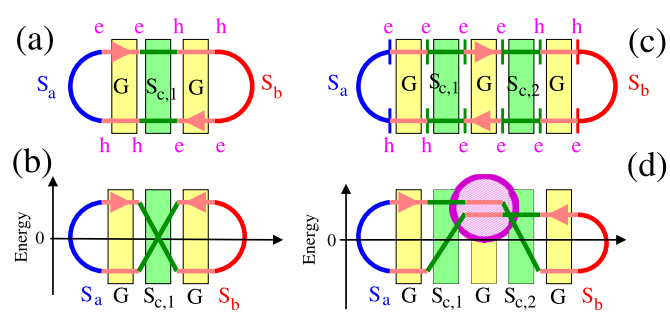

FIG. 6. Diffuson and energy pictures for the three-terminal $3TQ_1$ and for one of the contributions to the four-terminal 4TSQ: Panels (a) and (b) represent the three-terminal $3TQ_1$ in the diffuson and in the energy pictures, respectively. Panels (c) and (d) show similar representations for the four-terminal 4TSQ. The sequence of spin-up electron (e) and spin-down hole (h) Nambu labels is indicated in panels (a) and (c). The highlighted section of the four-terminal 4TSQ diagram in panel (d) shows long-range propagation over the mesoscopic phase coherence length l_φ in between S_{c_1} and S_{c_2}. The process on panels (c) and (d) is proportional to $x_0\, y_0^2$; see Eq. (84).

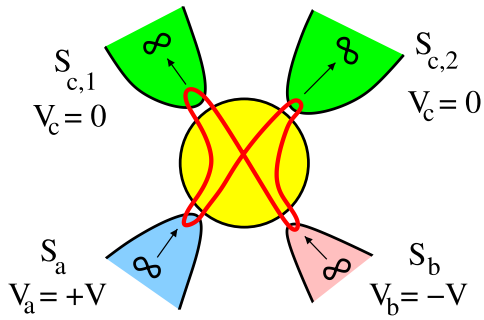

FIG. 7. The diagram encoding the *four-terminal statistical fluctuations of the split quartets* (4TFSQ) transmits one Cooper pair into S_{c_1} and another one into S_{c_2}. The four-terminal 4TFSQ diagrams encode a statistical fluctuation of the $\varphi_{q,3T}$-sensitive current, which does not scale with the number of channels. (This is because the Green's functions cannot be gathered in a pairwise manner in this diagram). The four-terminal 4TFSQ current-phase relation is given by Eq. (71).

(ii) The energy $(n_{c_1} + n_{c_2})eV_c = 0$ of the $n_{c_1} + n_{c_2}$ pairs transmitted into S_{c_1} and S_{c_2}, which are both grounded at $V_c = 0$.

Energy conservation on the quartet line implies $n_a eV_a + n_b eV_b = 0$ and thus $n_a = n_b$.

In addition, gauge invariance puts the constraint $n_a + n_b + n_{c,1} + n_{c,2} = 0$, which is compatible with Eqs. (38) and (39) being independent of α.

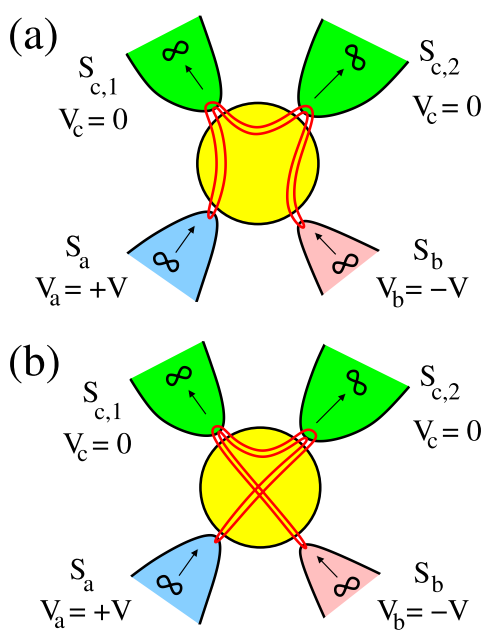

FIG. 8. Two of the four-terminal split quartet diagrams (4TSQs): Contrary to the previous four-terminal 4TFSQ diagram (see Fig. 7), these four-terminal 4TSQ diagrams yield a critical current that is not a small statistical fluctuation. On the contrary, the four-terminal 4TSQ current scales with the number of channels because the Green's functions are gathered in a pairwise manner on this figure. The process on panels (a) and (b) are proportional to $x_0 y_0^2$ and $x_0 z_0^2$ respectively; see Eq. (84).

C. The superconducting diffusion modes

Now, we discuss the importance of disorder in the superconductors that are supposed to be in the dirty limit, i.e., the elastic mean free path l_e is much shorter than the ballistic-limit coherence length $\xi_{\rm ball}(0)$ given by Eq. (5). This realistic assumption puts severe constraints on the diagrammatic perturbation theory: The nonlocal Green's functions are gathered in a pairwise manner in a real-space representation, even those crossing the ballistic 2D metal. In addition, small disorder in the 2D metal in the form of nonmagnetic impurities helps gather the Green's function in a pairwise manner. It is likely that the 4TSQs are robust against introducing a small concentration of nonmagnetic impurities in the 2D metal, assuming a localization length that is larger than the separation between the contacts. Clarifying this issue in future work requires understanding the fate of the quantum wake in the presence of disorder; see Sec. VII for the quantum wake in the absence of disorder.

Considering a superconductor in the dirty limit, the disorder-averaged single-particle Nambu Green's function oscillates with the Fermi wave vector k_F [see Eq. (20)], and its envelope decays exponentially over the elastic mean free path [36]. This puts a constraint of locality on the "unpaired" single-particle Green's function at each superconducting lead S_N.

Second, the superconducting diffusion modes are defined as pairs of single-particle Green's functions that scatter together on the same realization of the disorder. The range of the superconducting diffusion modes reaches the dirty-limit coherence length at subgap energies, which is much larger than the elastic mean free path for a superconductor such as aluminum in the dirty limit.

The calculation of the superconducting diffusion modes in the dirty limit generalizes Ref. [37]; see Appendix B. The superconducting diffusion modes have four Nambu labels $(\tau_1, \tau_2, \tau_3, \tau_4)$ attached to them; see Appendix B. The resulting $2^4 = 16$ terms are provided by Eqs. (B48)–(B54). They take the following form in the ladder approximation:

$$\int \frac{d\mathbf{k}}{(2\pi)^3} \overline{g_{\tau_1,\tau_2}(\mathbf{k},\omega) g_{\tau_3,\tau_4}(\mathbf{k}+\mathbf{q},\omega)} = \frac{1}{16\pi W} \frac{1}{2\sqrt{|\Delta|^2 - (\omega - i\eta)^2 + \mathscr{D} q^2}} \times F^{(\tau_3,\tau_4)}_{(\tau_1,\tau_2)}\left(\frac{\omega - i\eta}{|\Delta|}, \varphi_N\right), \tag{49}$$

where $\mathbf{k}$ and $\mathbf{q}$ are the wave vectors, $\mathscr{D} = v_F^2 \tau/3$ is the diffusion constant with τ the elastic scattering time, and φ_N is the superconducting phase variable of the superconducting lead S_N. The function $F^{(\tau_3,\tau_4)}_{(\tau_1,\tau_2)}$ appearing in Eq. (49) is deduced from Eqs. (B48)–(B54) in Appendix B, for instance

$$F^{(1,2)}_{(1,2)}\left(\frac{\omega - i\eta}{|\Delta|}, \varphi_N\right) = \frac{|\Delta|^2}{|\Delta|^2 - (\omega - i\eta)^2} \exp(2i\varphi_N), \tag{50}$$

$$F^{(1,2)}_{(1,1)}\left(\frac{\omega - i\eta}{|\Delta|}, \varphi_N\right) = \frac{(\omega - i\eta)|\Delta|}{|\Delta|^2 - (\omega - i\eta)^2} \exp(i\varphi_N). \tag{51}$$

The $\overline{g_{(1,2)} g_{(1,2)}}$ superconducting diffusion mode in Eq. (50) is relevant to the three-terminal $3TQ_1$, $3TQ_2$. Conversely, $\overline{g_{(1,1)} g_{(1,2)}}$ given by Eq. (51) is relevant

to the four-terminal 4TSQ, as well as to the normal metal–superconductor–superconductor double interface considered in Ref. [38]. Equations (50) and (51) are deduced from the corresponding Eqs. (B50) and (B53) in Appendix B.

Fourier transforming Eq. (49) from the wave vector $\mathbf{q}$ to the real-space coordinate R leads to

$$\overline{g_{\tau_1,\tau_2}g_{\tau_3,\tau_4}}(R,\omega) = \frac{c}{W^2}\left(\frac{\xi_{\rm dirty}(\omega-i\eta)}{l_e}\right) \times F^{(\tau_3,\tau_4)}_{(\tau_1,\tau_2)}\left(\frac{\omega-i\eta}{|\Delta|},\varphi_N\right)\exp\left(-\frac{R}{\xi_{\rm dirty}(\omega-i\eta)}\right), \quad (52)$$

where c is a constant of order unity, and

$$\xi_{\rm dirty}(\omega) \sim \sqrt{l_e\xi_{\rm ball}(\omega)} \quad (53)$$

denotes the superconducting coherence length in the dirty limit.

Next, we integrate Eq. (52) over the separation $R = |\mathbf{x}_1 - \mathbf{x}_2|$ between the tight-binding sites $\mathbf{x}_1$ and $\mathbf{x}_2$ at the interface. We distinguish between the following two situations:

(i) If $r_0 \gtrsim \xi_{\rm dirty}(0)$, then

$$\langle\langle g_{\tau_1,\tau_2}g_{\tau_3,\tau_4}\rangle\rangle \simeq \frac{c'}{2W^2}\frac{\xi_{\rm dirty}(\omega-i\eta)}{l_e}F^{(\tau_3,\tau_4)}_{(\tau_1,\tau_2)}\left(\frac{\omega-i\eta}{|\Delta|},\varphi_N\right), \quad (54)$$

where the contact radius r_0 is shown in Fig. 3(c), $\xi_{\rm dirty}(\omega)$ is given by Eq. (53), c' is a constant of order unity, and $\langle\langle\cdots\rangle\rangle$ stands for summation of $\overline{g_{\tau_1,\tau_2}g_{\tau_3,\tau_4}}$ over the separation R in Eq. (52).

(ii) Conversely, the assumption $r_0 \lesssim \xi_{\rm dirty}(0)$ leads to

$$\langle\langle g_{\tau_1,\tau_2}g_{\tau_3,\tau_4}\rangle\rangle \simeq \frac{d'}{2W^2}\frac{r_0}{l_e}F^{(\tau_3,\tau_4)}_{(\tau_1,\tau_2)}\left(\frac{\omega-i\eta}{|\Delta|},\varphi_N\right), \quad (55)$$

where d' is another constant of order unity.

The scaling in Eqs. (54) and (55) is linear in the dirty-limit coherence length or in the radius r_0 of the contact. This is consistent with the observation that the intersection between the 2D Brownian surfaces (resulting from scattering on disorder in the superconducting lead S_N) and the 2D interfaces generically forms a 1D object.

D. Approximation on disorder for finite bias voltage and arbitrary interface transparencies

Now, we present a technical introduction to the calculations of the forthcoming Sec. X about the interplay between disorder in the superconducting leads, arbitrary interface transparencies, and finite bias voltage V on the quartet line. We start with what we coin "model I" consisting of the four-terminal device in Figs. 1 and 3 with superconductors in the dirty limit connected to the 2D metal by clean interfaces; see the tunnel Hamiltonian given by Eq. (13).

Within this model I, we consider expansion of the current as the closed-loop diagrams mentioned above in Sec. IV B. After forming the superconducting diffusion modes of Sec. IV C, these diagrams consist of the elements shown in Fig. 4:

(i) The "superconducting diffusion modes" are pairs of nonlocal superconducting Green's functions propagating together in the superconductors over the dirty-limit coherence length given by Eq. (53).

(ii) The superconducting diffusion modes of item (i) bridge between the "nodes" shown by the dashed circles in Fig. 4. The nodes contain dressing by processes taking place locally between the 2D metal and the superconductors or nonlocal transmission through the 2D metal.

We consider now "model II" as the approximation to "model I"; see the following Hamiltonian for tunneling between the 2D metal and the superconductors within model II:

$$\mathscr{H}_{T,N,\rm eff} = -\sum_{\langle i,j\rangle}\sum_{\sigma=\uparrow,\downarrow}(J_{i\to j}c^+_{j,\sigma}c_{i,\sigma} + J_{j\to i}c^+_{i,\sigma}c_{j,\sigma}), \quad (56)$$

where the summation $\sum_{\langle i,j\rangle}$ runs over the pairs of sites on both sides of the contacts. The amplitude for hopping from i (in the 2D metal layer) to j (the corresponding site in the superconducting lead) is a complex number with a random phase:

$$J_{i\to j} = J_0\exp(i\psi_{i\to j}), \quad (57)$$

$$J_{j\to i} = J_0\exp(i\psi_{j\to i}), \quad (58)$$

where $\psi_{i\to j} = -\psi_{j\to i}$, and $\psi_{i\to j}$ is uniformly distributed in between 0 and 2π. The variables $\psi_{i\to j}$ and $\psi_{k\to l}$ are uncorrelated if $i,j \neq k,l$. Equations (57) and (58) automatically imply $\langle\langle(J_{i\to j})^2\rangle\rangle = 0$, which produces a vanishingly small value for the weak-localization-like diagrams [39] that intersect the interface with only two Green's functions. These weak-localization-like diagrams would not be washed out if disorder were introduced in the amplitudes $|J_{i\to j}| = |J_{j\to i}|$ instead of the random phases $\psi_{i\to j} = -\psi_{j\to i}$ in Eqs. (57) and (58).

However, the weak-localization-like diagrams that intersect the interfaces with four Green's functions at the same tight-binding site are not washed out by the random $\psi_{i\to j}$ in Eqs. (57) and (58). This is because $\langle\langle|J_{i\to j}|^4\rangle\rangle \neq 0$ can be written as $\langle\langle(J_{i\to j})^2(\overline{J_{i\to j}})^2\rangle\rangle$, where the terms $(J_{i\to j})^2$ and $(\overline{J_{i\to j}})^2$ match both ends of a weak-localization-like loop.

Now, we provide two additional remarks:

(i) Equations (B48)–(B54) and (C1)–(C7) in the dirty and ballistic limits, respectively, have the same dependence on energy-ω, apart from different prefactors; see Appendixes B and C, respectively.

(ii) The opposite signs of the $\langle\langle g_{(1,1)}g_{(1,2)}\rangle\rangle$ modes in the dirty and ballistic limits (see Sec. C 2 of Appendix C) are not relevant to the four-terminal 4TSQ, because the $\langle\langle g_{(1,1)}g_{(1,2)}\rangle\rangle$ modes come in pairs within each 4TSQ diagram. Their product has thus necessarily a positive sign.

Based on these remarks on the structure of perturbation theory in the presence of superconductors in the dirty limit, we propose now "model III," which is practically implemented in the forthcoming calculations of Sec. X and includes the same weak-localization-like diagrams as model I, such as those in Fig. 4. Model III makes use of the nondisordered interfaces of model I combined to the ballistic limit Green's functions of model II.

Specifically, in model III, the interfaces are described by Eq. (13), and now the $\{k_F R_{k,l}\}$ oscillations at the scale of the Fermi wave vector are averaged out in the expression of the critical currents, where $R_{k,l}$ denotes the separation between pairs of tight-binding sites at the four interfaces within each part of the circuit; see Eqs. (16)–(19) and (20).

These arguments show that replacing model I by model III can be considered as being legitimate as a physically motivated approximation to simulate disorder in the superconductors, i.e., to gather the superconducting Green's functions in a pairwise manner. Model III is used in the forthcoming Sec. X in the absence of other known method to address the interplay between disorder averaging, arbitrary interface transparencies, and finite bias voltage on the quartet line, taking also the 2D metal into account. Now, we proceed with presenting our results.

V. CURRENT-PHASE RELATIONS OF THE THREE-TERMINAL 3TQ AND THE FOUR-TERMINAL 4TSQ

In this section, we present a simple model for the microscopic processes contributing to the $\varphi_{q,3T}$-sensitive current on the quartet line. The gauge is given by Eqs. (10) and (11), and we calculate the currents in perturbation in the tunnel amplitudes and in the adiabatic limit. Section V A deals with the three-terminal quartets ($3TQ_1$) at the order $(J_0/W)^8$; see Fig. 2(d). Similarly, the $3TQ_2$ at the order $(J_0/W)^8$ are shown in Fig. 2(e). Section V B describes the "four-terminal statistical fluctuations of the split quartets" (4TFSQs) at the order $(J_0/W)^8$; see Fig. 2(f). Section V C presents the four-terminal split quartets (4TSQs) at the order $(J_0/W)^{12}$; see Fig. 2(f).

We microscopically calculate the current-phase relations:

(i) Equations (66) and (67) for the three-terminal $3TQ_1$ and the $3TQ_2$.

(ii) Equation (71) for the four-terminal 4TFSQs.

(iii) Equations (83) and (84) for the four-terminal 4TSQs with multichannel contacts.

These perturbative expansions nontrivially show that the three-terminal $3TQ_1$, $3TQ_2$ current-phase relations are π-shifted and the four-terminal 4TSQs are 0-shifted if the contact geometry is such that $r_0 \gg l_e$, where r_0 is shown in Fig. 3(c).

A. Three-terminal quartets ($3TQ_1$ and $3TQ_2$)

1. *Microscopic calculation of the three-terminal* $3TQ_1$, $3TQ_2$ *critical currents*

Now, we consider the three-terminal $3TQ_1$, $3TQ_2$ of Refs. [5,6] (see also Fig. 5), and we evaluate them at the order $(J_0/W)^8$ in perturbation in the tunnel amplitudes for the 2D metal, which is relevant to the Harvard group experiment [4]. The three-terminal $3TQ_1$, $3TQ_2$ transmit four fermions into the same superconducting lead, i.e., into $S_{c,1}$ for the $3TQ_1$ [see Fig. 5(a)] or into $S_{c,2}$ for the $3TQ_2$ [see Fig. 5(b)].

The first term $[\hat{J}_{a,\alpha}\hat{G}^A_{\alpha,a}]_{(1,1)}$ in the equilibrium current given by Eq. (34) takes the following form, at the lowest order $m = 8$ in an expansion in $(J_0/W)^m$ and in the adiabatic limit:

$$J_0\langle\langle G^{A,(-1,-1,2,0)}_{[8],S_{c,1},(\alpha,a),(1,1)}\rangle\rangle = J_0^8\langle\langle g^{A,(1,1)}_{\alpha,\gamma_{c_1}} g^{A,(1,2)}_{c_1,c_1} g^{A,(2,2)}_{\gamma_{c_1},\beta} g^{A,(2,1)}_{b,b} g^{A,(1,1)}_{\beta,\gamma_{c_1}} g^{A,(1,2)}_{c_1,c_1} g^{A,(2,2)}_{\gamma_{c_1},\alpha} g^{A,(2,1)}_{a,a}\rangle\rangle \tag{59}$$

$$= J_0^8\langle\langle g^{A,(2,1)}_{a,a}\rangle\rangle\langle\langle g^{A,(2,1)}_{b,b}\rangle\rangle\langle\langle (g^{A,(1,2)}_{c_1,c_1})^2\rangle\rangle\langle\langle g^{A,(1,1)}_{\alpha,\gamma_{c_1}} g^{A,(2,2)}_{\gamma_{c_1},\alpha}\rangle\rangle\langle\langle g^{A,(1,1)}_{\beta,\gamma_{c_1}} g^{A,(2,2)}_{\gamma_{c_1},\beta}\rangle\rangle \tag{60}$$

$$= \frac{c_{1/2}}{8}\left(\frac{J_0}{W}\right)^8 \frac{R_{c_1}}{l_e}\frac{1}{k_F R_{\alpha,\gamma_{c,1}}}\frac{1}{k_F R_{\beta,\gamma_{c,1}}}\frac{\Delta^4}{[\Delta^2-(\omega-i\eta)^2]^2}\exp\left[i\left(-\varphi_a-\varphi_b+2\varphi_{c_1}\right)\right], \tag{61}$$

where $(-1,-1,2,0)$ in the left-hand side superscript refers to the signs in the right-hand side $\exp[i(-\varphi_a-\varphi_b+2\varphi_{c_1})]$ combination. The notation (1,1) in the subscript is the same as in the preceding Sec. IV, i.e., it stands for the "electron-electron" Nambu component.

In agreement with the diagrams in Figs. 6(a) and 6(b), the $(1,1,-2,0)$ combination yielding $\exp[i(\varphi_a+\varphi_b-2\varphi_{c_1})]$ is vanishingly small at the order $(J_0/W)^8$ if the (1,1) electron-electron component is evaluated. Conversely, the (2,2) hole-hole component of the $(-1,-1,2,0)$ $\exp[i(-\varphi_a-\varphi_b+2\varphi_{c_1})]$ combination is vanishingly small at the order $(J_0/W)^8$.

The positive sign of Eq. (61) originates from the product of the two $\langle\langle g^{A,(1,1)}_{\alpha,\gamma_{c_1}} g^{A,(2,2)}_{\gamma_{c_1},\alpha}\rangle\rangle$ and $\langle\langle g^{A,(1,1)}_{\beta,\gamma_{c_1}} g^{A,(2,2)}_{\gamma_{c_1},\beta}\rangle\rangle$ transmission modes through the 2D metal, which both take negative values because they originate from taking the square of the pure imaginary complex number; see Eqs. (16) and (17).

The 1/8 coefficient in Eq. (61) originates from the following terms:

(i) Each of the 2D metal transmission modes $\langle\langle g^{A,(1,1)}_{\alpha,\gamma_{c_1}} g^{A,(2,2)}_{\gamma_{c_1},\alpha}\rangle\rangle$ and $\langle\langle g^{A,(1,1)}_{\beta,\gamma_{c_1}} g^{A,(2,2)}_{\gamma_{c_1},\beta}\rangle\rangle$ yields a $\langle\langle\cos^2(k_F R)\rangle\rangle = 1/2$ factor; see Eqs. (16) and (17).

(ii) A 1/2 coefficient is related by convention to the superconducting diffusion mode $\langle\langle (g^{A,(1,2)}_{c_1,c_1})^2\rangle\rangle$, which is taken to be dominated by nonlocal propagation over the dirty-limit coherence length on the $S_{c,1}$ side of the 2D metal-$S_{c,1}$ interface; see Eqs. (54) and (55).

Integrating the spectral current given by Eq. (61) over energy ω produces a positive sign because the residue at $\omega = -\Delta$ is positive; see Eqs. (D1)–(D3) in Appendix D 1. In the limit of zero temperature, the above Eqs. (59)–(61) and Eqs. (D1)–(D3) in Appendix D 1 lead to

$$\int_{-\infty}^{0} J_0\langle\langle G^{A,(-1,-1,2,0)}_{[8],S_{c,1},(\alpha,a),(1,1)}\rangle\rangle(\omega)d\omega = \frac{i\pi c'_{1/2}\Delta}{32}\left(\frac{J_0}{W}\right)^8\frac{\sqrt{\mathscr{S}_{\text{contact}}}}{l_e}\frac{y_0 z_0}{(k_F R_0)^2} \times \exp\left[i\left(-\varphi_a-\varphi_b+2\varphi_{c_1}\right)\right]. \tag{62}$$

Evaluating similarly all terms in Eqs. (34)–(37) leads to

$$I_{\alpha\to a,\mathrm{eq}} = I_{c,\,3\mathrm{TQ}_1}\sin\varphi_{q,\,3T,\,1}, \tag{63}$$

where

$$\varphi_{q,\,3T,\,1} = \varphi_a + \varphi_b - 2\varphi_{c_1}. \tag{64}$$

The SQ_1 critical current $I_{c,\,3\mathrm{TQ}_1}$ is negative, i.e., it is π-shifted:

$$I_{c,\,3\mathrm{TQ}_1} = -\frac{ec'_{1/2}\pi\Delta}{4\hbar}\left(\frac{J_0}{W}\right)^8\frac{\sqrt{\mathscr{S}_{\mathrm{contact}}}}{l_e}\frac{y_0 z_0}{(k_F R_0)^2}. \tag{65}$$

Finally, we define the remaining variables appearing in Eqs. (61)–(65).

The coefficients $c_{1/2}$ and $c'_{1/2}$ are positive and of order unity.

The dimensionless parameters y_0 and z_0 in Eqs. (62)–(65) depend on the shape of the four-terminal device, still within the short junction limit assumption; see Sec. III A 1 for a discussion of the short-junction limit and Fig. 3 for the definition of y_0 and z_0.

The $1/k_F R_{\alpha,\gamma_{c,1}}$ and $1/k_F R_{\beta,\gamma_{c,1}}$ terms in Eq. (61) originate from ballistic propagation through the 2D metal; see Eqs. (16)–(19).

In connection with Sec. IV C, we assumed small area $\mathscr{S}_{\mathrm{contact}} = \pi R_{c,1}^2$ for the circular contact between the 2D metal and the superconducting lead $S_{c,1}$, such that $R_{c,1} \lesssim \xi_{\mathrm{dirty}}(0)$, where the dirty-limit coherence length is given by Eq. (53) and the geometry is shown schematically in Fig. 3(c). The assumption $R_{c,1} \lesssim \xi_{\mathrm{dirty}}(0)$ yields the $R_{c,1}/l_e \sim \sqrt{\mathscr{S}_{\mathrm{contact}}}/l_e$ scaling in Eqs. (61), (62), and (65); see also the discussion in the preceding Sec. IV C.

2. Discussion

The following current-phase-flux relations are deduced from Eq. (63) in the gauge given by Eqs. (10) and (11):

$$I_{3\mathrm{TQ}_1}(\varphi_{q,\,3T},\Phi) = I_{c,\,3\mathrm{TQ}_1}\sin[\varphi_{q,\,3T}+\Phi], \tag{66}$$

$$I_{3\mathrm{TQ}_2}(\varphi_{q,\,3T},\Phi) = I_{c,\,3\mathrm{TQ}_2}\sin[\varphi_{q,\,3T}-\Phi], \tag{67}$$

where Eqs. (66) and (67) correspond to the three-terminal $3\mathrm{TQ}_1$, $3\mathrm{TQ}_2$, respectively. The phase variable entering Eq. (66) is $\varphi_{q,\,3T,\,1} \equiv \varphi_a + \varphi_b - 2\varphi_{c_1} \equiv \varphi_{q,\,3T} + \Phi$ and that entering Eq. (67) is $\varphi_{q,\,3T,\,2} \equiv \varphi_a + \varphi_b - 2\varphi_{c_2} \equiv \varphi_{q,\,3T} - \Phi$, where φ_{c_1} and φ_{c_2} are given by Eqs. (10) and (11), and $\varphi_{q,\,3T}$ is given by Eq. (6).

Figures 6(a) and 6(b) show two representations of the three-terminal $3\mathrm{TQ}_1$:

(i) Figure 6(a) shows a representation resembling the "diffusons" in the theory of disordered conductors.

(ii) Figure 6(b) shows energy on the y-axis, with respect to the chemical potential of the grounded S_c; see also Refs. [5,6].

In addition, an intuitive argument for the π-shift in the three-terminal $3\mathrm{TQ}_1$, $3\mathrm{TQ}_2$ current-phase relations Eqs. (63)–(67) is the following [7]:

The two Cooper pairs of the quartets imply taking the square of the single-pair wave function

$$\frac{1}{\sqrt{2}}(c^+_{a,\uparrow}c^+_{b,\downarrow} - c^+_{a,\downarrow}c^+_{b,\uparrow}) \tag{68}$$

according to

$$\tfrac{1}{2}(c^+_{a,\uparrow}c^+_{b,\downarrow} - c^+_{a,\downarrow}c^+_{b,\uparrow})^2. \tag{69}$$

Equation (69) takes the form of the opposite of a pair of pair:

$$(69) = -(c^+_{a,\uparrow}c^+_{a,\downarrow})(c^+_{b,\uparrow}c^+_{b,\downarrow}). \tag{70}$$

The minus sign appearing on the right-hand side of Eq. (70) is consistent with the π-shifted critical current in Eq. (65), which receives interpretation of macroscopic manifestation for the internal structure of a Cooper pair, i.e., the orbital and spin symmetries.

B. The four-terminal statistical fluctuations of the split quartet current

Before discussing in the next Sec. V C the four-terminal 4TSQ at the order $(J_0/W)^{12}$, we mention now a simpler "baby-4TSQ" at the order $(J_0/W)^8$; see Fig. 7. The critical current of this order-$(J_0/W)^8$ process is small, and it fluctuates around zero value. The reason is that the four one-particle Green's functions crossing the 2D metal in Fig. 7 cannot be gathered in a pairwise manner if the four contacts with the superconducting leads S_a, S_b, $S_{c,1}$, and $S_{c,2}$ make between them a distance that is much larger than the Fermi wavelength λ_F. The current associated with the four-terminal 4TFSQ of order $(J_0/W)^8$ in Fig. 7 is given by

$$I_{4\mathrm{TFSQ}}(\varphi_{q,\,4T}) = I_{c,\,4\mathrm{TFSQ}}\sin\varphi_{q,\,4T}, \tag{71}$$

where

$$\varphi_{q,\,4T} = \varphi_a + \varphi_b - \varphi_{c,1} - \varphi_{c,2}. \tag{72}$$

Equations (10) and (11) imply $\varphi_{q,\,4T} = \varphi_{q,\,3T}$, where $\varphi_{q,\,3T}$ is given by Eq. (6). Overall, multichannel averaging produces a vanishingly small critical current for the four-terminal 4TFSQ: $\langle\langle I_{c,\,4\mathrm{TFSQ}}\rangle\rangle = 0$.

C. Four-terminal split quartets

Now, we consider the four-terminal 4TSQ yielding a nonvanishingly small value for critical current with multichannel interfaces. Two types of diagrams appear at the order $(J_0/W)^{12}$, after a first selection has been operated with respect to gathering the nonlocal Green's functions through the 2D metal in a pairwise manner:

(i) *The diagrams containing products of three Nambu Green's functions within the same superconducting lead:* Their critical current is of order $\sqrt{\mathscr{S}_{\mathrm{contact}}}/l_e$; see the forthcoming Sec. V C 1 and Sec. II A in the Supplemental Material [29].

(ii) *The remaining diagrams* provide the leading-order $\mathscr{S}_{\mathrm{contact}}/l_e^2$ contribution to the critical current; see the forthcoming Sec. V C 2 and Sec. II B in the Supplemental Material [29].

1. The four-terminal 4TSQ current at the orders $(J_0/W)^{12}$ and $\sqrt{\mathscr{S}_{contact}}/l_e$

We provide now the microscopic calculation for the contributions to $J_{a,\alpha}G^A_{\alpha,a}$ at the orders $(J_0/W)^{12}$ and $\sqrt{\mathscr{S}_{\mathrm{contact}}}/l_e$.

The four terms given below in Eqs. (73)–(76) correspond to the following possibilities:

(i) The (1,1) "electron-electron" or the (2,2) "hole-hole" components of $J_{a,\alpha}G^{A}_{\alpha,a}$.

(ii) The $\exp[\pm i(+\varphi_a+\varphi_b-\varphi_{c,1}-\varphi_{c,2})]$ factors for the $(1,1,-1,-1)$ or $(-1,-1,1,1)$ labels, respectively.

We obtain the following:

$$J_0\langle\langle G^{A,(1,1,-1,-1)}_{[12],(\alpha,a),(1,1),(1)}\rangle\rangle_{\text{total}}(\omega)=\frac{c'_{1/2}}{8}\left(\frac{J_0}{W}\right)^{12}\frac{\sqrt{\mathscr{S}_{\text{contact}}}}{l_e}\frac{x_0y_0z_0}{(k_FR_0)^3}\frac{\Delta^6}{[\Delta^2-(\omega-i\eta)^2]^3}\exp\left[i\left(\varphi_a+\varphi_b-\varphi_{c_1}-\varphi_{c_2}\right)\right], \tag{73}$$

$$J_0\langle\langle G^{A,(-1,-1,1,1)}_{[12],(\alpha,a),(1,1),(1)}\rangle\rangle_{\text{total}}(\omega)=\frac{5c'_{1/2}}{8}\left(\frac{J_0}{W}\right)^{12}\frac{\sqrt{\mathscr{S}_{\text{contact}}}}{l_e}\frac{x_0y_0z_0}{(k_FR_0)^3}\frac{\Delta^6}{[\Delta^2-(\omega-i\eta)^2]^3}\exp\left[i\left(-\varphi_a-\varphi_b+\varphi_{c_1}+\varphi_{c_2}\right)\right], \tag{74}$$

$$J_0\langle\langle G^{A,(1,1,-1,-1)}_{[12],(\alpha,a),(2,2),(1)}\rangle\rangle_{\text{total}}(\omega)=\frac{5c'_{1/2}}{8}\left(\frac{J_0}{W}\right)^{12}\frac{\sqrt{\mathscr{S}_{\text{contact}}}}{l_e}\frac{x_0y_0z_0}{(k_FR_0)^3}\frac{\Delta^6}{[\Delta^2-(\omega-i\eta)^2]^3}\exp\left[i\left(\varphi_a+\varphi_b-\varphi_{c_1}-\varphi_{c_2}\right)\right], \tag{75}$$

$$J_0\langle\langle G^{A,(-1,-1,1,1)}_{[12],(\alpha,a),(2,2),(1)}\rangle\rangle_{\text{total}}(\omega)=\frac{c'_{1/2}}{8}\left(\frac{J_0}{W}\right)^{12}\frac{\sqrt{\mathscr{S}_{\text{contact}}}}{l_e}\frac{x_0y_0z_0}{(k_FR_0)^3}\frac{\Delta^6}{[\Delta^2-(\omega-i\eta)^2]^3}\exp\left[i\left(-\varphi_a-\varphi_b+\varphi_{c_1}+\varphi_{c_2}\right)\right]. \tag{76}$$

The microscopic process contributing to the $(-1,-1,1,1)$ terms given by Eqs. (74) and (76) is listed in Sec. II A of the Supplemental Material [29]. Specifically, Eq. (74) is the sum of Eqs. (10)–(39) in the Supplemental Material [29] and Eq. (76) is the sum of Eqs. (41)–(46), also in the Supplemental Material [29].

The overall positive sign of Eqs. (73)–(76) originates from the product of four negative contributions:

(i) A minus sign is associated with each of the three transmission modes through the 2D metal.

(ii) Another minus sign is due to averaging the product of three superconducting Green's functions; see Eqs. (D9)–(D13) in Appendix D 4.

In addition, the $\exp[i(-\varphi_a-\varphi_b+\varphi_{c_1}+\varphi_{c_2})]$ factor in Eqs. (74) and (76) produces a "(1,1)" electron-electron Nambu component 5/8 coefficient in Eq. (74), which is larger than the "(2,2)" hole-hole component 1/8 coefficient in Eq. (76). This is compatible with the observation that the "(2,2)" component associated with the $(-1,-1,2,0)$ combination is vanishingly small for the three-terminal $3TQ_1$; see the above Sec. V A.

In addition, the residue of the pole at $\omega=-\Delta$ is positive; see Eqs. (D4)–(D6) in Appendix D 2 concerning the integral over the energy ω.

Overall, Eqs. (29)–(32) and (73)–(76) lead to the following current-phase relation for the 4TSQ at the orders $(J_0/W)^{12}$ and $\sqrt{\mathscr{S}_{\text{contact}}}/l_e$:

$$I^{(1)}_{\alpha\to a,\text{eq}}=I^{(1)}_{c,\,4\text{TSQ}}\sin\varphi_{q,\,4T}, \tag{77}$$

where $\varphi_{q,\,4T}\equiv\varphi_a+\varphi_b-\varphi_{c,1}-\varphi_{c,2}\equiv\varphi_{q,\,3T}$, as for the 4TFSQ; see Eqs. (71) and (72).

The critical current $I^{(1)}_{c,\,4\text{TSQ}}$ appearing in Eq. (77) is negative, i.e., it is π-shifted:

$$I^{(1)}_{c,\,4\text{TSQ}}=-\frac{3ec'_{1/2}\pi\Delta}{4\hbar}\left(\frac{J_0}{W}\right)^{12}\frac{\sqrt{\mathscr{S}_{\text{contact}}}}{l_e}\frac{x_0y_0z_0}{(k_FR_0)^3}. \tag{78}$$

2. The four-terminal 4TSQ current at the orders $(J_0/W)^{12}$ and $\mathscr{S}_{contact}/l_e^2$

Next, we calculate the four-terminal 4TSQ critical current at the orders $(J_0/W)^{12}$ and $\mathscr{S}_{\text{contact}}/l_e^2$. Again, we separate the "electron-electron" from the "hole-hole" Nambu components, and the $\exp[\pm i(+\varphi_a+\varphi_b-\varphi_{c,1}-\varphi_{c,2})]$ sensitivity on the superconducting phase variables:

$$J_0\langle\langle G^{A,(1,1,-1,-1)}_{[12],(\alpha,a),(1,1),(2)}\rangle\rangle_{\text{total}}(\omega)=-\frac{c'_1}{32}\left(\frac{J_0}{W}\right)^{12}\frac{\mathscr{S}_{\text{contact}}}{l_e^2}\frac{y_0z_0^2+y_0^2z_0+x_0z_0^2+x_0y_0^2}{(k_FR_0)^3}\frac{(\omega-i\eta)^2\Delta^4}{[\Delta^2-(\omega-i\eta)^2]^3}e^{i(\varphi_a+\varphi_b-\varphi_{c_1}-\varphi_{c_2})}, \tag{79}$$

$$J_0\langle\langle G^{A,(-1,-1,1,1)}_{[12],(\alpha,a),(1,1),(2)}\rangle\rangle_{\text{total}}(\omega)=-\frac{5c'_1}{32}\left(\frac{J_0}{W}\right)^{12}\frac{\mathscr{S}_{\text{contact}}}{l_e^2}\frac{y_0z_0^2+y_0^2z_0+x_0z_0^2+x_0y_0^2}{(k_FR_0)^3}\frac{(\omega-i\eta)^2\Delta^4}{[\Delta^2-(\omega-i\eta)^2]^3}e^{i(-\varphi_a-\varphi_b+\varphi_{c_1}+\varphi_{c_2})}, \tag{80}$$

$$J_0\langle\langle G^{A,(1,1,-1,-1)}_{[12],(\alpha,a),(2,2),(2)}\rangle\rangle_{\text{total}}(\omega)=-\frac{5c'_1}{32}\left(\frac{J_0}{W}\right)^{12}\frac{\mathscr{S}_{\text{contact}}}{l_e^2}\frac{y_0z_0^2+y_0^2z_0+x_0z_0^2+x_0y_0^2}{(k_FR_0)^3}\frac{(\omega-i\eta)^2\Delta^4}{[\Delta^2-(\omega-i\eta)^2]^3}e^{i(\varphi_a+\varphi_b-\varphi_{c_1}-\varphi_{c_2})}, \tag{81}$$

$$J_0\langle\langle G^{A,(-1,-1,1,1)}_{[12],(\alpha,a),(2,2),(2)}\rangle\rangle_{\text{total}}(\omega)=-\frac{c'_1}{32}\left(\frac{J_0}{W}\right)^{12}\frac{\mathscr{S}_{\text{contact}}}{l_e^2}\frac{y_0z_0^2+y_0^2z_0+x_0z_0^2+x_0y_0^2}{(k_FR_0)^3}\frac{(\omega-i\eta)^2\Delta^4}{[\Delta^2-(\omega-i\eta)^2]^3}e^{i(-\varphi_a-\varphi_b+\varphi_{c_1}+\varphi_{c_2})}. \tag{82}$$

Equation (80) is the sum of Eqs. (48)–(107) in Sec. II B of the Supplemental Material [29]. Equation (82) is the sum of Eqs. (109)–(120) in the Supplemental Material [29].

The minus sign in Eqs. (79)–(82) is due to the product of three (negative) transmission modes through the 2D metal.

In addition, the $\exp[i(-\varphi_a-\varphi_b+\varphi_{c_1}+\varphi_{c_2})]$ combination yields the 5/32 coefficient for the "(1,1)" component, which is larger than 1/32 for the "(2,2)" component; see Eqs. (80) and (82), respectively. This is compatible with the discussion following the above Eqs. (73)–(76).

A (positive) residue is taken into account in the integral over energy; see Eqs. (D7) and (D8) in Appendix D 3.

It is deduced that Eqs. (34)–(37) and Eqs. (79)–(82) lead to the following contribution to the equilibrium current $I_{\alpha\to a,\mathrm{eq}}$ at the orders $(J_0/W)^{12}$ and $\mathscr{S}_{\mathrm{contact}}/l_e^2$:

$$I^{(2)}_{\alpha\to a,\mathrm{eq}} = I^{(2)}_{c,\,4\mathrm{TSQ}} \sin\varphi_{q,\,4T}, \tag{83}$$

where $\varphi_{q,\,4T}$ is given by Eq. (72) and the critical current $I^{(2)}_{c,\,4\mathrm{TSQ}}$ is positive, i.e., it is 0-shifted:

$$I^{(2)}_{c,\,4\mathrm{TSQ}} = \frac{3ec_1'\Delta}{16\hbar}\left(\frac{J_0}{W}\right)^{12}\frac{\mathscr{S}_{\mathrm{contact}}}{l_e^2}\frac{y_0z_0^2+y_0^2z_0+x_0z_0^2+x_0y_0^2}{(k_FR_0)^3}. \tag{84}$$

3. Discussion

Two of the four-terminal 4TSQ diagrams appearing at the orders $(J_0/W)^{12}$ and $\mathscr{S}_{\mathrm{contact}}/l_e^2$ are shown in Figs. 8(a) and 8(b). The diffuson and the energy representations in Figs. 6(c) and 6(d), respectively, illustrate that the four-terminal 4TSQ of orders $(J_0/W)^{12}$ and $\mathscr{S}_{\mathrm{contact}}/l_e^2$ involve the product of two superconducting diffusion modes of the $\langle\langle g_{(1,1)}g_{(1,2)}\rangle\rangle$-type. For instance, the superconducting diffusion modes propagating in $S_{c,1}$ or in $S_{c,2}$ in Figs. 8(a) and 8(b) correspond to the $x_0y_0^2$ or $x_0z_0^2$ contributions to Eqs. (79)–(82), respectively [see also Eq. (84)].

The 0-shifted four-terminal 4TSQ current [see Eqs. (83) and (84)] is interpreted as the intermediate state

$$c^+_{S_{c_1},\uparrow}c^+_{S_{c_1},\downarrow}c^+_{S_{c_2},\uparrow}c^+_{S_{c_2},\downarrow} \tag{85}$$

made with two Cooper pairs from S_a and S_b biased at $\pm V$. Anticommuting the $(S_{c_1},\uparrow)$ and the $(S_{c_2},\uparrow)$ partners in Eq. (85) leads to a minus sign, which implies 0-shift for the four-terminal 4TSQ current-phase relation [see Eqs. (83) and (84)] in comparison with the previous π-shift of the three-terminal $3\mathrm{TQ}_1$ and $3\mathrm{TQ}_2$ [see Eqs. (63)–(65)]. Indeed, the three-terminal $3\mathrm{TQ}_1$ and $3\mathrm{TQ}_2$ do not contain the additional two-fermion exchange of the 4TSQ, which is made possible by the 2D quantum wake; see the forthcoming Sec. VII.

VI. INTERFERENCE BETWEEN THE THREE-TERMINAL $3\mathrm{TQ}_1$, $3\mathrm{TQ}_2$ AND THE FOUR-TERMINAL 4TSQ

We proceed by further considering that, in the gauge given by Eqs. (10) and (11), the $\varphi_{q,\,3T}$-sensitive critical current is the result of an interference between the three-terminal $3\mathrm{TQ}_1$, $3\mathrm{TQ}_2$ (see Sec. V A), and the four-terminal 4TSQ (see Sec. V C):

$$I_c(\Phi/\Phi_0) = \max_{\varphi_{q,\,3T}}[I_{3\mathrm{TQ}_1}(\varphi_{q,\,3T},\Phi) + I_{3\mathrm{TQ}_2}(\varphi_{q,\,3T},\Phi) + I_{4\mathrm{TSQ}}(\varphi_{q,\,3T})]. \tag{86}$$

The contact areas $\mathscr{S}_{\mathrm{contact}}$ are considered to be large compared to $(l_e)^2$, i.e., $\mathscr{S}_{\mathrm{contact}} \gg l_e^2$. This realistic assumption yields $|I^{(1)}_{c,\,4\mathrm{TSQ}}| \ll I^{(2)}_{c,\,4\mathrm{TSQ}}$. The four-terminal 4TSQ critical current is approximated as $I_{4\mathrm{TSQ}}(\varphi_{q,\,3T}) \simeq I^{(2)}_{c,\,4\mathrm{TSQ}}$. The resulting current-phase relation

$$I_{4\mathrm{TSQ}}(\varphi_{q,\,3T}) \simeq I^{(2)}_{c,\,4\mathrm{TSQ}}\sin\varphi_{q,\,3T} \tag{87}$$

is independent of the value of the magnetic flux Φ; see the expression of $\varphi_{q,\,3T}$ given by Eq. (6) and $I^{(2)}_{c,\,4\mathrm{TSQ}}$ in Eq. (84).

Equation (86) is 2π-periodic in Φ, while the previous $\max_{\varphi_{q,\,3T}}[I_{3\mathrm{TQ}_1}(\varphi_{q,\,3T},\Phi) + I_{3\mathrm{TQ}_2}(\varphi_{q,\,3T},\Phi)]$ was π-periodic.

More specifically, specializing to $\Phi/\Phi_0 = 0$ and to $\Phi/\Phi_0 = 1/2$ leads to

$$I_c(0) = \left|I_{c,\,3\mathrm{TQ}_1} + I_{c,\,3\mathrm{TQ}_2} + I_{c,\,4\mathrm{TSQ}}\right|, \tag{88}$$

which is different from

$$I_c(1/2) = \left|I_{c,\,3\mathrm{TQ}_1} + I_{c,\,3\mathrm{TQ}_2} - I_{c,\,4\mathrm{TSQ}}\right|. \tag{89}$$

VII. WHY THE FOUR-TERMINAL 4TSQ APPEAR ONLY IN TWO DIMENSIONS

The preceding Sec. V presented the calculation (in perturbation in J_0/W and in the adiabatic limit $V = 0^+$) of the sign and the amplitude of the π-shifted three-terminal $3\mathrm{TQ}_1$, $3\mathrm{TQ}_2$, and the 0-shifted four-terminal 4TSQ critical currents. We proceed further by discussing why the four-terminal 4TSQ yields a vanishingly small current if a 1D or 3D metal is used instead of the 2D metal such as graphene gated away from the Dirac point in the Harvard group experiment [4].

We establish a link between Eqs. (16)–(19) for the Green's function of a ballistic 2D metal, and the general theory of the "wake" in the solution of the even-dimensional wave equation, starting in Sec. VII A with the classical wave equation. The 2D quantum wake in nanoscale electronic devices is considered in Sec. VII B. Synchronizing two Josephson junctions with quasiparticles "surfing" on the 2D quantum wake is discussed in Sec. VII C, in connection with the features of the four-terminal 4TSQ diagram; see one of the 4TSQ diagrams in Fig. 6(d). A summary of this Sec. VII is presented in Sec. VII D.

At this point, we also make reference to a very recent unpublished work [40] about the production of quantum wakes with ultracold atoms.

A. The wake effect in the classical wave equation

Volterra was the first to understand that the solutions of the wave equation are drastically different in even or odd space dimension. Let us assume that an excitation is produced at a given location and time. A detector is at a distance R from the location of the excitation. In all cases, the signal reaches R after the time delay $t_0 = R/v$, where v is the speed of wave propagation. In odd dimensions (such as in one or three dimensions), the detected signal consists of the sharp pulse associated with the wavefront. But in even dimension (such as in two dimensions), the detected signal oscillates long after the time delay t_0. This "classical wake" appears in even space dimensions but not in odd dimensions, and it agrees with the common sense idea regarding a boat propagating on a calm sea.

B. The 2D quantum wake in meso- or nanoscale devices

The signal at the detector mentioned above results from a convolution of the initial excitation with the D-dimensional Green's functions. It turns out that Green's functions are at the heart of the calculation of the electronic transport properties in meso- or nanoscale devices.

The normal-state Green's function at a distance R is a plane wave in one dimension:

$$g^A_{1\mathrm{D},\,(1,1)}(R,\omega) \sim \exp(ikR), \tag{90}$$

where k is the wave vector at the considered energy ω, and "(1,1)" refers to the "spin-up electron" Nambu component. The 3D Green's function is also a plane wave:

$$g^A_{3\mathrm{D},\,(1,1)}(R,\omega) \sim \frac{\exp(ikR)}{kR}, \tag{91}$$

which is normalized by the factor kR arising from probability conservation. In two dimensions, the Green's function is a Bessel function that behaves like

$$g^A_{2\mathrm{D},\,(1,1)}(R,\omega) \sim i\frac{\cos(kR-\pi/4)}{\sqrt{kR}} \tag{92}$$

at large $R \gg 1/k$; see the above Eq. (16) and Appendix A for the demonstration of Eqs. (16) and (92).

C. Synchronizing two Josephson junctions by the 2D quantum wake

The difference between the 1D or 3D $\exp(ikR)$ oscillations in Eqs. (90) and (91), and the 2D $\cos(kR-\pi/4)$ oscillations in Eq. (92), is now discussed in connection with synchronizing two Josephson junctions.

Specifically, we focus on the highlighted section of the four-terminal 4TSQ diagram in Fig. 6(d), which involves taking the square of the advanced Green's function according to $[g^A_{(1,1)}(R)]^2$. Multichannel interfaces are simulated by averaging $[g^A_{(1,1)}(R)]^2$ over R around the value R_0 such that $\lambda_F \ll R_0 \lesssim l_\varphi$. Averaging over the separation R between $S_{c,1}$ and $S_{c,2}$ in an interval of width $\Delta R \sim 2\pi/k$ around $R = R_0$ yields

$$\langle\langle[g^A_{1D,\,(1,1)}(R)]^2\rangle\rangle = 0, \tag{93}$$

$$\langle\langle[g^A_{2D,\,(1,1)}(R)]^2\rangle\rangle \simeq -\frac{1}{2W^2k_FR_0}, \tag{94}$$

$$\langle\langle[g^A_{3D,\,(1,1)}(R)]^2\rangle\rangle = 0. \tag{95}$$

Equations (93)–(95) are deduced from Eqs. (90), (16), and (91), respectively. These Eqs. (93)–(95) imply short range coupling over λ_F if a 1D or a 3D metal is used instead of a 3D metal, which is in agreement with the general theory of the 2D wake mentioned above.

To summarize, it is only in 2D that the 4TSQ diagrams in Figs. 6(c) and 6(d) are nonvanishingly small, due to the nonvanishingly small $\langle\langle[g^A_{(1,1)}(R)]^2\rangle\rangle \neq 0$ connecting S_{c_1} and S_{c_2} in Fig. 6(d), and physically encoding the exchange of a quasiparticle via the 2D quantum wake.

D. Summary of this section

The microscopic theory of the four-terminal 4TSQ was discussed:

(i) The four-terminal 4TSQs are specific to 2D, and they are related to the quantum limit of the wake in the even-dimensional wave equation.

(ii) The four-terminal 4TSQs realize *quantum mechanical* synchronization between Josephson junctions by coherently exchanging a quasiparticle between them. The quasiparticle that is exchanged propagates on the 2D quantum wake.

(iii) The four-terminal 4TSQs couple the Andreev bound states of the two Josephson junctions in the simple limit of equilibrium with bias voltage $V = 0$, and in the adiabatic limit with $V = 0^+$ on the quartet line; see also the remarks on the long-range coupling of the four-terminal 4TSQ in the concluding Sec. XI C.

Finally, we note that the four-terminal 4TSQs do not contribute to the current in the previous Grenoble group experiment [13]. In this experiment, the intermediate region connecting the superconducting leads consists of an evaporated "T-shaped" Copper lead which is 3D, as opposed to the atomically thin 2D sheet of graphene used in the Harvard group experiment [4]. The 2D quantum wake is also not expected to play a role in the Weizmann Institute group experiment [14] made with a semiconducting nanowire.

VIII. INVERSION BETWEEN $\Phi/\Phi_0 = 0$ AND $\Phi/\Phi_0 = 1/2$

In this section, we show that the relative shift of π between the three-terminal $3\mathrm{TQ}_1$, $3\mathrm{TQ}_2$, and the four-terminal 4TSQ obtained in the above Sec. V implies the emergence of the inversion $I_c(0) < I_c(1/2)$ between $\Phi/\Phi_0 = 0$ and $\Phi/\Phi_0 = 1/2$ in the reduced flux Φ/Φ_0 dependence of the critical current $I_c(\Phi/\Phi_0)$ given by Eqs. (86) and (87).

In addition, we address the reverse question of the information that is deduced from "*Observation of inversion in* $I_c(\Phi/\Phi_0)$ *between* $\Phi/\Phi_0 = 0$ *and* $\Phi/\Phi_0 = 1/2$," regarding the sign of the three-terminal $3\mathrm{TQ}_1$, $3\mathrm{TQ}_2$, and the four-terminal 4TSQ current-phase relations.

The assumptions about the 0- and π-shifted current-phase relations are presented in Sec. VIII A. The reasoning is presented in Sec. VIII B. The consequences for the Harvard group experiment are provided in Sec. VIII C.

A. The assumptions

This subsection is based on the following assumptions:

(i) We have information about the Φ/Φ_0-sensitivity of the critical current I_c, more specifically about whether $I_c(0)$ is smaller or larger than $I_c(1/2)$.

(ii) The signs of the three-terminal $3\mathrm{TQ}_1$, $3\mathrm{TQ}_2$, and the four-terminal 4TSQ critical currents are left as free parameters, while they interfere according to the preceding Eq. (86).

B. General statements

Let us now assume that inversion $I_c(0) < I_c(1/2)$ between $\Phi/\Phi_0 = 0$ and $\Phi/\Phi_0 = 1/2$ is observed. Combining Eqs. (88) and (89) with Eq. (121) in Sec. III of the

Supplemental Material [29] yields the following "logical chain":

$$I_c(0) < I_c(1/2) \tag{96}$$

$$\iff \left|I_{c,\,3\mathrm{TQ}_1} + I_{c,\,3\mathrm{TQ}_2} + I_{c,\,4\mathrm{TSQ}}\right| \tag{97}$$

$$< \left|I_{c,\,3\mathrm{TQ}_1} + I_{c,\,3\mathrm{TQ}_2} - I_{c,\,4\mathrm{TSQ}}\right|$$

$$\iff I_{c,\,3\mathrm{TQ}_1} + I_{c,\,3\mathrm{TQ}_2} \text{ and } I_{c,\,4\mathrm{TSQ}} \tag{98}$$

have opposite signs.

C. Conclusion on the Harvard group experiment [4]

In this subsection, we present the consequences for the Harvard group experiment [4].

As is mentioned above, perturbation theory in the tunnel amplitudes J_0/W combined with the adiabatic limit $V = 0^+$ imply the π-shifted three-terminal $3\mathrm{TQ}_1$, $3\mathrm{TQ}_2$, and 0-shifted four-terminal 4TSQ; see Sec. V. Given that Eq. (98) implies Eq. (96), we conclude that perturbation theory and the adiabatic limit imply "inversion in the critical current $I_c(\Phi/\Phi_0)$ between $\Phi/\Phi_0 = 0$ and $\Phi/\Phi_0 = 1/2$," i.e., $I_c(0) < I_c(1/2)$.

Conversely, "experimental evidence for inversion" implies

"*Evidence that the three-terminal* $3\mathrm{TQ}_1$, $3\mathrm{TQ}_2$ *are* π*-shifted and the four-terminal 4TSQ are 0-shifted*,"

or, alternatively,

"*Evidence for 0-shifted* $3\mathrm{TQ}_1$, $3\mathrm{TQ}_2$, *and* π*-shifted 4TSQ*.

No information is gained about which of the three-terminal $3\mathrm{TQ}_1$, $3\mathrm{TQ}_2$, or the four-terminal 4TSQ is π-shifted, the other being 0-shifted.

IX. GATE VOLTAGE DEPENDENCE OF THE MAGNETIC FIELD OSCILLATIONS

A. Notations for the phenomenological model

The previous calculations are summarized in the following phenomenological form of the critical current-flux Φ relation:

$$J_c(\Phi/\Phi_0) = J_c^{(0)}\max_{\varphi_{q,\,3T}}\big\{\alpha_{3\mathrm{TQ}_1}\sin(\varphi_{q,\,3T} + \Phi) + \alpha_{3\mathrm{TQ}_2}\sin(\varphi_{q,\,3T} - \Phi) + \alpha_{4\mathrm{TSQ}}\sin\varphi_{q,\,3T}\big\}, \tag{99}$$

which is deduced from the previous Eq. (86).

The factorized scaling parameter $J_c^{(0)}$ is positive and it has dimension of a critical current. The dimensionless parameters $\alpha_{3\mathrm{TQ}_1}$, $\alpha_{3\mathrm{TQ}_2}$, and $\alpha_{4\mathrm{TSQ}}$ characterize the relative weights and signs of the three-terminal $3\mathrm{TQ}_1$, $3\mathrm{TQ}_2$ and the four-terminal 4TSQ critical currents.

The perturbative calculations presented in the above Sec. V lead to $\alpha_{3\mathrm{TQ}_1} < 0$, $\alpha_{3\mathrm{TQ}_2} < 0$, and to $\alpha_{4\mathrm{TSQ}} > 0$. Following the previous Sec. VIII, we assume more generally that the three-terminal $\alpha_{3\mathrm{TQ}_1}$, $\alpha_{3\mathrm{TQ}_2}$ and the four-terminal $\alpha_{4\mathrm{TSQ}}$ can have arbitrary positive or negative relative signs.

General positive or negative signs of $\alpha_{3\mathrm{TQ}_1}$, $\alpha_{3\mathrm{TQ}_2}$, and $\alpha_{4\mathrm{TSQ}}$ could be relevant to higher transparency of the contacts between the 2D metal and the superconducting leads. However, it has not yet been examined whether increasing the contact transparency *via* the parameter J_0/W can produce change of sign in these coefficients.

B. Analogy with interferometric detection of the π-shift [41]

Now, we mention a connection between the following:

(i) The SQUID containing a 0 and a π-junction which was realized experimentally in Ref. [41].

(ii) The relative π-shift between the three-terminal $3\mathrm{TQ}_1$, $3\mathrm{TQ}_2$ and the four-terminal 4TSQ.

More specifically,

(i) Half-period shift of the critical current magnetic oscillations is observed in Ref. [41] with a SQUID containing a π-shifted and a 0-shifted Josephson junction, in comparison with a SQUID containing two 0-shifted Josephson junctions.

(ii) Half-period shift in the critical current of the four-terminal Josephson junction shown in Figs. 1 and 3 is produced in our theory when changing "relative shift of π between the three-terminal $3\mathrm{TQ}_1$, $3\mathrm{TQ}_2$" and the four-terminal 4TSQ into "relative shift of 0."

C. Gate voltage dependence of the critical current magnetic oscillations in the perturbative limit

Figures 9 and 10 show in panels (a1)–(e1) the magnetic oscillations of the critical current given by Eq. (99), and their Fourier coefficients H_n are shown in panels (a2)–(e2):

$$H_n = \int \frac{d\Phi}{2\pi}\cos\left(\frac{2\pi n\Phi}{\Phi_0}\right)J_c\left(\frac{\Phi}{\Phi_0}\right), \tag{100}$$

where $J_c(\Phi/\Phi_0)$ is given by Eq. (99). The parameters $\alpha_{3\mathrm{TSQ}_1} = \alpha_{3\mathrm{TSQ}_2} = -1$ used in Figs. 9 and 10 have the meaning of the π-shifted three-terminal $3\mathrm{TQ}_1$, $3\mathrm{TQ}_2$ critical currents deduced from perturbation theory in J_0/W; see Sec. V.

The parameter $\alpha_{4\mathrm{TSQ}} \geqslant 0$ is used in Fig. 9, thus with relative π-shift between the three-terminal $3\mathrm{TQ}_1$, $3\mathrm{TQ}_2$ and the four-terminal 4TSQ: $\alpha_{4\mathrm{TSQ}} = 0$ [panels (a1) and (a2)], $\alpha_{4\mathrm{TSQ}} = 0.5$ [panels (b1) and (b2)], $\alpha_{4\mathrm{TSQ}} = 1$ [panels (c1) and (c2)], $\alpha_{4\mathrm{TSQ}} = 1.5$ [panels (d1) and (d2)], and to $\alpha_{4\mathrm{TSQ}} = 2$ [panels (e1) and (e2)].

Figure 10 shows the corresponding data with $\alpha_{4\mathrm{TSQ}} \leqslant 0$, i.e., with a 0-shift between the three-terminal $3\mathrm{TQ}_1$, $3\mathrm{TQ}_2$ and the four-terminal 4TSQ: $\alpha_{4\mathrm{TSQ}} = 0$ [panels (a1) and (a2)], $\alpha_{4\mathrm{TSQ}} = -0.5$ [panels (b1) and (b2)], $\alpha_{4\mathrm{TSQ}} = -1$ [panels (c1) and (c2)], $\alpha_{4\mathrm{TSQ}} = -1.5$ [panels (d1) and (d2)], and to $\alpha_{4\mathrm{TSQ}} = -2$ [panels (e1) and (e2)].

Figures 9(a1)–9(e1) and 10(a1)–10(e1) illustrate the logical chain of Eqs. (96)–(98): Figures 9(a1)–9(e1) with relative π-shift between the three-terminal $3\mathrm{TQ}_1$, $3\mathrm{TQ}_2$, and the four-terminal 4TSQ reveal the inversion $J_c(0) < J_c(1/2)$ between $J_c(\Phi/\Phi_0)$ at $\Phi/\Phi_0 = 0$ and $\Phi/\Phi_0 = 1/2$. Conversely, Figs. 10(a1)–10(e1) with relative 0-shift feature the noninverted behavior $J_c(0) > J_c(1/2)$.

In addition, Figs. 9 and 10 are deduced from each other by a half-period shift of $\Phi/2\pi$ on the x-axis, which is in agreement with the analogous SQUID containing a 0- and a π-shifted Josephson junction; see Ref. [41] and the preceding Sec. IX B.

Gating the 2D metal away from the center of the band has the effect of increasing the density of states, which increases J_0/W and favors the four-terminal 4TSQ over the three-terminal $3\mathrm{TQ}_1$, $3\mathrm{TQ}_2$, because they appear in perturbation at the different orders $(J_0/W)^8$ and $(J_0/W)^{12}$, respectively; see Sec. V.

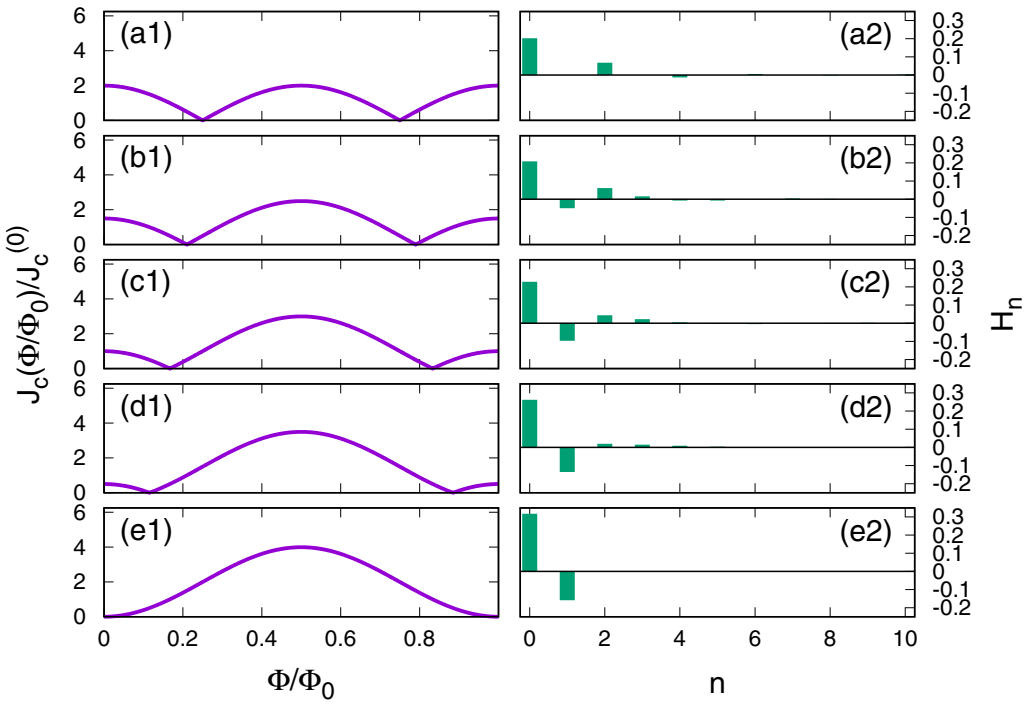

FIG. 9. Critical current-flux relations [panels (a1)–(e1)] and the corresponding Fourier coefficients [panels (a2)–(e2)]: The parameters $\alpha_{3TQ_1} = \alpha_{3TQ_2} = -1$ are used, and $\alpha_{4TSQ} = 0,\ 0.5,\ 1,\ 1.5,\ 2$ in panels (a1)–(a2), (b1)–(b2), (c1)–(c2), (d1)–(d2), and (e1)–(e2), respectively. The opposite signs of $\alpha_{3TQ_1} < 0$, $\alpha_{3TQ_2} < 0$ and $\alpha_{4TSQ} \geqslant 0$ correspond to relative shift of π between the three-terminal $3TQ_1$, $3TQ_2$ and the four-terminal 4TSQ. This relative π-shift is the result of lowest-order perturbation theory in the tunnel amplitudes; see Sec. V.

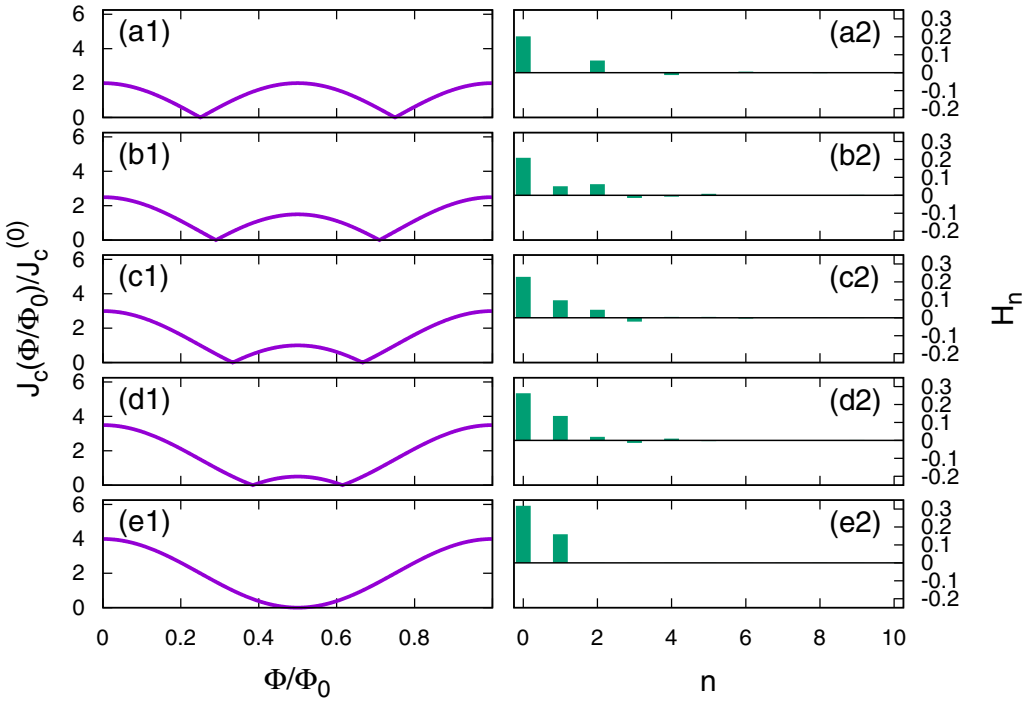

FIG. 10. Critical current-flux relations [panel (a1)–(e1)] and the corresponding Fourier coefficients [panels (a2)–(e2)]: The parameters $\alpha_{3TQ_1} = \alpha_{3TQ_2} = -1$ are used, and $\alpha_{4TSQ} = 0,\ -0.5,\ -1,\ -1.5,\ -2$ in panels (a1)–(a2), (b1)–(b2), (c1)–(c2), (d1)–(d2), and (e1)–(e2), respectively. The signs of $\alpha_{3TQ_1} < 0$, $\alpha_{3TQ_2} < 0$, and $\alpha_{4TSQ} \leqslant 0$ correspond to relative 0-shift between the three-terminal $3TQ_1$, $3TQ_2$, and the four-terminal 4TSQ.

It is deduced from Figs. 9(a2)–9(e2) and 10(a2)–10(e2) that tuning gate voltage away from the Dirac point increases $|H_1|$ and reduces H_2 [where H_1 and H_2 are defined as the $n = 1, 2$ in Eq. (100)], which favors the Φ_0 harmonics over the $2\Phi_0$ one. Figures 9 and 10 reveal in addition the expected negative $H_1 < 0$ for relative π-shift between the three-terminal $3TQ_1$, $3TQ_2$, and the four-terminal 4TSQ, and $H_1 > 0$ for a relative 0-shift, which is in agreement with the perturbative calculations of Sec. V.

We conclude this section by emphasizing that our theory is in qualitative agreement with the Harvard group's experimental data [4] regarding the gate voltage dependence of the critical current magnetic oscillations on the quartet line. Figures 9 and 10 are related to Fig. 3 in the recent work of the Harvard group [4].

X. GENERALIZATION TO ARBITRARY INTERFACE TRANSPARENCIES AND FINITE BIAS VOLTAGE

The three-terminal $3TQ_1$, $3TQ_2$ transmit an even number of Cooper pairs into S_{c_1} or S_{c_2} while the four-terminal 4TSQs transmit an odd number of Cooper pairs. This characterization based on the parity of the number of Cooper pairs transmitted into $S_{c,1}$ or $S_{c,2}$ is now generalized in the following section to arbitrary interface transparencies and finite bias voltage.

Given the arguments of Sec. IV D, we replace the "realistic model I of clean interfaces and superconductors in the dirty limit" by the "physically motivated approximation of the model III," i.e., clean interfaces and superconductors in the ballistic limit, and averaging over $\{k_F R_{k,l}\}$.

We start in Sec. X A by demonstrating the generalized Ambegaokar-Baratoff formula in the $V = 0^+$ adiabatic limit at arbitrary interface transparencies. Section X B generalizes this argument to finite voltage V on the quartet line, instead of the previous $V = 0^+$ adiabatic limit. Discussion of the Harvard group experiment [4] is presented in Secs. X A 2 and X B 2.

A. Generalized Ambegaokar-Baratoff formula in the $V = 0^+$ adiabatic limit

We start in this subsection with the $V = 0^+$ adiabatic limit. Subsection X A 1 demonstrates the generalized Ambegaokar-Baratoff formula for the quartet current-flux relation; see the forthcoming Eq. (105). Section X A 2 presents experimental consequences.

1. Demonstration of the generalized Ambegaokar-Baratoff formula at $V = 0^+$

Now, we calculate the quartet current in the $V = 0^+$ adiabatic limit, for arbitrary interface transparencies, and within the model III presented in the above Sec. IV D.

The first term $J_{a,\alpha}\hat{G}^A_{\alpha,a}$ appearing in Eq. (34) on the quartet line is written as

$$J_{a,\alpha}\hat{G}^A_{\alpha,a} = \sum_n \sum_{m_a,m_b,m_{c_1},m_{c_2}} X_n^{(m_a,m_b,m_{c_1},m_{c_2}),A} \times J_a^{2m_a} J_b^{2m_b} J_{c_1}^{2m_{c_1}} J_{c_2}^{2m_{c_2}} \exp(in\varphi_{q,3T}). \quad (101)$$

Conversely, $J_{a,\alpha}\hat{G}^R_{\alpha,a}$ involving the retarded Green's function takes the form

$$J_{a,\alpha}\hat{G}^R_{\alpha,a} = \sum_n \sum_{m_a,m_b,m_{c_1},m_{c_2}} X_n^{(m_a,m_b,m_{c_1},m_{c_2}),R} \times J_a^{2m_a} J_b^{2m_b} J_{c_1}^{2m_{c_1}} J_{c_2}^{2m_{c_2}} \exp(in\varphi_{q,3T}). \quad (102)$$

The bare Green's functions [i.e., Eqs. (16)–(19) and (20)] are used to produce a relation between the "advanced" and the "retarded" Green's functions by taking the complex conjugate and changing the sign of the superconducting phases. This symmetry is then generalized to the fully dressed advanced and retarded Green's functions by making use of the Dyson Eq. (23). The resulting $\hat{G}^A(\omega, R_0, \psi_F, \varphi_N) = [\hat{G}^R(\omega, R_0, \psi_F, -\varphi_N)]^*$ leads to

$$X_n^{(m_a,m_b,m_{c_1},m_{c_2}),R} = \left[X_n^{(m_a,m_b,m_{c_1},m_{c_2}),A}\right]^*. \quad (103)$$

Thus,

$$J_{a,\alpha}\hat{G}^A_{\alpha,a} - J_{a,\alpha}\hat{G}^R_{\alpha,a} = 2i \sum_n \sum_{m_a,m_b,m_{c_1},m_{c_2}} \mathrm{Im}\left[X_n^{(m_a,m_b,m_{c_1},m_{c_2}),R}\right] \times J_a^{2m_a} J_b^{2m_b} J_{c_1}^{2m_{c_1}} J_{c_2}^{2m_{c_2}} \exp(in\varphi_{q,3T}), \quad (104)$$

where the variable n stands for $n \equiv n_a = n_b$; see the notations in Eq. (48). Equations (34)–(37) imply the following decomposition of the critical current in the $V = 0^+$ adiabatic limit on the quartet line:

$$I'_c(\Phi/\Phi_0) = \max_{\varphi_c} \sum_{n,p} X(2n, p) \times \sin\left[(2n-p)\left(\varphi_c - \frac{\Phi}{2}\right) + p\left(\varphi_c + \frac{\Phi}{2}\right)\right], \quad (105)$$

where the quartet phase is expressed in the gauge given by Eqs. (10) and (11). Equation (104) shows that the coefficients $X(2n, p)$ appearing in the Ambegaokar-Baratoff formula Eq. (105) are real-valued. A number n of Cooper pairs is taken from the superconducting lead S_a biased at $V_a = +V$, and n other pairs are taken from S_b biased at $V_b = -V$. The integer p in Eq. (105) denotes the partition between the p pairs transmitted into S_{c_2} contact and the remaining $2n - p$ pairs transmitted into S_{c_1}.

2. Experimental consequences

In this subsection, we proceed further with the same assumptions as in the preceding Sec. X A 1, and we establish a link between the following:

(i) The emergence of different values for the critical current at fluxes $\Phi/\Phi_0 = 0$ and $\Phi/\Phi_0 = 1/2$ [i.e., $I_c(0) \neq I_c(1/2)$].

(ii) Evidence for interference between quantum processes transmitting even or odd numbers of Cooper pairs into S_{c_1} or S_{c_2}.

Specifically, we make the change of variables $\varphi_c \to \varphi_c + \Phi/2$ in Eq. (105), which is equivalent to changing the gauge

from Eqs. (10) and (11) to $\varphi_{c_1} = \varphi_c$ and $\varphi_{c_2} = \varphi_c + \Phi$:

$$I_c'(\Phi/\Phi_0) = \max_{\varphi_c} \sum_{n,p} X(2n, p) \sin[(2n-p)\varphi_c + p(\varphi_c + \Phi)]. \tag{106}$$

Equation (106) simplifies as

$$I_c'(\Phi/\Phi_0) = \max_{\varphi_c} \sum_{n,p} X(2n, p) \sin[2n\varphi_c + p\Phi]. \tag{107}$$

It is deduced that

$$I_c'(0) = \max_{\varphi_c} \sum_{n,p} X(2n, p) \sin[2n\varphi_c], \tag{108}$$

$$I_c'(1/2) = \max_{\varphi_c} \sum_{n,p} X(2n, p)(-)^p \sin[2n\varphi_c]. \tag{109}$$

Separating the terms with p even or odd according to

$$Y_{\text{even}}(\varphi_c) = \sum_{p\,\text{even}} \sum_n X(2n, p) \sin[2n\varphi_c], \tag{110}$$

$$Y_{\text{odd}}(\varphi_c) = \sum_{p\,\text{odd}} \sum_n X(2n, p) \sin[2n\varphi_c], \tag{111}$$

leads to

$$I_c'(0) = \max_{\varphi_c}[Y_{\text{even}}(\varphi_c) + Y_{\text{odd}}(\varphi_c)], \tag{112}$$

$$I_c'(1/2) = \max_{\varphi_c}[Y_{\text{even}}(\varphi_c) - Y_{\text{odd}}(\varphi_c)]. \tag{113}$$

The following logical link is deduced within the assumptions mentioned above:

"*Experimental observation for different values of the critical current between reduced fluxes* $\Phi/\Phi_0 = 0$ *and* $\Phi/\Phi_0 = 1/2$ *at arbitrary transparency*" [i.e., $I_c'(0) \neq I_c'(1/2)$ in Eqs. (112) and (113)]

is equivalent to

"*Evidence for interference between processes transmitting even or odd number of Cooper pairs into* S_{c_1} *and* S_{c_2}."

B. Generalization to finite bias voltage on the quartet line

Now, we generalize to finite bias voltage V and arbitrary interface transparencies. Disorder is treated within the model III introduced in Sec. IV D.

Specifically, we show in Sec. X B 1 that the Ambegaokar-Baratoff formula Eq. (105) holds at finite V within our treatment. Consequences for the proposed interpretation of the Harvard group experiment are discussed in Sec. X B 2.

1. Demonstration of the Ambegaokar-Baratoff formula at finite bias voltage

Now, at finite bias voltage V on the quartet line, we show that the currents transmitted at the $S_{c,1}$ or $S_{c,2}$ contacts take the form of the generalized Ambegaokar-Baratoff formula Eq. (105), where the coefficients $X(2n, p)$ appearing in the $V = 0^+$ Eq. (105) are replaced by their values $X(2n, p, eV/\Delta)$ at finite bias voltage V.

The Keldysh Green's function given by Eq. (27) is written as $\hat{G}^{+,-} = \hat{G}_A^{+,-} + \hat{G}_B^{+,-}$, where the "quasiequilibrium" and the "nonequilibrium" $\hat{G}_A^{+,-}$ and $\hat{G}_B^{+,-}$ are given by

$$\hat{G}_A^{+,-} = \hat{n}_F \hat{G}^A - \hat{G}^R \hat{n}_F, \tag{114}$$

$$\hat{G}_B^{+,-} = \hat{G}^R[\hat{J}\hat{n}_F - \hat{n}_F\hat{J}]\hat{G}^A, \tag{115}$$

respectively. The matrices appearing in Eqs. (114) and (115) are now defined both in Nambu and in the infinite set of harmonics of the Josephson frequencies. In the following, we use the notations $\check{\varphi} = (\varphi_a, \varphi_b, \varphi_{c,1}, \varphi_{c,2})$ for the superconducting phases and $\check{n} = (n_a, n_b, n_{c,1}, n_{c,2})$ for labeling the multiples of the voltage frequency $eV/\hbar$. The $\check{n}$ vector belongs to the set $S_{\check{n}}$ of quadruplets, which fulfill the constraints

$$n_a + n_b + n_{c,1} + n_{c,2} = 0, \tag{116}$$

$$n_a = n_b; \tag{117}$$

see the discussion following Eq. (48).

We start with the quasiequilibrium contribution I_A deduced from Eqs. (29)–(32):

$$\begin{aligned} -I_A &\equiv -I_{A,\gamma_{c_1}\to c_1} \\ &= \frac{e}{\hbar}\sum_p \int d\omega \Big\{ \big[\hat{J}_{c_{1,p},\gamma_{c_{1,p}}} \hat{G}^{+,-}_{A,\gamma_{c_{1,p}},c_{1,p}}\big]_{(1,1)/(0,0)} \\ &\quad \times (\omega, \check{\varphi}, \{\psi_{F,k,l}\}, V) \end{aligned} \tag{118}$$

$$-\big[\hat{J}_{c_{1,p},\gamma_{c_{1,p}}} \hat{G}^{+,-}_{A,\gamma_{c_{1,p}},c_{1,p}}\big]_{(2,2)/(0,0)}(\omega, \check{\varphi}, \{\psi_{F,k,l}\}, V) \tag{119}$$

$$-\big[\hat{J}_{\gamma_{c_{1,p}},c_{1,p}} \hat{G}^{+,-}_{A,c_{1,p},\gamma_{c_{1,p}}}\big]_{(1,1)/(0,0)}(\omega, \check{\varphi}, \{\psi_{F,k,l}\}, V) \tag{120}$$

$$+[\hat{J}_{\gamma_{c_{1,p}},c_{1,p}} \hat{G}^{+,-}_{A,c_{1,p},\gamma_{c_{1,p}}}]_{(2,2)/(0,0)}(\omega, \check{\varphi}, \{\psi_{F,k,l}\}, V)\Big\}, \tag{121}$$

where $\hat{G}_A^{+,-}$ is given by Eq. (114). The notation $\{\psi_{F,k,l}\}$ stands for the phases oscillating at the scale of the Fermi wavelength in a multichannel configuration, as they appear in the 2D metal and superconductor Green's functions; see Eqs. (16)–(19) and (20), respectively. Namely, $\psi_{F,k,l} = k_F R_{k,l} - \pi/4$ for the 2D metal [see Eqs. (16)–(19)], and $\psi_{F,k,l} = k_F R_{k,l}$ for the ballistic 3D superconductors [see Eq. (20)].

The Dyson Eq. (23) implies that the fully dressed advanced and retarded Green's functions take the following form:

$$\hat{G}^A(\omega, \check{\varphi}, \{\psi_{F,k,l}\}, V) = \sum_{\check{n}\in S_{\check{n}}} \hat{G}^A_{\check{n}}(\omega, \{\psi_{F,k,l}\}, V) e^{i\check{n}\cdot\check{\varphi}}, \tag{122}$$

$$\hat{G}^R(\omega, \check{\varphi}, \{k_F R_{k,l}\}) = \sum_{\check{n}\in S_{\check{n}}} \hat{G}^R_{\check{n}}(\omega, \{\psi_{F,k,l}\}) e^{i\check{n}\cdot\check{\varphi}}. \tag{123}$$

To relate $\hat{G}^A_{\check{n}}$ to $\hat{G}^R_{\check{n}}$ in Eqs. (122) and (123), we note that the bare Green's functions given by Eqs. (16)–(19) and (20) are such that

$$\hat{\mathscr{T}}_{\text{Nambu}} \hat{g}^{A,R}(\omega, \check{\varphi}, \{\psi_{F,k,l}\}, V) = \hat{g}^{A,R}(\omega, -\check{\varphi}, \{-\psi_{F,k,l}\}, -V), \tag{124}$$

where the transformation $\hat{\mathscr{T}}_{\text{Nambu}}$ exchanges the "1" and "2" Nambu components for "spin-up electron" and "spin-down hole," respectively. The Dyson equation given by Eq. (23)

yields

$$\hat{\mathscr{T}}_{\text{Nambu}}\hat{J}_{a,\gamma_{c_1}}\hat{G}^{A,R}_{\gamma_{c_1},c_1}(\omega,\check{\varphi},\{\psi_{F,k,l}\},V) = \hat{J}_{a,\gamma_{c_1}}\hat{G}^{A,R}_{\gamma_{c_1},c_1}(\omega,-\check{\varphi},\{-\psi_{F,k,l}\},-V). \quad (125)$$

Combining Eq. (114) with Eq. (125) leads to

$$\sum_p\int d\omega n_F(\omega)\{\langle\langle\hat{J}_{c_{1,p},\gamma_{c_{1,p}}}\hat{G}^A_{\gamma_{c_{1,p}},c_{1,p}}(\omega,\{\psi_{F,k,l}\},V,\check{\varphi})\rangle\rangle_{(1,1)} - \langle\langle\hat{J}_{c_{1,p},\gamma_{c_{1,p}}}\hat{G}^A_{\gamma_{c_{1,p}},c_{1,p}}(\omega,\{\psi_{F,k,l}\},-V,\check{\varphi})\rangle\rangle_{(2,2)}\} = 2i\sum_p\int d\omega n_F(\omega)\sum_{\check{n}\in S_{\check{n}}} \langle\langle\hat{J}_{c_{1,p},\gamma_{c_{1,p}}}\mathrm{Im}[G^A_{\gamma_{c_{1,p}},c_{1,p},\check{n}}(\omega,\{\psi_{F,k,l}\},V)]\rangle\rangle_{(1,1)}\sin(\check{n}\cdot\check{\varphi}). \quad (126)$$

Within the considered model III, averaging over disorder is mimicked by integrating over the phases $\{\psi_{F,k,l}\}$ in the $[0,2\pi]$ interval. The terms that are odd in $k_F R_{k,l}$ do not contribute to this integral, and thus

$$\langle\langle\hat{J}_{c_{1,p},\gamma_{c_{1,p}}}\hat{G}^A_{\gamma_{c_{1,p}},c_{1,p}}(\omega,\check{\varphi},\{\psi_{F,k,l}\},V)\rangle\rangle_{(1,1)} = \langle\langle\hat{J}_{c_{1,p},\gamma_{c_{1,p}}}\hat{G}^A_{\gamma_{c_{1,p}},c_{1,p}}(\omega,-\check{\varphi},\{\psi_{F,k,l}\},-V)\rangle\rangle_{(2,2)} \quad (127)$$

is independent of whether $\hat{G}^A_{\gamma_{c_{1,p}},c_{1,p}}(\omega,-\check{\varphi},\{\psi_{F,k,l}\},V)$ or $\hat{G}^A_{\gamma_{c_{1,p}},c_{1,p}}(\omega,-\check{\varphi},\{-\psi_{F,k,l}\},V)$ is averaged over $\{\psi_{F,k,l}\}$. In addition, the calculation is specific to the "quartet current" I_q, which is even if the voltage V changes sign.

The subtracted "retarded" terms are deduced from the "advanced" ones by taking the complex conjugate and changing $\check{\varphi}$ into $-\check{\varphi}$; see Sec. X A 1. We deduce the following expression of $\langle\langle I_{q,A}\rangle\rangle$:

$$\langle\langle I_{q,A}\rangle\rangle = \frac{2e}{\hbar}\sum_p\int d\omega n_F(\omega)\sum_{\check{n}\in S_{\check{n}}} \times\mathrm{Im}\langle\langle J_{c_{1,p},\gamma_{c_{1,p}}}G^A_{\check{n},\gamma_{c_{1,p}},c_{1,p}}(\omega,\{\psi_{F,k,l}\},V)\rangle\rangle\sin(\check{n}\cdot\check{\varphi}) + (V\to -V), \quad (128)$$

which takes the form of the Ambegaokar-Baratoff formula Eq. (105) for $I_{q,A}(V) = [I_A(V)+I_A(-V)]/2$.

Now, Eqs. (29)–(32) and Eq. (115) yield the following "nonequilibrium" contribution I_B to the current:

$$-I_B \equiv -I_{B,\gamma_{c_1}\to c_1} = \frac{e}{\hbar}\sum_p\int d\omega\{[\hat{J}_{c_{1,p},\gamma_{c_{1,p}}}\hat{G}^{+,-}_{B,\gamma_{c_{1,p}},c_{1,p}}]_{(1,1)/(0,0)} \times(\omega,\check{\varphi},\{\psi_{F,k,l}\},V) \quad (129)$$

$$-[\hat{J}_{c_{1,p},\gamma_{c_{1,p}}}\hat{G}^{+,-}_{B,\gamma_{c_{1,p}},c_{1,p}}]_{(2,2)/(0,0)}(\omega,\check{\varphi},\{\psi_{F,k,l}\},V) \quad (130)$$

$$-[\hat{J}_{\gamma_{c_{1,p}},c_{1,p}}\hat{G}^{+,-}_{B,c_{1,p},\gamma_{c_{1,p}}}]_{(1,1)/(0,0)}(\omega,\check{\varphi},\{\psi_{F,k,l}\},V) \quad (131)$$

$$+[\hat{J}_{\gamma_{c_{1,p}},c_{1,p}}\hat{G}^{+,-}_{B,c_{1,p},\gamma_{c_{1,p}}}]_{(2,2)/(0,0)}(\omega,\check{\varphi},\{\psi_{F,k,l}\},V)\}, \quad (132)$$

where $\hat{G}^{+,-}_B$ is given by Eq. (115).

We make use of the transformation $\mathscr{T}_{\text{Nambu}}$ given by Eq. (124) to obtain

$$[\hat{J}_{c_{1,p},\gamma_{c_{1,p}}}\hat{G}^{+,-}_{B,\gamma_{c_{1,p}},c_{1,p}}]_{(1,1)/(0,0)}(\omega,\check{\varphi},\{\psi_{F,k,l}\},V) - [\hat{J}_{c_{1,p},\gamma_{c_{1,p}}}\hat{G}^{+,-}_{B,\gamma_{c_{1,p}},c_{1,p}}]_{(2,2)/(0,0)}(\omega,\check{\varphi},\{\psi_{F,k,l}\},-V) = 2i\sum_{\check{n}\in S_{\check{n}}}[\hat{J}_{c_{1,p},\gamma_{c_{1,p}}}\hat{G}^{+,-}_{B,\gamma_{c_{1,p}},c_{1,p},\check{n}}]_{(1,1)/(0,0)}(\omega,\check{\varphi},\{\psi_{F,k,l}\},V) \times\sin(\check{n}\cdot\check{\varphi}). \quad (133)$$

Now, we note that $\hat{J}^\dagger = \hat{J}$ combined with

$$[\hat{g}^{A,R}(\omega,\check{\varphi},\{\psi_{F,k,l}\},V)]^\dagger = \hat{g}^{R,A}(\omega,\check{\varphi},\{\psi_{F,k,l}\},V) \quad (134)$$

and with the Dyson Eq. (23) leads to $(\hat{G}^{A,R})^\dagger = \hat{G}^{R,A}$. Conversely, combining with Eq. (115) yields $(\hat{G}^{+,-}_B)^\dagger = \hat{G}^{+,-}_B$. We deduce that $\langle\langle I_{q,B}\rangle\rangle$ takes the following form of the Ambegaokar-Baratoff formula:

$$\langle\langle I_{q,B}\rangle\rangle = \frac{2e}{\hbar}\sum_p\int d\omega n_F(\omega)\sum_{\check{n}\in S_{\check{n}}} \times\mathrm{Im}\langle\langle J_{c_{1,p},\gamma_{c_{1,p}}}G^{+,-}_{B,\check{n},\gamma_{c_{1,p}},c_{1,p}}(\omega,\{\psi_{F,k,l}\},V)\rangle\rangle\sin(\check{n}\cdot\check{\varphi}) + (V\to -V), \quad (135)$$

where $I_{q,B}(V) = [I_B(V)+I_B(-V)]/2$.

It is concluded that both Eq. (128) for the "quasiequilibrium quartet current" $\langle\langle I_{q,A}\rangle\rangle$ entering or exiting $S_{c,1}$ and Eq. (135) for the "nonequilibrium quartet current" $\langle\langle I_{q,B}\rangle\rangle$ take the form of the "generalized Ambegaokar-Baratoff formula" Eq. (105) where the coefficients $X(2n,p)$ acquire a dependence on the voltage V.

2. Conclusion on the Harvard group experiment [4]

It is deduced that the assumption of arbitrary interface transparencies and finite bias voltage V, combined with mimicking disorder in the superconducting leads by averaging over $\{k_F R_{k,l}\}$, leads to the following statement:

"*Experimental evidence for $I_c'(0)\neq I_c'(1/2)$*" implies "*Evidence for transmission of an odd number of Cooper pairs into S_{c_1} or S_{c_2}.*"

This statement implies "*Evidence for microscopic processes containing an odd number of electron-hole or hole-electron conversions in lead $S_{c,1}$.*"

Going one step further, we note that multiple quartet superconducting diffusion modes of the $\langle\langle g_{(1,2)}g_{(1,2)}\rangle\rangle$ type in Eqs. (49) and (50) necessarily imply even numbers of electron-hole or hole-electron conversions. Thus, the requirement of an odd number of electron-hole or hole-electron conversions in lead $S_{c,1}$ implies that at least one $\langle\langle g_{(1,1)}g_{(1,2)}\rangle\rangle$ mode of the 4TSQ-type is involved in the corresponding diagram; see Eqs. (49) and (51).

This argument relies on gathering the nonlocal Green's functions in a pairwise manner. It would break down for localized contacts such that $r_0 \lesssim l_e$, because the unpaired "local" electron-hole conversions would have to be taken into account on the same footing as the pairs of nonlocal Green's functions.

The paper is concluded with the following remark regarding the Harvard group experiment [4]:

"*Experimental evidence for different values of the critical currents between* $\Phi/\Phi_0 = 0$ *and* $\Phi/\Phi_0 = 1/2$*," i.e.,* $I_c'(0) \neq I_c'(1/2)$

implies

"*Evidence for the four-terminal 4TSQ.*"

This statement holds for arbitrary device parameters, and it was demonstrated within the physically motivated approximation of the model III discussed in the above Sec. IV D.

XI. CONCLUSIONS

Now, we provide a summary of the paper in Sec. XI A, specific conclusions on the Harvard group experiment in Sec. XI B, and final remarks and outlook in Sec. XI C.

A. Summary of the paper

In this paper, we provided a possible mechanism for the inversion in the critical current $I_c(\Phi/\Phi_0)$ on the quartet line in a four-terminal Josephson junction (see Figs. 1 and 3), in connection with the recent Harvard group experiment [4].

The Harvard group experiment [4] uses graphene gated away from the Dirac point, which was modeled as a simple 2D metal with a circular Fermi surface. We took the two dimensions of the graphene sheet into account while ignoring the effects related to the Dirac cones.

Specifically, we calculated microscopically the Josephson relations from lowest-order perturbation theory in the tunnel amplitudes, assuming in addition the adiabatic limit. We found that the three- and four-terminal quartet channels interfere with each other in the critical current on the quartet line. The "standard" three-terminal $3TQ_1$ transmit two pairs into $S_{c,1}$ and the three-terminal $3TQ_2$ transmit two pairs into $S_{c,2}$. The nonstandard four-terminal 4TSQs transmit two Coopers in the same quantum process but in a split manner, i.e., one pair into $S_{c,1}$ and the other one into $S_{c,2}$.

We found that the four-terminal 4TSQs do not contribute to the dc-current if a 1D or a 3D metal and multichannel contacts are used instead of the considered 2D metal. The importance of 2D is related to the general properties of the solutions of the wave equation, which imply a wake in even dimension (such as 2D) but not in odd dimension (such as 1D or 3D). We demonstrated that the "2D quantum wake" can synchronize two Josephson junctions by the exchange of a quasiparticle at the S_{c_1} and S_{c_2} contacts, yielding a nonvanishingly small four-terminal 4TSQ critical current.

We demonstrated that, with a 2D metal, lowest-order perturbation theory and the adiabatic limit produce π- and 0-shifted current-phase relations for the three-terminal $3TQ_1$, $3TQ_2$ and for the four-terminal 4TSQ, respectively. This implies inversion $I_c(0) < I_c(1/2)$ between the critical currents $I_c(0)$ and $I_c(1/2)$ at fluxes $\Phi/\Phi_0 = 0$ and $\Phi/\Phi_0 = 1/2$, respectively. In turn, experimental evidence for inversion implies $(\pi, 0)$ or $(0, \pi)$ shifts for the three-terminal $3TQ_1$, $3TQ_2$, and the four-terminal 4TSQ, respectively. This type of experiment cannot determine which of the three-terminal $3TQ_1$, $3TQ_2$, or the four-terminal 4TSQ is π-shifted, the other being 0-shifted.

We proposed an analogy with experiments on a SQUID containing π- and 0-shifted Josephson junctions [41]. In this analogy with Ref. [41], the π- and 0-shifted three-terminal $3TQ_1$, $3TQ_2$, and the four-terminal 4TSQ play the role of the π- or 0-shifted two-terminal Josephson junctions inserted in the SQUID loop, respectively.

In addition, the perturbative calculation predicts that the relative weight of the three-terminal $3TQ_1$, $3TQ_2$, and the four-terminal 4TSQ changes with gate voltage on the 2D metal, in a way that is compatible with the experimental data of the Harvard group [4].

We also generalized our theory to arbitrary interface transparencies and finite bias voltage V on the quartet line. This generalization was based on the even or odd parity of the number of Cooper pairs transmitted into $S_{c,1}$ or $S_{c,2}$ by the three-terminal $3TQ_1$, $3TQ_2$, and the four-terminal 4TSQ.

We treated the ingredients of "arbitrary interface transparencies" and "finite bias voltage" within a physically motivated approximation for disorder. The current entering or exiting $S_{c,1}$ takes the form of the generalized Ambegaokar-Baratoff relation from which we could infer that the 4TSQs imply different values for critical current $I_c(\Phi/\Phi_0)$ at $\Phi/\Phi_0 = 0$ and $\Phi/\Phi_0 = 1/2$. We argued within this framework of physically motivated approximation that "$I_c(0) \neq I_c(1/2)$" implies "evidence for the nonstandard four-terminal 4TSQ."

B. Specific conclusion on the Harvard group experiment [4]

To summarize, our theory teaches the following on the Harvard group experimental data [4]:

(i) Perturbation theory in the tunnel amplitudes combined with the $V = 0^+$ adiabatic limit produces the "inversion in $I_c(\Phi/\Phi_0)$ between $\Phi/\Phi_0 = 0$ and $\Phi/\Phi_0 = 1/2$" which is observed in the Harvard group experiment [4].

(ii) The calculated gate voltage dependence of the critical current oscillations as a function of magnetic field is compatible with the Harvard group experimental results [4].

(iii) We argued that "experimental evidence for $I_c(0) \neq I_c(1/2)$" implies "evidence for the four-terminal 4TSQ." Thus, our model implies that the Harvard group experiment [4] is evidence for the four-terminal 4TSQ.

C. Final remarks and outlook

The four-terminal 4TSQs shown in Figs. 6(c) and 6(d) and in Fig. 8 are robust against taking the long junction limit $R_0/x_0 \lesssim l_\varphi$ along the x-axis direction, where l_φ is the mesoscopic phase coherence length of the 2D metal. It is assumed in addition that the device remains short along the y-direction, i.e., $R_0/y_0 \lesssim \xi_{\rm dirty}(0)$. The device geometry is shown in Fig. 3.

More precisely, the nonlocal $\langle\langle g_{(1,1)} g_{(1,1)}\rangle\rangle$ mode connects $S_{c,1}$ and $S_{c,2}$ through the 2D metal by the quantum wake; see the highlighted section of the four-terminal 4TSQ diagram in Fig. 6(d). Equation (16) provides the expression of each one-particle Green's function $g_{(1,1)}$ entering the $\langle\langle g_{(1,1)} g_{(1,1)}\rangle\rangle$ mode through the 2D metal. Both nonlocal $g_{(1,1)}$ are in the "electron-electron" channel and they are both evaluated at the same wave vector $k_e = k_F + \omega/v_F$. Thus, $\langle\langle g_{(1,1)} g_{(1,1)}\rangle\rangle$ is not washed out by multichannel averaging if the energy ω is larger

than the Thouless energy $\hbar v_F/R$ associated with the separation R between the contacts. This is why the four-terminal 4TSQ critical current given by the diagram in Fig. 8(d) remains large as long as the device dimension R_0/x_0 along the x-axis is in the mesoscopic domain, i.e., $R_0/x_0 \lesssim l_\varphi$.

In addition, the $V = 0$ limit of phase-biased superconductors (instead of the $V = 0^+$ adiabatic limit of a voltage-biased device) also involves long-distance coupling between the Andreev bound states associated with each pair of Josephson junctions sharing a 2D metal as a common weak link, according to $R_0/x_0 \lesssim l_\varphi$ mentioned above in the geometry in Fig. 3.

These arguments show that the four-terminal 4TSQs constitute a nonstandard "mesoscopic" channel of quantum coherent synchronization, which operates in between the quartets at the smallest scale and the early 1980s synchronization of macroscopic Josephson circuits [42,43]. An interesting complementary point of view is to approach this mesoscopic regime from the classical limit, i.e., to incorporate quantum fluctuation in the classical circuit models.

We also note that comparing Eq. (65) for the three-terminal $3TQ_1$ critical current $I_{c,\,3TQ_1}$ to Eq. (84) for the four-terminal 4TSQ critical current $I^{(2)}_{c,\,4TSQ}$ leads to the following order of magnitude for their ratio:

$$K = \left|\frac{I^{(2)}_{c,\,4TSQ}}{I_{c,\,3TQ_1}}\right| \approx \left(\frac{J_0}{W}\right)^4 \frac{\sqrt{\mathscr{S}_{\text{contact}}}}{l_e}. \tag{136}$$

It was assumed implicitly in this paper that perturbation theory is converging, which implies $K < 1$. Paper III of the series [24] will address resummations of the perturbative expansions if the diffusion modes proliferate for $K > 1$.

Finally, we point out that, in the presence of Coulomb interactions, the charging energy is larger for the three-terminal $3TQ_1$ and $3TQ_2$ (involving four fermions in $S_{c,1}$ or four fermions in $S_{c,2}$) than for the four-terminal 4TSQ (involving one pair in $S_{c,1}$ and another one in $S_{c,2}$). Thus, static Coulomb interactions favor the nonstandard four-terminal 4TSQ over the three-terminal $3TQ_1$, $3TQ_2$. It would be interesting to address dynamical Coulomb blockade [44] for the device in Figs. 1 and 3.

ACKNOWLEDGMENTS

The author acknowledges the stimulating collaboration with the Harvard group (K. Huang, Y. Ronen, and P. Kim) on Secs. V A and V B. The author wishes to thank R. Danneau and B. Douçot for their collaboration on an early attempt to find signatures of the 2D quantum wake in the signal of multiple Andreev reflection through bilayer graphene. R. Danneau also provided useful comments on an early version of the manuscript. The author acknowledges fruitful discussions with D. Feinberg. The author thanks the Infrastructure de Calcul Intensif et de Données (GRICAD) for use of the resources of the Mésocentre de Calcul Intensif de l'Université Grenoble-Alpes (CIMENT). The author acknowledges support from the French National Research Agency (ANR) in the framework of the Graphmon project (ANR 19-CE47-0007).

APPENDIX A: GREEN'S FUNCTION OF A 2D METAL

We start this Appendix with the Fourier transform of the Green's function between two tight-binding sites separated by distance R:

$$g^{A,(1,1)/(2,2)}(R,\omega) = \int_{-\pi}^{\pi} d\theta \int_0^{+\infty} \frac{kdk}{(2\pi)^2} \exp(ikR\cos\theta) g^{A,(1,1)/(2,2)}(\mathbf{k},\omega), \tag{A1}$$

where

$$g^{A,(1,1)}(\mathbf{k},\omega) = \frac{1}{\omega - \xi_{\mathbf{k}} - i\eta}, \tag{A2}$$

$$g^{A,(2,2)}(\mathbf{k},\omega) = \frac{1}{\omega + \xi_{\mathbf{k}} - i\eta}, \tag{A3}$$

with $\xi_{\mathbf{k}}$ the kinetic energy of the 2D plane-wave state $\mathbf{k}$ with respect to the chemical potential $\mu = \hbar^2 k_F^2/2m$, and where k_F and m are the Fermi wave vector and the band mass, respectively. The superscripts "(1,1)" or "(2,2)" in Eqs. (A1)–(A3) refer to propagation in the electron-electron or hole-hole channels, respectively.

Equation (A1) is written as

$$g^A(R,\omega) = \int_0^{+\infty} \frac{kdk}{(2\pi)} \frac{J_0(kR)}{\omega - \varepsilon\xi_{\mathbf{k}} - i\eta}, \tag{A4}$$

where the Bessel function

$$J_0(x) = \frac{1}{2\pi}\int_{-\pi}^{\pi} \exp(ix\cos\theta) d\theta \tag{A5}$$

was introduced in Eq. (A4). The parameter ε takes the values $\varepsilon = \pm 1$ for the (1,1) and (2,2) components, respectively. We consider a pole at

$$k \equiv k_0 \simeq k_F + \frac{\varepsilon(\omega - i\eta)}{v_F} \tag{A6}$$

and the residue is evaluated according to

$$\omega - \varepsilon\xi_{k_0+\delta k} - i\eta \simeq -\frac{\hbar^2}{2m}\varepsilon k_0 \delta k \simeq -\varepsilon v_F k_0 \delta k. \tag{A7}$$

Considering in addition that $\text{sgn}(\text{Im}k_0) = -\varepsilon$ and using contour integration in the complex k plane leads to

$$g^{A,(1,1)}(R) = g^{A,(2,2)}(R) = \frac{i}{W} J_0(k_F R), \tag{A8}$$

$$g^{R,(1,1)}(R) = g^{R,(2,2)}(R) = -\frac{i}{W} J_0(k_F R), \tag{A9}$$

where the limit $\omega R/v_F \lesssim 1$ is considered. Noting that ω has a typical order of magnitude set by the superconducting gap, the condition $\omega R/v_F \lesssim 1$ yields the short junction limit $R \lesssim \xi_{\text{ball}}(0)$ for each pair of superconductor–2D metal–superconductor Josephson junction, where the ballistic superconducting coherence length is given by Eqs. (5) and (21).

Equations (A8) and (A9) lead to Eqs. (16)–(19) if the realistic condition $2\pi/k_F \ll R \lesssim \xi_{\text{ball}}(0)$ is fulfilled on the separation R.

APPENDIX B: SUPERCONDUCTING DIFFUSION MODES IN THE DIRTY LIMIT

The goal of this Appendix is to treat disorder in the superconducting leads of the considered four-terminal device. The calculations are based on Ref. [37].

Averaging the one-particle Green's functions over disorder in the Born approximation is summarized in Appendix B 1. Appendix B 2 presents the calculation of the disorder-averaged superconducting modes in the dirty limit.

The superconducting modes are formed with products of Nambu Green's functions scattering together on the same configuration of disorder; see Sec. IV C.

Now, the superconducting diffusion modes are calculated in the ladder approximation.

1. One-particle Green's function averaged over disorder

We start with the expression of the average over disorder of the one-particle Green's functions [36].

Using the notations of Ref. [37], the average superconducting Green's function takes the following form in the Born approximation:

$$\hat{g}^{A,R}(\xi_{\mathbf{k}},\omega)=\frac{\hat{\mathscr{N}}_{\mathbf{k}}(\omega)}{\mathscr{D}_{\mathbf{k}}(\omega)}, \tag{B1}$$

with

$$\hat{\mathscr{N}}_{\mathbf{k}}(\omega)=\overline{\omega}\mp i\eta+\xi_{\mathbf{k}}\hat{\tau}_3+\overline{\Delta}\hat{\tau}_1, \tag{B2}$$

$$\mathscr{D}_{\mathbf{k}}(\omega)=(\overline{\omega}\mp i\eta)^2-\overline{\Delta}^2-\xi_{\mathbf{k}}^2, \tag{B3}$$

where ω and $\mathbf{k}$ refer to the energy and wave vector, respectively. The notations $\overline{\omega}$, $\overline{\Delta}$, and $s(\omega)$ stand for

$$\overline{\omega}=\omega\left(1+\frac{1}{s(\omega)\tau}\right), \tag{B4}$$

$$\overline{\Delta}=\Delta\left(1+\frac{1}{s(\omega)\tau}\right), \tag{B5}$$

$$s^2(\omega)=\Delta^2-\omega^2. \tag{B6}$$

2. Product of two Green's functions averaged over disorder

Now, we evaluate the average over disorder of the product of two Nambu Green's functions. An intermediate result on two integrals is presented in Appendix B 2 a. The resummation of the ladders is presented in Appendix B 2 b.

a. Intermediate result on evaluation of useful integrals

Following Ref. [37], we evaluate the following integrals at energy $|\omega|<\Delta$ within the gap:

$$\mathscr{I}_{\alpha}^{A,A}(\mathbf{q},\omega)=v^2\int\frac{d\mathbf{k}}{(2\pi)^3}\hat{\tau}_3\hat{g}^A(\xi_{\mathbf{k}},\omega)\hat{\tau}_\alpha\hat{g}^A(\xi_{\mathbf{k}+\mathbf{q}},\omega)\hat{\tau}_3, \tag{B7}$$

$$\mathscr{I}_{\alpha}^{A,R}(\mathbf{q},\omega)=v^2\int\frac{d\mathbf{k}}{(2\pi)^3}\hat{\tau}_3\hat{g}^A(\xi_{\mathbf{k}},\omega)\hat{\tau}_\alpha\hat{g}^R(\xi_{\mathbf{k}+\mathbf{q}},\omega)\hat{\tau}_3, \tag{B8}$$

where $\hat{\tau}_\alpha$ are the 2×2 Pauli matrices.

The first step of the calculation is to combine the relation

$$\int\frac{d\mathbf{k}}{(2\pi)^3}=\frac{1}{8\pi^2}\int_{-1}^{1}du\int_{-\infty}^{+\infty}k^2dk\exp(ikRu) \tag{B9}$$

to contour integration for the integral over k.

The poles of $\hat{g}^A(\xi_{\mathbf{k}},\omega)$ are given by the solutions of $\mathscr{D}_{\mathbf{k}}^A(\omega)=0$ at $k=k_0$, namely

$$\xi_{\mathbf{k}_0}^2=\overline{\omega}^2-\overline{\Delta}^2-2i\eta\overline{\omega}=0. \tag{B10}$$

A branch-cut along the $\omega<0$ axis leads to

$$\xi_{\mathbf{k}_0}^{(\varepsilon)}(\omega)=i\varepsilon\sqrt{\overline{\Delta}^2-\overline{\omega}^2}, \tag{B11}$$

with

$$\varepsilon=\mathrm{sgn}(-\eta\overline{\omega}). \tag{B12}$$

The solutions of Eq. (B11) for $k_0>0$ or $k_0<0$ are given by

$$k_0^{(\varepsilon,\varepsilon')}(\omega)=\varepsilon'\left(k_F+\frac{i\varepsilon\overline{s}(\omega)}{\hbar v_F}\right), \tag{B13}$$

with $\varepsilon'=\pm$.

No reason is advocated for why a constraint holds between $\mathrm{Re}[k_0(\omega)]$ and $\mathrm{Im}[k_0(\omega)]$. Instead, the four solutions are relevant to a double interface, i.e., those with exponential growth or decay along the positive or negative directions of propagation. For instance, the four waves are involved in the solution of the Bogoliubov–de Gennes equations within the Blonder-Tinkham-Klapwijk approach [45] for a normal metal–superconductor–normal metal double junction [46], with separation between the contacts comparable to the superconducting coherence length. Thus, the four wave vectors $k_0^{(\varepsilon,\varepsilon')}$ in Eq. (B13) are taken into account in the following, where ε and ε' are free to take the values $\varepsilon=\pm$ and $\varepsilon'=\pm$.

To obtain the residue, we evaluate $\mathscr{D}_{\mathbf{k}}(\omega)$ for $k=k_0^{(\varepsilon,\varepsilon')}(\omega)+\delta k$ in the limit $\delta k\to 0$:

$$\mathscr{D}_{k_0+\delta k}(\omega)\simeq -2\frac{\hbar^2}{m}k_0^{(\varepsilon,\varepsilon')}(\omega)\xi_{k_0}^{(\varepsilon)}(\omega)\delta k. \tag{B14}$$

Next, we expand $\mathscr{D}_{\mathbf{k}_0+\mathbf{q}}(\omega)$ according to

$$\mathscr{D}_{\mathbf{k}_0+\mathbf{q}}(\omega)\simeq -\frac{\hbar^2}{m}k_0^{(\varepsilon,\varepsilon')}(\omega)qu\left\{2\xi_{\mathbf{k}_0}^{(\varepsilon)}(\omega)+\frac{\hbar^2}{m}k_0^{(\varepsilon,\varepsilon')}(\omega)qu\right\} \tag{B15}$$

and we expand $\hat{\mathscr{N}}_{\mathbf{k}_0+\mathbf{q}}(\omega)$ according to

$$\hat{\mathscr{N}}_{\mathbf{k}_0+\mathbf{q}}(\omega)\simeq\hat{\mathscr{N}}_{\mathbf{k}_0}(\omega)+qu\left(\frac{\hbar^2k_0^{(\varepsilon,\varepsilon')}(\omega)}{m}\hat{\tau}_3\right). \tag{B16}$$

Evaluating the contribution proportional to qu in Eq. (B16) leads to a term that is subleading in the limit of a dirty superconductor, i.e., if the elastic scattering time is much smaller than $\hbar/\Delta$.

Contour integration leads to the dominant contribution of the pole at $k_0^{(\varepsilon,\varepsilon')}(\omega)$ in $\hat{g}^A(\xi_{\mathbf{k}},\omega)$ in Eqs. (B7)

and (B8):

$$\mathscr{I}_{\alpha}^{A,A}(\mathbf{q},\omega,\hat{\tau}_{\alpha}) = \mathscr{I}_{\alpha}^{A,R}(\mathbf{q},\omega,\hat{\tau}_{\alpha}) = \frac{i\varepsilon\varepsilon' v^2}{4\pi}\int_{-1}^{1} du \sum_{\varepsilon,\varepsilon'=\pm} \frac{\hat{\tau}_3\big(\overline{\omega}+\xi_{k_0}^{(\varepsilon)}\hat{\tau}_3+\overline{\Delta}\hat{\tau}_1\big)\hat{\tau}_{\alpha}\big(\overline{\omega}+\tilde{\xi}_{k_0}^{(\varepsilon)}\hat{\tau}_3+\overline{\Delta}\hat{\tau}_1\big)\hat{\tau}_3}{\big(\frac{-2\hbar^2 k_0^{(\varepsilon,\varepsilon')}(\omega)}{m}\big)^2\big(1+\frac{\hbar^2 k_0^{(\varepsilon,\varepsilon')}(\omega)qu}{2m\xi_{k_0}^{(\varepsilon)}}\big)qu}, \tag{B17}$$

to which is added the "$u \to -u$" contribution from the pole k_1 of $\hat{g}^{A,R}(\xi_{\mathbf{k}+\mathbf{q}},\omega)$ in Eqs. (B7) and (B8), defined as $\mathscr{D}^{A}_{\mathbf{k}_1+\mathbf{q}}(\omega)=0$.

Selecting $\tilde{\xi}_{k_0}^{(\varepsilon)} = (\xi_{k_0}^{(\varepsilon)})^*$ in Eq. (B17) involves the product mentioned above of "forward-moving exponentially decay" and "backward-moving exponentially growth," which leads to

$$\mathscr{I}_{\alpha}^{A,A}(\mathbf{q},\omega,\hat{\tau}_{\alpha}) = \mathscr{I}_{\alpha}^{A,R}(\mathbf{q},\omega,\hat{\tau}_{\alpha}). \tag{B18}$$

This identity is compatible with the real-valued $\hat{g}^{A}_{\mathbf{x}_1,\mathbf{x}_2}(\omega) = \hat{g}^{R}_{\mathbf{x}_1,\mathbf{x}_2}(\omega)$ if $|\omega| < \Delta$ and $\eta = 0^+$; see Eq. (20). Namely, the real-space Dyson equations used to describe scattering on disorder take real values, which is compatible with the preceding Eq. (B18) obtained from integration over the wave vector $\mathbf{k}$.

The next step is to evaluate the numerator of Eq. (B17) for all Pauli matrices $\hat{\tau}_{\alpha}$. We separate between the following contributions:

$$(\overline{\omega}+i\overline{s}\hat{\tau}_3+\overline{\Delta}\hat{\tau}_1)\hat{\tau}_{\alpha}(\overline{\omega}-i\overline{s}\hat{\tau}_3+\overline{\Delta}\hat{\tau}_1) = \hat{X}^{(1)}+\hat{X}^{(2)}, \tag{B19}$$

with

$$\hat{X}^{(1)}(\hat{\tau}_{\alpha}) = (\overline{\omega}+\overline{\Delta}\hat{\tau}_1)\hat{\tau}_{\alpha}(\overline{\omega}+\overline{\Delta}\hat{\tau}_1)+\overline{s}^2\hat{\tau}_3\hat{\tau}_{\alpha}\hat{\tau}_3, \tag{B20}$$

$$\hat{X}^{(2)}(\hat{\tau}_{\alpha}) = i\overline{s}[\hat{\tau}_3\hat{\tau}_{\alpha}(\overline{\omega}+\overline{\Delta}\hat{\tau}_1)-(\overline{\omega}+\overline{\Delta}\hat{\tau}_1)\hat{\tau}_3\hat{\tau}_{\alpha}]. \tag{B21}$$

A straightforward calculation leads to

$$\hat{X}^{(1)}(\hat{I}) = 2\overline{\Delta}^2\hat{I}+2\overline{\omega}\overline{\Delta}\hat{\tau}_1, \tag{B22}$$

$$\hat{X}^{(1)}(\hat{\tau}_1) = 2\overline{\omega}\overline{\Delta}\hat{I}+2\overline{\omega}^2\hat{\tau}_1, \tag{B23}$$

$$\hat{X}^{(1)}(\hat{\tau}_3) = 0, \tag{B24}$$

$$\hat{X}^{(1)}(\hat{\tau}_3\hat{\tau}_1) = -2(\overline{\Delta}^2-\overline{\omega}^2)\hat{\tau}_3\hat{\tau}_1. \tag{B25}$$

Expanding Eq. (B17) to order u^2 and integrating over the variable u leads to the following contributions to Eq. (B17):

$$\begin{aligned}\mathscr{I}^{A,A,(1)}(\mathbf{q},\omega,\hat{I}) &= \mathscr{I}^{A,R,(1)}(\mathbf{q},\omega,\hat{I})\\ &= \mathscr{A}[\overline{\Delta}^2\hat{I}-\overline{\omega}\overline{\Delta}\hat{\tau}_1],\end{aligned} \tag{B26}$$

$$\begin{aligned}\mathscr{I}^{A,A,(1)}(\mathbf{q},\omega,\hat{\tau}_1) &= \mathscr{I}^{A,R,(1)}(\mathbf{q},\omega,\hat{\tau}_1)\\ &= \mathscr{A}[\overline{\omega}\overline{\Delta}\hat{I}-\overline{\omega}^2\hat{\tau}_1],\end{aligned} \tag{B27}$$

$$\begin{aligned}\mathscr{I}^{A,A,(1)}(\mathbf{q},\omega,\hat{\tau}_3) &= \mathscr{I}^{A,R,(1)}(\mathbf{q},\omega,\hat{\tau}_3)\\ &= 0,\end{aligned} \tag{B28}$$

$$\begin{aligned}\mathscr{I}^{A,A,(1)}(\mathbf{q},\omega,\hat{\tau}_3\hat{\tau}_1) &= \mathscr{I}^{A,R,(1)}(\mathbf{q},\omega,\hat{\tau}_3\hat{\tau}_1)\\ &= -\mathscr{A}(\overline{\Delta}^2-\overline{\omega}^2)\hat{\tau}_3\hat{\tau}_1,\end{aligned} \tag{B29}$$

with

$$\mathscr{A} = \frac{k_F^3}{16\pi[\overline{s}(\omega)]^3\varepsilon_F}\left[1-\frac{v_F^2q^2}{12[\overline{s}(\omega)]^2}\right]. \tag{B30}$$

The notation $\overline{s}(\omega)$ in Eq. (B30) stands for $[\overline{s}(\omega)]^2 = \overline{\Delta}^2-\overline{\omega}^2$, where $\overline{\omega}$ and $\overline{\Delta}$ are given by Eqs. (B4) and (B5), respectively.

b. Summing the 2 × 2 matrix geometric series in the ladder approximation

Iterating Eqs. (B26) and (B27) to form the first "rungs" of the superconducting diffusion modes in the ladder approximation yields

$$\begin{aligned}&\mathscr{I}^{A,A,(1)}(\mathbf{q},\omega,\mathscr{I}^{A,A,(1)}(\mathbf{q},\omega,\hat{I}))\\ &\quad= \mathscr{A}[\overline{\Delta}^2-\overline{\omega}^2]\mathscr{I}^{A,A,(1)}(\mathbf{q},\omega,\hat{I}),\end{aligned} \tag{B31}$$

$$\begin{aligned}&\mathscr{I}^{A,A,(1)}(\mathbf{q},\omega,\mathscr{I}^{A,A,(1)}(\mathbf{q},\omega,\hat{\tau}_1))\\ &\quad= \mathscr{A}[\overline{\Delta}^2-\overline{\omega}^2]\mathscr{I}^{A,A,(1)}(\mathbf{q},\omega,\hat{\tau}_1),\end{aligned} \tag{B32}$$

where $\mathscr{A}$ is given by Eq. (B30).

We find the following at the next order:

$$\begin{aligned}&\mathscr{I}^{A,A,(1)}(\mathbf{q},\omega,\mathscr{I}^{A,A,(1)}(\mathbf{q},\omega,\mathscr{I}^{A,A,(1)}(\mathbf{q},\omega,\hat{I})))\\ &\quad= [\mathscr{A}[\overline{\Delta}^2-\overline{\omega}^2]]^2\mathscr{I}^{A,A,(1)}(\mathbf{q},\omega,\hat{I}),\end{aligned} \tag{B33}$$

$$\begin{aligned}&\mathscr{I}^{A,A,(1)}(\mathbf{q},\omega,\mathscr{I}^{A,A,(1)}(\mathbf{q},\omega,\hat{\tau}_1))\\ &\quad= [\mathscr{A}[\overline{\Delta}^2-\overline{\omega}^2]]^2\mathscr{I}^{A,A,(1)}(\mathbf{q},\omega,\hat{\tau}_1).\end{aligned} \tag{B34}$$

Summing all terms to infinite order leads to the disorder-averaged superconducting diffusion modes:

$$\begin{aligned}\overline{\hat{g}\hat{I}\hat{g}}(q,\omega) &= \frac{1}{16\pi W}\frac{1}{2\sqrt{\Delta^2-\omega}+\mathscr{D}q^2}\\ &\quad\times\frac{\Delta^2\hat{I}+\omega\Delta\hat{\tau}_1}{\Delta^2-\omega^2},\end{aligned} \tag{B35}$$

$$\begin{aligned}\overline{\hat{g}\hat{\tau}_1\hat{g}}(q,\omega) &= \frac{1}{16\pi W}\frac{1}{2\sqrt{\Delta^2-\omega^2}+\mathscr{D}q^2}\\ &\quad\times\frac{\omega\Delta\hat{I}-\omega^2\hat{\tau}_1}{\Delta^2-\omega^2},\end{aligned} \tag{B36}$$

$$\overline{\hat{g}\hat{\tau}_3\hat{g}}(q,\omega) = 0, \tag{B37}$$

$$|\overline{\hat{g}\hat{\tau}_3\hat{\tau}_1\hat{g}}(q,\omega)| \ll |\overline{\hat{g}\hat{I}\hat{g}}(q,\omega)|, \tag{B38}$$

$$|\overline{\hat{g}\hat{\tau}_3\hat{\tau}_1\hat{g}}(q,\omega)| \ll |\overline{\hat{g}\hat{\tau}_1\hat{g}}(q,\omega)|, \tag{B39}$$

where the diffusion constant is $\mathscr{D} = v_F^2\tau/3$.

Expanding the Nambu components of Eq. (B36) leads to

$$[\overline{\hat{g}\hat{I}\hat{g}}(q,\omega)]_{(1,1)} = \overline{\hat{g}_{(1,1)}\hat{g}_{(1,1)}}(q,\omega)+\overline{\hat{g}_{(1,2)}\hat{g}_{(2,1)}}(q,\omega), \tag{B40}$$

$$[\overline{\hat{g}\hat{I}\hat{g}}(q,\omega)]_{(1,2)} = \overline{\hat{g}_{(1,1)}\hat{g}_{(1,2)}}(q,\omega)+\overline{\hat{g}_{(1,2)}\hat{g}_{(2,2)}}(q,\omega), \tag{B41}$$

$$[\overline{\hat{g}\hat{I}\hat{g}}(q,\omega)]_{(1,1)} = \overline{\hat{g}_{(2,1)}\hat{g}_{(1,1)}}(q,\omega)+\overline{\hat{g}_{(2,2)}\hat{g}_{(2,1)}}(q,\omega), \tag{B42}$$

$$[\overline{\hat{g}\hat{f}\hat{g}}(q,\omega)]_{(1,2)} = \overline{\hat{g}_{(2,1)}\hat{g}_{(1,2)}}(q,\omega) + \overline{\hat{g}_{(2,2)}\hat{g}_{(2,2)}}(q,\omega). \tag{B43}$$

Similarly, expanding the Nambu components of Eq. (B36) leads to

$$[\overline{\hat{g}\hat{\tau}_1\hat{g}}]_{(1,1)}(q,\omega) = \overline{\hat{g}_{(1,1)}\hat{g}_{(2,1)}}(q,\omega) + \overline{\hat{g}_{(1,2)}\hat{g}_{(1,1)}}(q,\omega), \tag{B44}$$

$$[\overline{\hat{g}\hat{\tau}_1\hat{g}}]_{(1,2)}(q,\omega) = \overline{\hat{g}_{(1,1)}\hat{g}_{(2,2)}}(q,\omega) + \overline{\hat{g}_{(1,2)}\hat{g}_{(1,2)}}(q,\omega), \tag{B45}$$

$$[\overline{\hat{g}\hat{\tau}_1\hat{g}}]_{(1,1)}(q,\omega) = \overline{\hat{g}_{(2,1)}\hat{g}_{(2,1)}}(q,\omega) + \overline{\hat{g}_{(2,2)}\hat{g}_{(1,1)}}(q,\omega), \tag{B46}$$

$$[\overline{\hat{g}\hat{\tau}_1\hat{g}}]_{(1,2)}(q,\omega) = \overline{\hat{g}_{(2,1)}\hat{g}_{(2,2)}}(q,\omega) + \overline{\hat{g}_{(2,2)}\hat{g}_{(1,2)}}(q,\omega). \tag{B47}$$

Combining Eqs. (B35)–(B39) and Eqs. (B40)–(B43) with Eqs. (B44)–(B47), and then replacing Eqs. (B38) and (B39) by $\overline{\hat{g}\hat{\tau}_3\hat{\tau}_1\hat{g}}(q,\omega) = 0$ yields

$$\overline{g_{(1,1)}g_{(1,1)}}(q,\omega) = \overline{g_{(2,2)}g_{(2,2)}}(q,\omega) = \frac{1}{16\pi W}\frac{1}{2\sqrt{|\Delta|^2-\omega}+\mathscr{D}q^2}\frac{|\Delta|^2}{|\Delta|^2-\omega^2}, \tag{B48}$$

$$\overline{g_{(1,2)}g_{(2,1)}}(q,\omega) = \overline{g_{(2,1)}g_{(1,2)}}(q,\omega) = \frac{1}{16\pi W}\frac{1}{2\sqrt{|\Delta|^2-\omega}+\mathscr{D}q^2}\frac{|\Delta|^2}{|\Delta|^2-\omega^2}, \tag{B49}$$

where Eqs. (B48) and (B49) are relevant to elastic cotunneling (EC) [25,26] and crossed Andreev reflection (CAR) [25–27] in a three-terminal normal metal–superconductor–normal metal device, with contacts separated by distance comparable to the superconducting coherence length.

Equations (B35)–(B39), (B40)–(B43), and (B44)–(B47) yield

$$\overline{g_{(1,2)}g_{(1,2)}}(q,\omega) = \frac{1}{16\pi W}\frac{1}{2\sqrt{|\Delta|^2-\omega}+\mathscr{D}q^2}\frac{|\Delta|^2\exp(2i\varphi_N)}{|\Delta|^2-\omega^2}, \tag{B50}$$

$$\overline{g_{(2,1)}g_{(2,1)}}(q,\omega) = \frac{1}{16\pi W}\frac{1}{2\sqrt{|\Delta|^2-\omega}+\mathscr{D}q^2}\frac{|\Delta|^2\exp(-2i\varphi_N)}{|\Delta|^2-\omega^2}, \tag{B51}$$

where φ_N is the macroscopic phase variable of the considered superconductor S_N. Equation (B50) is relevant to double crossed Andreev reflection [5,6] and to the three-terminal $3TQ_1$, $3TQ_2$ in the presence of biasing at opposite voltages, with distance between the interfaces approximately set by the superconducting coherence length.

Equations (B35)–(B39), (B40)–(B43) and (B44)–(B47) imply

$$\overline{g_{(1,1)}g_{(2,2)}}(q,\omega) = \overline{g_{(2,2)}g_{(1,1)}}(q,\omega) = \frac{1}{16\pi W}\frac{1}{2\sqrt{|\Delta|^2-\omega}+\mathscr{D}q^2}\frac{2\omega^2-|\Delta|^2}{|\Delta|^2-\omega^2}, \tag{B52}$$

which is relevant to double elastic cotunneling [5] (dEC) in a three-terminal Josephson junction biased at identical voltages.

Finally, the following superconducting diffusion modes are relevant to the four-terminal 4TSQ that is the subject of this paper, and it is also relevant to the normal metal–superconductor–superconductor double junction of Ref. [38]:

$$\overline{g_{(1,1)}g_{(1,2)}}(q,\omega) = \overline{g_{(2,2)}g_{(1,2)}}(q,\omega) = \overline{g_{(1,2)}g_{(1,1)}}(q,\omega) = \overline{g_{(1,2)}g_{(2,2)}}(q,\omega) = \frac{1}{16\pi W}\frac{1}{2\sqrt{|\Delta|^2-\omega}+\mathscr{D}q^2}\frac{\omega|\Delta|\exp(i\varphi_N)}{|\Delta|^2-\omega^2} \tag{B53}$$

and

$$\overline{g_{(2,2)}g_{(2,1)}}(q,\omega) = \overline{g_{(1,1)}g_{(2,1)}}(q,\omega) = \overline{g_{(2,1)}g_{(2,2)}}(q,\omega) = \overline{g_{(2,1)}g_{(1,1)}}(q,\omega) = \frac{1}{16\pi W}\frac{1}{2\sqrt{|\Delta|^2-\omega}+\mathscr{D}q^2} \times\frac{\omega|\Delta|\exp(-i\varphi_N)}{|\Delta|^2-\omega^2}. \tag{B54}$$

Equations (50) and (51) in Sec. IV C are deduced from Eqs. (B50) and (B53), respectively.

APPENDIX C: THE BALLISTIC LIMIT

This Appendix addresses the limit of ballistic superconducting leads, which is relevant to the model III introduced in Sec. IV D.

The expression of the ballistic superconducting diffusion modes is provided in Appendix C 1. Appendix C 2 provides an explanation for different signs in the dirty and ballistic limits of $\langle\langle g_{(1,1)}g_{(1,2)}\rangle\rangle$.

1. Expression of the superconducting modes of a ballistic superconductor

Now, we provide the expression of the ballistic superconducting modes propagating in the superconducting lead S_N with phase φ_N on the basis of averaging over $k_F R_1$ the product of Nambu superconducting Green's functions given in Eq. (20):

$$\overline{g^A_{(1,1)}(R_{\alpha,\beta},\omega)g^A_{(1,1)}(R_{\beta,\alpha},\omega)} = \overline{g^A_{(2,2)}(R_{\alpha,\beta},\omega)g^A_{(2,2)}(R_{\beta,\alpha},\omega)} = \frac{1}{2W^2(k_F R_1)^2}\frac{\Delta^2}{\Delta^2-\omega^2}\exp\left(-\frac{2R_1}{\xi_{\rm ball}(\omega)}\right), \tag{C1}$$

$$\overline{g^A_{(1,2)}(R_{\alpha,\beta},\omega)g^A_{(2,1)}(R_{\beta,\alpha},\omega)} = \overline{g^A_{(2,1)}(R_{\alpha,\beta},\omega)g^A_{(2,1)}(R_{\beta,\alpha},\omega)} = \frac{1}{2W^2(k_F R_1)^2}\frac{\Delta^2}{\Delta^2-\omega^2}\exp\left(-\frac{2R_1}{\xi_{\rm ball}(\omega)}\right), \tag{C2}$$

$$\overline{g^A_{(1,2)}(R_{\alpha,\beta},\omega)g^A_{(1,2)}(R_{\beta,\alpha},\omega)} = \frac{1}{2W^2(k_F R_1)^2}\frac{\Delta^2}{\Delta^2-\omega^2}\exp\left(-\frac{2R_1}{\xi_{\rm ball}(\omega)}\right)\exp(2i\varphi_N), \tag{C3}$$

$$\overline{g^A_{(2,1)}(R_{\alpha,\beta},\omega)g^A_{(2,1)}(R_{\beta,\alpha},\omega)} = \frac{1}{2W^2(k_F R_1)^2}\frac{\Delta^2}{\Delta^2-\omega^2}\exp\left(-\frac{2R_1}{\xi_{\rm ball}(\omega)}\right)\exp(-2i\varphi_N), \tag{C4}$$

$$\overline{g^A_{(1,1)}(R_{\alpha,\beta},\omega)g^A_{(2,2)}(R_{\beta,\alpha},\omega)} = \overline{g^A_{(2,2)}(R_{\alpha,\beta},\omega)g^A_{(1,1)}(R_{\beta,\alpha},\omega)} = \frac{1}{2W^2(k_F R_1)^2}\frac{2\omega^2-\Delta^2}{\Delta^2-\omega^2}\exp\left(-\frac{2R_1}{\xi_{\rm ball}(\omega)}\right), \tag{C5}$$

$$\begin{aligned}\overline{g^A_{(1,1)}(R_{\alpha,\beta},\omega)g^A_{(1,2)}(R_{\beta,\alpha},\omega)} &= \overline{g^A_{(2,2)}(R_{\alpha,\beta},\omega)g^A_{(1,2)}(R_{\beta,\alpha},\omega)} = \overline{g^A_{(1,2)}(R_{\alpha,\beta},\omega)g^A_{(1,1)}(R_{\beta,\alpha},\omega)} = \overline{g^A_{(1,2)}(R_{\alpha,\beta},\omega)g^A_{(1,2)}(R_{\beta,\alpha},\omega)}\\ &= \frac{1}{2W^2(k_F R_1)^2}\frac{-\omega\Delta}{\Delta^2-\omega^2}\exp\left(-\frac{2R_1}{\xi_{\rm ball}(\omega)}\right)\exp(i\varphi_N),\end{aligned} \tag{C6}$$

$$\begin{aligned}\overline{g^A_{(1,1)}(R_{\alpha,\beta},\omega)g^A_{(2,1)}(R_{\beta,\alpha},\omega)} &= \overline{g^A_{(2,2)}(R_{\alpha,\beta},\omega)g^A_{(2,1)}(R_{\beta,\alpha},\omega)} = \overline{g^A_{(2,1)}(R_{\alpha,\beta},\omega)g^A_{(1,1)}(R_{\beta,\alpha},\omega)} = \overline{g^A_{(2,1)}(R_{\alpha,\beta},\omega)g^A_{(2,1)}(R_{\beta,\alpha},\omega)}\\ &= \frac{1}{2W^2(k_F R_1)^2}\frac{-\omega\Delta}{\Delta^2-\omega^2}\exp\left(-\frac{2R_1}{\xi_{\rm ball}(\omega)}\right)\exp(-i\varphi_N),\end{aligned} \tag{C7}$$

where $R_1 \equiv R_{\alpha,\beta} = R_{\beta,\alpha}$ denotes the separation between the tight-binding sites α and β. The overline in Eqs. (C1)–(C7) denotes averaging over the $k_F R_1$ oscillations in the superconducting Green's function, and the $1/2$ coefficient appearing in front of Eqs. (C1)–(C7) originates from $\overline{\cos^2(k_F R_1)} = \overline{\sin^2(k_F R_1)} = 1/2$; see the ballistic-limit superconducting Green's function given by Eq. (20).

Equations (C1) and (C2) for elastic cotunneling (EC) [25,26] and crossed Andreev reflection (CAR) [25–27] in the ballistic limit are associated with Eqs. (B48) and (B49) in the dirty limit, respectively. Equations (C3) and (C4) for the quartets [5,6] correspond to Eqs. (B50) and (B51). Equation (C5) for double elastic cotunneling (dEC) [5] is associated with Eqs. (B52). Equations (C6) and (C7), which are relevant to the four-terminal 4TSQ and to a normal metal–superconductor–superconductor double junction [38], have Eqs. (B53) and (B54) as their dirty-limit analog.

2. Discussion of the opposite signs of Eqs. (B53) and (B54) and Eqs. (C6) and (C7)

The $\langle\langle g_{(1,1)}g_{(1,2)}\rangle\rangle$ mode relevant to the four-terminal 4TSQ is found to have opposite signs in the dirty and ballistic limits; see Eqs. (B53) and (B54) in the dirty limit and Eqs. (C6) and (C7) in the ballistic limit, respectively. We provide now an explanation for the different signs appearing in the dirty and ballistic limits.

Specifically, we mimic the disorder scattering potential v [see Eqs. (B7) and (B8)] by a tunnel barrier. Namely, we replace an $S_a I S_0 I S_b$ double junction (where I is an insulator) by an $S_a I S_1 I S_2 I S_b$ triple junction, where S_1 and S_2 are two ballistic superconductors separated by an insulating tunnel barrier.

We start with the simple $\langle\langle g_{(1,1)}g_{(1,2)}\rangle\rangle$ four-terminal 4TSQ diagram in an $S_a I S_0 I S_b$ double junction; see Fig. 11(a):

$$\mathscr{D}^{A,(0)} = \langle\langle J^{(1,1)}_{a,\alpha} g^{A,(1,1)}_{\alpha,\beta} J^{(1,1)}_{\beta,b} g^{A,(1,2)}_{b,b} J^{(2,2)}_{b,\beta} g^{A,(2,1)}_{\beta,\alpha} J^{(1,1)}_{\alpha,a} g^{A,(1,1)}_{a,a}\rangle\rangle \tag{C8}$$

$$= -J_0^4\langle\langle g^{A,(1,1)}_{a,a}\rangle\rangle\langle\langle g^{A,(1,2)}_{b,b}\rangle\rangle\langle\langle g^{A,(1,1)}_{\alpha,\beta} g^{A,(2,1)}_{\beta,\alpha}\rangle\rangle. \tag{C9}$$

Thus, $\mathscr{D}^{A,(0)}$ in Eqs. (C8) and (C9) is given by

$$\mathscr{D}^{A,(0)} = -J_0^4\langle\langle g^{A,(1,1)}_{a,a}\rangle\rangle\langle\langle g^{A,(1,2)}_{b,b}\rangle\rangle\mathscr{A}_{\alpha,\gamma}, \tag{C10}$$

where Eq. (C7) was written as

$$\langle\langle g^{A,(1,1)}_{\alpha,\gamma} g^{A,(2,1)}_{\gamma,\alpha}\rangle\rangle = -\mathscr{A}_{\alpha,\gamma}\frac{(\omega-i\eta)|\Delta|}{|\Delta|^2-(\omega-i\eta)^2}\exp(-i\varphi_c), \tag{C11}$$

and the "geometrical" prefactor $\mathscr{A}_{\alpha,\gamma}$ is given by

$$\mathscr{A}_{\alpha,\gamma} = \frac{1}{2W^2}\frac{1}{(k_F R_{\alpha,\gamma})^2}\exp\left(-\frac{2R_{\alpha,\gamma}}{\xi_{\rm ball}(\omega-i\eta)}\right). \tag{C12}$$

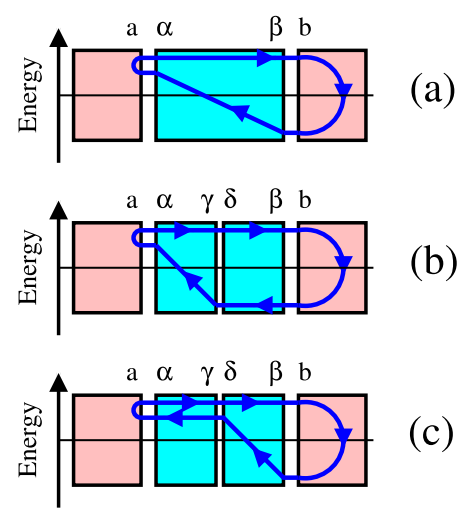

FIG. 11. Panel (a) shows the $\langle\langle g_{(1,1)}g_{(1,2)}\rangle\rangle$ mode at lowest order in the tunnel amplitudes in an $S_a I S_0 I S_b$ double junction [$\mathscr{D}^{A,(0)}$ term in Eq. (C8)]. Panels (b) and (c) show schematically the $\mathscr{D}^{A,(1)}$ and $\mathscr{D}^{A,(2)}$ terms in an $S_a I S_1 I S_2 I S_b$ triple junction; see Eqs. (C13) and (C14) and Eqs. (C15) and (C16), respectively.

Now, we consider an $S_aIS_1IS_2IS_b$ triple junction and start with the diagrams $\mathscr{D}^{A,(1)}$ and $\mathscr{D}^{A,(2)}$ appearing at the lowest order $(J_0/W)^6$ in the tunnel amplitudes; see Figs. 11(b) and 11(c), respectively:

$$\mathscr{D}^{A,(1)} = \langle\langle J^{(1,1)}_{a,\alpha} g^{A,(1,1)}_{\alpha,\gamma} J^{(1,1)}_{\gamma,\delta} g^{A,(1,1)}_{\delta,\beta} J^{(1,1)}_{\beta,b} g^{A,(1,2)}_{b,b} J^{(2,2)}_{b,\beta} g^{A,(2,2)}_{\beta,\delta} J^{(2,2)}_{\delta,\gamma} g^{A,(2,1)}_{\gamma,\alpha} J^{(1,1)}_{\alpha,a} g^{A,(1,1)}_{a,a}\rangle\rangle \tag{C13}$$

$$= J_0^{12}\langle\langle g^{A,(1,1)}_{a,a}\rangle\rangle\langle\langle g^{A,(1,2)}_{b,b}\rangle\rangle\langle\langle g^{A,(1,1)}_{\alpha,\gamma} g^{A,(2,1)}_{\gamma,\alpha}\rangle\rangle\langle\langle g^{A,(1,1)}_{\delta,\beta} g^{A,(2,2)}_{\beta,\delta}\rangle\rangle \tag{C14}$$

and

$$\mathscr{D}^{A,(2)} = \langle\langle J^{(1,1)}_{a,\alpha} g^{A,(1,1)}_{\alpha,\gamma} J^{(1,1)}_{\gamma,\delta} g^{A,(1,1)}_{\delta,\beta} J^{(1,1)}_{\beta,b} g^{A,(1,2)}_{b,b} J^{(2,2)}_{b,\beta} g^{A,(2,1)}_{\beta,\delta} J^{(1,1)}_{\delta,\gamma} g^{A,(1,1)}_{\gamma,\alpha} J^{(1,1)}_{\alpha,a} g^{A,(1,1)}_{a,a}\rangle\rangle \tag{C15}$$

$$= J_0^{12}\langle\langle g^{A,(1,1)}_{a,a}\rangle\rangle\langle\langle g^{A,(1,2)}_{b,b}\rangle\rangle\langle\langle g^{A,(1,1)}_{\alpha,\gamma} g^{A,(1,1)}_{\gamma,\alpha}\rangle\rangle\langle\langle g^{A,(1,1)}_{\delta,\beta} g^{A,(2,1)}_{\beta,\delta}\rangle\rangle. \tag{C16}$$

Equation (C5) leads to

$$\langle\langle g^{A,(1,1)}_{\delta,\beta} g^{A,(2,2)}_{\beta,\delta}\rangle\rangle = \mathscr{A}_{\beta,\delta}\frac{2(\omega-i\eta)^2-|\Delta|^2}{|\Delta|^2-(\omega-i\eta)^2}. \tag{C17}$$

We deduce the following:

$$\mathscr{D}^{A,(0)} = -\mathscr{B}\frac{(\omega-i\eta)^2|\Delta|^2}{[|\Delta|^2-(\omega-i\eta)^2]^2}, \tag{C18}$$

$$\mathscr{D}^{A,(1)} = \mathscr{C}\frac{(\omega-i\eta)^2|\Delta|^2[2(\omega-i\eta)^2-|\Delta|^2]}{[|\Delta|^2-(\omega-i\eta)^2]^3}, \tag{C19}$$

$$\mathscr{D}^{A,(2)} = \mathscr{C}\frac{(\omega-i\eta)^2|\Delta|^4}{[|\Delta|^2-(\omega-i\eta)^2]^3}, \tag{C20}$$

where $\mathscr{B}$ and $\mathscr{C}$ have the same sign. Thus,

$$\mathscr{D}^{A,(1)} + \mathscr{D}^{A,(2)} = \frac{2\mathscr{C}(\omega-i\eta)^4|\Delta|^2}{[|\Delta|^2-(\omega-i\eta)^2]^3} \tag{C21}$$

has a sign that is opposite to that of $\mathscr{D}^A_0$.

It is concluded that a change of sign appears in $\langle\langle g_{(1,1)}g_{(1,2)}\rangle\rangle$ between the following situations:

(i) Equation (C18) for $\mathscr{D}^{A,(0)}$ in an $S_LIS_0IS_R$ double ballistic tunnel junction.

(ii) Equation (C21) for $\mathscr{D}^{A,(1)} + \mathscr{D}^{A,(2)}$ in an $S_aIS_1IS_2IS_b$ triple ballistic tunnel junction.

This resolves the apparent paradox that emerged between the preceding calculations of the $\langle\langle g_{(1,1)}g_{(1,2)}\rangle\rangle$ mode:

(iii) Equations (C6) and (C7) for $\langle\langle g_{(1,1)}g_{(1,2)}\rangle\rangle$ in the ballistic limit.

(iv) Equations (B53) and (B54) for impurity scattering the $\langle\langle g_{(1,1)}g_{(1,2)}\rangle\rangle$ superconducting diffusion mode at the order v^2.

APPENDIX D: DETAILS ON THE CALCULATION OF THE CURRENT-PHASE RELATIONS

1. Demonstration of Eq. (65) for $I_{c,3TQ_1}$

We evaluate the following integral:

$$I_1 = \int_{-\infty}^{0}\frac{\Delta^4}{[\Delta^2-(\omega-i\eta)^2]^2}d\omega. \tag{D1}$$

We expand according to $\omega - i\eta = -\Delta + \varepsilon$. Assuming $|\varepsilon| \ll \Delta$ leads to

$$\frac{\Delta^4}{[\Delta^2-(\omega-i\eta)^2]^2} \simeq \frac{\Delta^2}{4\varepsilon^2} + \frac{\Delta}{8\varepsilon} + \cdots. \tag{D2}$$

If $\eta \ll \Delta$, contour integration yields

$$I_1 = \frac{i\pi\Delta}{4}. \tag{D3}$$

Equation (D3) is used in Sec. V A to deduce the quartet current-phase relations Eqs. (63)–(65) from Eq. (62).

2. Demonstration of Eq. (78) for $I^{(1)}_{c,4TSQ}$

Now, we evaluate

$$I_2 = \int_{-\infty}^{0}\frac{\Delta^6}{[\Delta^2-(\omega-i\eta)^2]^3}d\omega. \tag{D4}$$

Expanding around $\omega - i\eta = -\Delta + \varepsilon$ with $|\varepsilon| \ll \Delta$ leads to

$$\frac{\Delta^6}{[\Delta^2-(\omega-i\eta)^2]^3} \simeq \frac{\Delta^3}{8\varepsilon^3} + \frac{3\Delta^2}{16\varepsilon^2} + \frac{3\Delta}{16\varepsilon} + \cdots. \tag{D5}$$

The residue of the simple pole is $3\Delta/16$. Contour integration yields

$$I_2 = \frac{3i\pi\Delta}{8} \tag{D6}$$

if $\eta \ll \Delta$. Equation (D6) is used in Sec. V C 1 to deduce the four-terminal 4TSQ current-phase relations Eqs. (77) and (78) from Eq. (76).

3. Demonstration of Eq. (84) for $I^{(2)}_{c,4TSQ}$

The integral

$$I_3 = \int_{-\infty}^{0}\frac{(\omega-i\eta)^2\Delta^4}{[\Delta^2-(\omega-i\eta)^2]^3}d\omega \tag{D7}$$

is equal to

$$I_3 = I_2 \tag{D8}$$

if $\eta \ll \Delta$, where I_2 is given by Eq. (D6). The leading-order four-terminal 4TSQ current-phase relations Eqs. (83) and (84) are deduced from Eq. (82) by making use of Eqs. (D7) and (D8); see Sec. V C 2.

4. Averaging the product of three superconducting Green's functions

The average over disorder of the product of three Green's functions

$$\mathscr{C}_3 = \langle\langle g_{(1,1)}g_{(1,2)}g_{(2,2)}\rangle\rangle \tag{D9}$$

appears in the expression of the four-terminal 4TSQ at the orders $(J_0/W)^{12}$ and $\sqrt{\mathscr{S}_{\rm contact}}/l_e$; see Eqs. (9)–(46) in Sec. II A of the Supplemental Material [29].

Each of the three Green's function appearing in Eq. (D9) can propagate locally or nonlocally within the superconducting lead S_N having superconducting phase variable φ_N.

The Wick theorem leads to

$$\mathscr{C}_3 = \langle\langle g_{(1,1)} g_{(1,2)}\rangle\rangle\langle\langle g_{(2,2)}\rangle\rangle + \langle\langle g_{(1,1)} g_{(2,2)}\rangle\rangle\langle\langle g_{(1,2)}\rangle\rangle + \langle\langle g_{(1,1)}\rangle\rangle\langle\langle g_{(1,2)} g_{(2,2)}\rangle\rangle, \tag{D10}$$

where Eqs. (B4) and (B5) imply the following for the local Green's functions of the disordered superconductor S_N:

$$\langle\langle g_{(1,1)}\rangle\rangle = \langle\langle g_{(2,2)}\rangle\rangle = \frac{1}{W}\frac{-(\omega - i\eta)}{\sqrt{|\Delta|^2 - (\omega - i\eta)^2}}, \tag{D11}$$

$$\langle\langle g_{(1,2)}\rangle\rangle = = \frac{1}{W}\frac{|\Delta|}{\sqrt{|\Delta|^2 - (\omega - i\eta)^2}}\exp(i\varphi_N). \tag{D12}$$

Combining with the energy dependence of Eqs. (B52) and (B53) implies the minus sign in

$$\mathscr{C}_3 \sim -\frac{\Delta^3}{W^2[|\Delta|^2 - (\omega - i\eta)^2]^{3/2}}\exp(i\varphi_N), \tag{D13}$$

which is taken into account in the four-terminal 4TSQ critical current at the orders $(J_0/W)^{12}$ and $\sqrt{\mathscr{S}_{\rm contact}}/l_e$; see Eq. (78) in the main body of the paper and Sec. II A in the Supplemental Material [29].

[1] P. W. Anderson, Random-phase approximation in the theory of superconductivity, Phys. Rev. **112**, 1900 (1958).

[2] P. W. Anderson, Plasmons, gauge invariance, and mass, Phys. Rev. **130**, 439 (1963).

[3] B. D. Josephson, Possible new effects in superconductive tunnelling, Phys. Lett. **1**, 251 (1962).

[4] K. F. Huang, Y. Ronen, R. Mélin, D. Feinberg, K. Watanabe, T. Taniguchi, and P. Kim, Interference of Cooper quartet Andreev bound states in a multi-terminal graphene-based Josephson junction, arXiv:2008.03419 [cond-mat] (2020).

[5] A. Freyn, B. Douçot, D. Feinberg, and R. Mélin, Production of Non-Local Quartets and Phase-Sensitive Entanglement in a Superconducting Beam Splitter, Phys. Rev. Lett. **106**, 257005 (2011).

[6] R. Mélin, D. Feinberg, and B. Douçot, Partially resummed perturbation theory for multiple Andreev reflections in a short three-terminal Josephson junction, Eur. Phys. J. B **89**, 67 (2016).

[7] T. Jonckheere, J. Rech, T. Martin, B. Douçot, D. Feinberg, and R. Mélin, Multipair DC Josephson resonances in a biased all-superconducting bijunction, Phys. Rev. B **87**, 214501 (2013).

[8] J. Rech, T. Jonckheere, T. Martin, B. Douçot, D. Feinberg, and R. Mélin, Proposal for the observation of nonlocal multipair production, Phys. Rev. B **90**, 075419 (2014).

[9] R. Mélin, M. Sotto, D. Feinberg, J.-G. Caputo, and B. Douçot, Gate-tunable zero-frequency current cross-correlations of the quartet mode in a voltage-biased three-terminal Josephson junction, Phys. Rev. B **93**, 115436 (2016).

[10] R. Mélin, J.-G. Caputo, K. Yang, and B. Douçot, Simple Floquet-Wannier-Stark-Andreev viewpoint and emergence of low-energy scales in a voltage-biased three-terminal Josephson junction, Phys. Rev. B **95**, 085415 (2017).

[11] R. Mélin, R. Danneau, K. Yang, J.-G. Caputo, and B. Douçot, Engineering the Floquet spectrum of superconducting multiterminal quantum dots, Phys. Rev. B **100**, 035450 (2019).

[12] B. Douçot, R. Danneau, K. Yang, J.-G. Caputo, and R. Mélin, Berry phase in superconducting multiterminal quantum dots, Phys. Rev. B **101**, 035411 (2020).

[13] A. H. Pfeffer, J. E. Duvauchelle, H. Courtois, R. Mélin, D. Feinberg, and F. Lefloch, Subgap structure in the conductance of a three-terminal Josephson junction, Phys. Rev. B **90**, 075401 (2014).

[14] Y. Cohen, Y. Ronen, J. H. Kang, M. Heiblum, D. Feinberg, R. Mélin, and H. Strikman, Non-local supercurrent of quartets in a three-terminal Josephson junction, Proc. Natl. Acad. Sci. USA **115**, 6991 (2018).

[15] J. E. Zimmerman and A. H. Silver, Macroscopic quantum interference effects through superconducting point contacts, Phys. Rev. **141**, 367 (1966).

[16] J. D. Pillet, V. Benzoni, J. Griesmar, J.-L. Smirr, and Ç. Ö. Girit, Nonlocal Josephson effect in Andreev molecules, Nano Lett. **19**, 7138 (2019).

[17] J.-D. Pillet, V. Benzoni, J. Griesmar, J.-L. Smirr, and Ç. Ö Girit, Scattering description of Andreev molecules, SciPost Phys. Core **2**, 009 (2020).

[18] R.-P. Riwar, M. Houzet, J. S. Meyer, and Y. V. Nazarov, Multi-terminal Josephson junctions as topological materials, Nat. Commun. **7**, 11167 (2016).

[19] E. Eriksson, R.-P. Riwar, M. Houzet, J. S. Meyer, and Y. V. Nazarov, Topological transconductance quantization in a four-terminal Josephson junction, Phys. Rev. B **95**, 075417 (2017).

[20] E. Strambini, S. D'Ambrosio, F. Vischi, F. S. Bergeret, Yu. V. Nazarov, and F. Giazotto, The ω-SQUIPT as a tool to phase-engineer Josephson topological materials, Nat. Nanotech. **11**, 1055 (2016).

[21] A. W. Draelos, M.-T. Wei, A. Seredinski, H. Li, Y. Mehta, K. Watanabe, T. Taniguchi, I. V. Borzenets, F. Amet, and G. Finkelstein, Supercurrent flow in multiterminal graphene Josephson junctions, Nano Lett. **19**, 1039 (2019).

[22] N. Pankratova, H. Lee, R. Kuzmin, K. Wickramasinghe, W. Mayer, J. Yuan, M. G. Vavilov, J. Shabani, and V. E. Manucharyan, Multi-Terminal Josephson Effect, Phys. Rev. X **10**, 031051 (2020).

[23] R. Mélin and B. Douçot, Inversion in a four-terminal superconducting device on the quartet line. II. Quantum dot and Floquet theory, Phys. Rev. B **102**, 245436 (2020).

[24] R. Mélin (unpublished).

[25] G. Falci, D. Feinberg, and F. W. J. Hekking, Correlated tunneling into a superconductor in a multiprobe hybrid structure, Europhys. Lett. **54**, 255 (2001).

[26] R. Mélin and D. Feinberg, Sign of the crossed conductances at a ferromagnet/superconductor/ferromagnet double interface, Phys. Rev. B **70**, 174509 (2004).

[27] G. Deutscher and D. Feinberg, Coupling superconducting-

ferromagnetic point contacts by Andreev reflections, Appl. Phys. Lett. **76**, 487 (2000).

[28] T. H. Stoof and Yu. V. Nazarov, Flux effect in superconducting hybrid Aharonov-Bohm rings, Phys. Rev. B **54**, R772(R) (1996).

[29] See Supplemental Material at http://link.aps.org/supplemental/10.1103/PhysRevB.102.245435 for technical details of the calculations.

[30] S. B. Kaplan, C. C. Chi, D. N. Langenberg, J. J. Chang, S. Jafarey, and D. J. Scalapino, Quasiparticle and phonon lifetimes in superconductors, Phys. Rev. B **14**, 4854 (1976).

[31] R. C. Dynes, V. Narayanamurti, and J. P. Garno, Direct Measurement of Quasiparticle-Lifetime Broadening in a Strong-Coupled Superconductor, Phys. Rev. Lett. **41**, 1509 (1978).

[32] J. P. Pekola, V. F. Maisi, S. Kafanov, N. Chekurov, A. Kemppinen, Yu. A. Pashkin, O.-P. Saira, M. Möttönen, and J. S. Tsai, Environment-Assisted Tunneling as an Origin of the Dynes Density of States, Phys. Rev. Lett. **105**, 026803 (2010).

[33] O.-P. Saira, A. Kemppinen, V. F. Maisi, and J. P. Pekola, Vanishing quasiparticle density in a hybrid Al/Cu/Al single-electron transistor, Phys. Rev. B **85**, 012504 (2012).

[34] C. Caroli, R. Combescot, P. Nozières and D. Saint-James, Direct calculation of the tunneling current, J. Phys. C **4**, 916 (1971).

[35] J. C. Cuevas, A. Martín-Rodero, and A. Levy Yeyati, Hamiltonian approach to the transport properties of superconducting quantum point contacts, Phys. Rev. B **54**, 7366 (1996).

[36] A. A. Abrikosov, L. P. Gorkov, and I. E. Dzyaloshinski, *Methods of Quantum Field Theory in Statistical Physics*, 1st ed. (Prentice Hall, Englewood Cliffs, NJ, 1963).

[37] R. A. Smith and V. Ambegaokar, Weak-localization correction to the number density of superconducting electrons, Phys. Rev. B **45**, 2463 (1992).

[38] D. Gosselin, G. Hornecker, R. Mélin, and D. Feinberg, Phase-sensitive transport at a normal metal-superconductor interface close to a Josephson junction, Phys. Rev. B **89**, 075415 (2014).

[39] R. Mélin, Contribution of weak localization to nonlocal transport at normal metal/superconductor double interfaces, Phys. Rev. B **73**, 174512 (2006).

[40] M. Wampler, P. Schauss, E. B. Kolomeisky, and I. Klich, Quantum wakes in lattice fermions, arXiv:2006.09469.

[41] W. Guichard, M. Aprili, O. Bourgeois, T. Kontos, J. Lesueur, and P. Gandit, Phase Sensitive Experiments in Ferromagnetic-Based Josephson Junctions, Phys. Rev. Lett. **90**, 167001 (2003).

[42] M. A. H. Nerenberg, J. A. Blackburn, and D. W. Jillie, Voltage locking and other interactions in coupled superconducting weak links. I. Theory, Phys. Rev. B **21**, 118 (1980).

[43] D. W. Jillie, M. A. H. Nerenberg, and J. A. Blackburn, Voltage locking and other interactions in coupled superconducting weak links. II. Experiment, Phys. Rev. B **21**, 125 (1980).

[44] A. Levy Yeyati, F. S. Bergeret, A. Martín-Rodero, and T. M. Klapwijk, Entangled Andreev pairs and collective excitations in nanoscale superconductors, Nat. Phys. **3**, 455 (2007).

[45] G. E. Blonder, M. Tinkham, and T. M. Klapwijk, Transition from metallic to tunneling regimes in superconducting microconstrictions: Excess current, charge imbalance, and supercurrent conversion, Phys. Rev. B **25**, 4515 (1982).

[46] M. Flöser, D. Feinberg, and R. Mélin, Absence of split pairs in the cross-correlations of a highly transparent normal metal-superconductor-normal metal electron beam splitter, Phys. Rev. B **88**, 094517 (2013).